2018-08-03

Towards the Fabrication of a Fibrin Based Vascular Network

Johanna Eleanor Santos
Worcester Polytechnic Institute

Towards the Fabrication of a Fibrin Based Vascular Network

Johanna Eleanor Santos

A thesis to be submitted to the faculty of Worcester Polytechnic Institute in partial fulfillment of the requirements for the Degree of Master of Science

Submitted by:

Johanna E. Santos
Department of Biomedical Engineering

Approved by:

George Pins, PhD, Advisor
Professor
Department of Biomedical Engineering

Committee Chair: Jeannine Coburn, PhD.
Assistant Professor
Department of Biomedical Engineering

Catherine Whittington, PhD.
Assistant Professor
Department of Biomedical Engineering

August 2018

Acknowledgements

I would first and foremost like to thank my committee members, Jeannine Coburn, PhD, and Catherine Whittington, PhD, for their feedback and for their participation in this major event in my educational and professional career and development.

Special thanks to:

My advisor, George Pins, PhD, for his continuous help, patience and guidance through this process. FWorking with him has taught me to become a better scientist, and to have more confidence both in my work and in myself.

The Pins lab: Meagan Carnes, Kailey Castellano, Megan Chrobak, PhD, Elizabeth English, and Marianne Kanellias, and all of our wonderful undergraduate students for making the lab a fun place to be, and always being there to answer my many questions.

Jyotsna Patel, for teaching me the ins and outs of histology, always being ready to help and answer questions, and for being a delight to see every day around lab.

Keith Gagnon and Thomas Moutinho for answering questions about their MQP three years after the completion of their project.

Jack Rivadeneira for teaching me how to use the laser cutter, assisting with builds, and for impulse buying a fancy 3D printer and letting me use it.

Olivia Mack, for providing a platform for future development with the inspired use of Shrinky Dinks.

Nicole Beinstein, for keeping me supplied with a steady stream of baked good and calculus advice and being my editor-in-chief.

Special thanks to Hugh Long for his artistic prowess and contributing figures to this final paper.

Finally, I would like to thank all of my friends and family, especially Joanna Luo, Evan Baum, and my wonderful parents for supporting me through graduate school, helping me maintain my sanity, and for not letting me give up. Your love and support has meant the world to me.

Abstract

Physiologically relevant scaffold-based tissue engineered structures have been limited in scope and viability by the diffusion limits of oxygen and other nutrients and functions provided by native vasculature *in vivo.* This has prevented the maintenance of healthy cell populations in scaffolds that are more than 200µm thick. Combining concepts from microfluidics with biomaterials engineering, this project set out to engineer a perfusable fibrin-based vascular network capable of physiologically relevant flow properties as well as diffusion that supports viable cell populations. To create this system, a small artery sized (1.5 mm wide) gelatin sacrificial structure was embedded inside of a block of robust fibrin gel (4.26% w/v fibrin) then melted and rinsed out to create a perfusable vascular network. Characterization consisted of morphometric and histological analyses for channel sizes compared to the sacrificial structures, particle tracking to observe flow properties, and fluorescent dextran diffusion to measure diffusivity into the fibrin scaffold. We found that channels derived from sacrificial structures maintain their size and shape inside of the gel. Flow properties of the fluid through the channels were found to be both laminar and within expected physiological rates compared to native vessels of similar sizes. Cells on the surface of the fibrin vascular device expressed fluorescent markers that were delivered through the vascular network and perfused through the fibrin scaffold. These findings suggest that a fibrin based vascular system may provide a platform creating a functional vascular layer and for developing tissue engineered systems of increased size and complexity.

Table of Contents

Table of Figures

Table of Tables

Table of Equations

Chapter 1: Introduction

With very few exceptions, cells are not capable of survival more than 200µm away from a source of oxygen, a source of nutrients, and metabolic waste removal [1]. *In vivo*, this source takes the form of the vascular network, which is made of a complex branching system of veins, arteries, arterioles, and capillaries which contact every area of tissue and organ [2]. Should the vasculature become damaged, diseased, or removed, as in the case of myocardial infarction or volumetric muscle loss, the lack of blood flow to the area causes tissue death. This dead tissue cannot be regenerated. In its place will be avascular scar tissue, which does not function the same way as the ischemic tissue [3], [4].

The need for vascularization has also been a major limitation in the development of full thickness tissue engineered constructs and grafts [1]. Vascular engineering has become a large and varied field aimed at addressing this concern. A wide variety of both natural and synthetic materials are used to fabricate vasculature *in vitro.* Synthetic materials have been very successful in producing geometrically complex systems. However, they tend to see only limited bioactivity [1], [5]. Natural materials, such as collagen, ECM, and fibrin, are more capable of supporting healthy cell populations and provide better remodeling, but suffer in their ability to make complex channel geometries, mechanical properties, and have been found to leak [1], [5, 6]. Both methods have proven viable for applications, like drug testing and *in vitro* modeling, but overall, there is neither a perfect method of nor a perfect material for vascular engineering [7].

The goal of this project was to develop a novel method for the fabrication of a single layered fibrin based vascular network that was able to reliably produce channels, had flow properties that were physiologically relevant, and had diffusion rates that were capable of sustaining a viable cell population on the surface. For the purpose of this study, a larger channel size was targeted, one that mimicked small arteries rather than microvasculature. That is because this thesis was a large-scale proof of concept exploring the feasibility and functionality of such a system.

The objectives of these studies were centered around the development and characterization of a perfusable fibrin based vascular network. Once the network fabrication was successful, several characteristics were measured to establish consistency and compare to physiological values. These were as follows:

- A morphometric and histological analysis of sacrificial structure and channel sizes to establish consistency and reliability of channel fabrication methods
- Flow analysis focused on the ability of the system to maintain expected flow rates, laminar flow, and wall shear stress values similar to physiological values to ensure the system was physiologically relevant
- Diffusivity calculations to measure and understand the ability of the system to diffuse micro- and macromolecules outside of the channels
- Evaluate cell viability on the surface of the fibrin vascular device to establish the ability of the system to maintain cell populations

A variety of techniques were used to address each of the goals listed above. The sacrificial structure technique was selected to fabricate the channels within the fibrin vascular devices due to its versatility and simplicity, as well as the ease at which a single layered system could be created to address frequent problems with hydrogel based vascular engineering, like backflow and leakage [6]. Histology and microscope imaging were used for the morphometric analysis of channels and sacrificial structures. The findings showed no statistical difference between them, and that they achieved the goal of mimicking small arterial dimensions [8, 9]. The flow analysis was performed by perfusing polystyrene microbeads through the fibrin vascular device. The average particle speed obtained from this study allowed the calculation of a variety of flow properties, including volumetric flow rate, which closely matched expected values, Reynolds number, which showed our flow to be laminar, as it is *in vivo*, and wall shear stress which was below the physiological maximum within our system [10]. Perfusion of two

different molecular weights of fluorescent dextran were used to measure the diffusive properties of the gel. Finally, a perfusion of calcein AM dye was used to observe cellular uptake on a cover slip on the surface of a fibrin vascular device, to prove that fibrin vascular devices can supply cells with nutrients.

Overall, the morphological, diffusive, and flow properties of a monolayered fibrin vascular device showed strong correlation to physiological values. Channel areas were an average of 1.10 mm^2 and showed no significant difference between the size of the channels and the size of the sacrificial structures. An average flow rate of 0.204 mm^3/s, a Reynolds number of 1.15×10^{-3} and a wall shear stress of 0.385 N/m^2 all fall within physiological values. These experiments also successfully addressed several problems common with hydrogel based fluidic systems. These promising results provide a strong argument for the continuation of development of this system, with the end goal of creating a functional microvascular network for an array of uses, including vascularization of full thickness tissue engineered constructs, and as a platform for *in vitro* drug testing assays.

Chapter 2: Background

This project centers around the fabrication and characterization of a novel engineered vasculature for the purposes of developing full thickness engineered tissues, patches, and even as an *in vitro* platform for drug testing. The development of this device requires a background understanding of the purpose of vasculature, existing engineered tissue, and what is being researched in the world of vascular engineering and microfluidics for the purpose of vascular engineering. Finally, this section will discuss the materials chosen for this project, and the logic behind those choices in order to develop vasculature that is biocompatible and functional.

2.1: Vasculature Function

The vascular network is the system of arteries, veins, arterioles, and capillaries that carry blood from the heart to nearly every tissue and organ throughout the body [2]. Blood vessels in this network, with diameters ranging from arteries up to 6mm to capillaries as small as 5µm, are made of smooth muscle with a single layer of endothelial cells lining the inside [8, 9]. As outlined in Figure 1 to the right, vasculature provides nearby cells with oxygen and other nutrients, and serves as the mechanism for the removal of metabolic waste. Due to the diffusion limit and consumption of oxygen, cells are unable to survive more than 200µm from the closest blood vessel, meaning that capillaries are widespread and numerous [1,

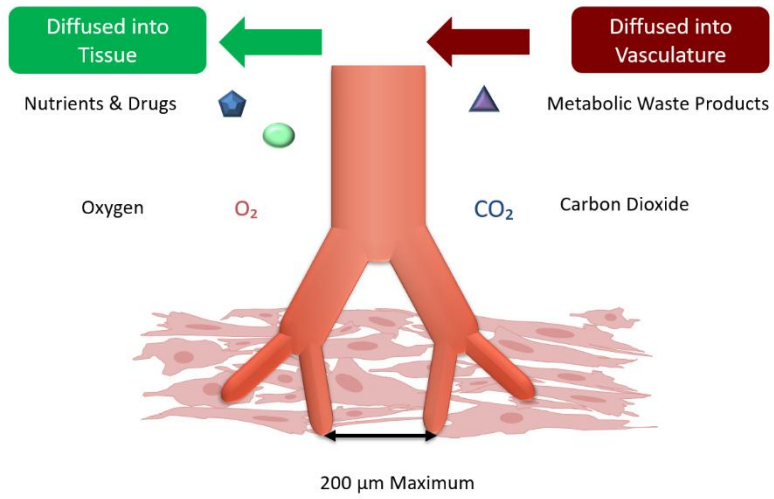

Figure 1: Schematic of vascular function. Adapted from Novesel et al.

11]. It also means that when vasculature is damaged or otherwise dysfunctional, there are major repercussions in the health of the individual, including myocardial infarction in the event of cardiac vasculature becoming compromised and volumetric muscle loss within skeletal muscle tissue.

2.1.1: Myocardial Infarction

The treatment of patients with damage to their organs or tissues accounts for over half of all medical costs in the United States of America [7]. Between 2011 and 2014, over 7.9 million of the patients responsible for this cost, approximately 4.9 million of whom were men, suffered from a myocardial infarction, or heart attack [12]. In 2014, 114,000 of these cases resulted in death [12]. Myocardial infarction occurs due to a thrombic occlusion of a cardiac artery that lasts for longer than 20 minutes [3], [13]. The resulting ischemia, or lack of blood flow, causes the death of myocardial tissue [3].

Unfortunately, the mammalian heart has limited regenerative properties, meaning that the ischemic area fills in with avascular collagenous scar tissue rather than functional cardiac muscle [3]. While this scar tissue is initially useful in providing mechanical support for the heart and preventing further damage to the heart wall, they also change the ventricle geometry and alter the mechanical properties of the heart, thus changing the way it beats [4]. This alteration of the cardiac tissue caused by this fibrosis eventually results in heart dilation, which can ultimately cause heart failure [4, 14]. In summary, the damage of vascular tissue in the heart is dangerous and frequently deadly due to the inability of cardiac muscle to remodel in the absence of nutrients and oxygen.

2.1.2: Volumetric Muscle Loss

When an injury destroys more than 20% of a specific muscle, it is considered to be an area of volumetric muscle loss [15]. This means the tissue in the area is incapable of regenerating in the same way a smaller injury could. This is due to the destruction of the basement membrane, connective tissue, and vascular tissue in the area. Removal of these tissues means that the biochemical, structural, and mechanical cues that the body normally uses to regenerate are not present [15]. Vasculature is

especially difficult to regenerate, and, much like the heart after myocardial infarction, the lack of nutrients and waste removal leads to the area filling with avascular scar tissue [15]. The results of excess scar tissue in the injured area are also similar to occurrences in the heart. The muscle in the area is never able to regain its full strength and function, and as of now, there are no treatments available to restore full function in these injuries [15]. In extreme cases of volumetric muscle loss, full limb amputation becomes necessary due to the inability of the body to regenerate function [15]. This is another case where the lack of vascular tissue in an area causes severe and irreparable damage to the body and has a massive impact on health and quality of life. It is for these reasons that it is important to find a way to reliably produce engineered vasculature to replace damaged or diseased tissue, and why it has become a major focus of the tissue engineering community.

2.2: Microvascular grafts

Vascular grafts are the current gold standard of treatment for damaged or diseased vasculature. The first vascular autograft was performed in 1949 [5]. This is a graft made with a patient's own endothelial cells and fibroblasts, and, while not a perfect treatment, it has seen considerable success [7]. Depending on the needs of the patient, there are two types of vasculature that can be grafted: macrovasculature, such as veins and arteries, and microvasculature. Should there be a need for a macrovascular autograft, a patient's own veins can be transplanted to the appropriate area of the body. In other cases where a microvascular graft is necessary, it is more common to use a pedicle flap.

Microvascular grafts work differently than their larger counterparts. Rather than harvesting a patient's vein to replace a large portion of damaged tissue, microvasculature is replaced using something called a pedicle flap. These are autologous tissue lifted from a donor site and moved to the implant site. This is often done underneath the healthy tissue. It is performed in this manner because the donated flap is not disconnected from its blood supply until a new, properly functional blood supply has been formed at the site of implantation. Pedicle flaps have been used in and have seen significant

success across multiple applications, including the treatment of severe burns or trauma, breast reconstruction, and at sites of tumor resection [16], [17], [18]. Unfortunately, these pedicle flap grafts have several limitations. It is difficult to maintain these grafts in an angle and position that does not damage the blood supply to the flap. The vein can become compressed, and if not properly attached, the entire flap can shift [17]. There is also a large amount of donor site morbidity, and difficulties have arisen with the vascular inosculation of donor and implant site blood vessels [16].

While autografts have seen great success in many cases, they are not an ideal choice for all situations or patients. They also apply exclusively to vascular damage; autografts have not been used in other engineered tissue. A pressing need remains for engineered vasculature, both for the purposes of full thickness tissue engineering, as well as *in vitro* models for drug testing and vascular disease modeling [1].

2.3: Vascular Engineering

As previously discussed, the creation of a vascular substitute is vital for the creation of full thickness engineered tissue, and it has thus been a major area of research [19, 20]. The ultimate goal of tissue engineering is to create functional tissues *in vitro* and transplant them *in vivo* or to use them as *in vitro* models, an example schematic of which is in Figure 2 [1]. The most successful tissue engineered constructs have involved three major parts: cells, a scaffold for extracellular matrix (ECM), and signals to direct repair and regeneration [7]. Unfortunately, due to difficulties with the creation of vasculature, the current state of engineering

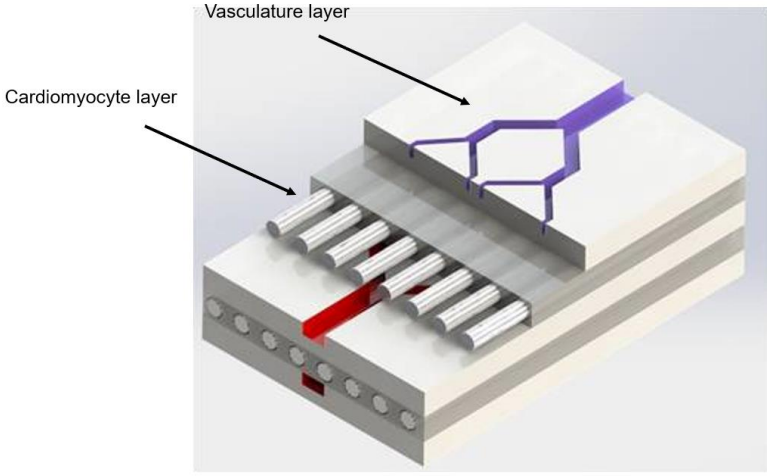

Figure 2:Schematic of a full thickness vascularized patch. Credit to Alexander Hallet

technology focuses more on repair and regeneration of damaged tissue than replacement [5]. There are two major approaches to vascular engineering: acellular scaffold based methods, and cellular methods. Each of these methods have benefits and limitations.

2.3.1: Acellular Vasculature Engineering Strategies

Acellular scaffold guided vascular regeneration has been a major area of exploration for engineers in the tissue engineering field [5]. Acellular scaffolds encompass a very broad range of materials and techniques, including use of both synthetic and natural materials, and addressing vasculature of multiple sizes [5]. The few universal requirements include sufficient porosity to promote cell growth, and allowance for the exchange of nutrients and waste [5]. It is also ideal for scaffolds intended for grafting to have a burst pressure greater than 1700 mmHg and the ability to resist fatigue from cyclic loading for at least 30 days *in vitro* without dilation [5]. These values make the developed scaffold more likely to be useful *in vivo*. With these factors in mind, a variety of both synthetic and natural materials have been used to model vasculature.

Synthetic materials for vascular grafts must be carefully considered across a range of criteria. Among these are the thromboresistance and mechanical compliance [5]. Additionally, it is preferable that the chosen material does not induce hyperplasia as a result of being implanted into the body [5]. These all must be considered in order to prevent total failure of the engineered graft, either due to mechanical strain, immune rejection, or thrombosis. Materials that have proven themselves viable according to these parameters include Dacron and Teflon [5].

These materials are ideal, not only for their response in the body, but also their versatility to be used in multiple fabrication techniques. They can be made in high volumes, and formed into extremely small and complex geometries, without sacrificing their desirable and easily manipulated mechanical properties [5]. Unfortunately, these synthetic materials do have a major drawback: their lack of

bioactivity [1], [5]. This means that while cells are capable of living on scaffolds made from these materials, they often do not do very much to promote cell growth and healing.

To promote a more active healing environment, it is common to use natural materials in place of synthetic materials in a scaffold. These materials have many benefits over their synthetic counterparts: the bioactivity previously mentioned, and being biocompatible in bulk tissue [1]. These materials often also have relevant geometries, such as pores, already in place [1]. Materials such as fibrin, collagen, and ECM have become popular due to their ability to mimic necessary properties of native tissue [7]. It is also common to utilize natural structures that have been decellularized with detergents, leaving only a scaffold. These scaffolds range in material from cellulose based spinach leaves to full ECM organs [21, 22]. In all cases, however, these structures are fully perfusable and, while they suffer in mechanical properties, maintain a complex vascular structure able to be seeded with cells [21, 22]. Overall, these natural scaffolds provide far better remodeling than has been seen with synthetic scaffolds [5]. There are, however, limitations to using these natural materials.

The most prominent problem with the use of natural material is the mismatch of mechanical properties between these natural scaffolds and native tissue. Specifically with collagen, a clear compliance mismatch was seen, and the addition of a material like Dacron has been shown to cause negative responses [5]. Despite the use of adding other natural fibers, like silk, and laminating layers of biomaterial together, mechanical properties of the natural material scaffolds remain inferior to synthetic materials. It is also difficult to standardize and reproduce natural scaffolds [1].

The use of acellular scaffolds for vascular engineering is an active and powerful area of research with many varied materials, techniques, and limitations associated with it. Synthetic scaffolds provide excellent mechanical properties and are easily used to make reproducible small geometries, but are severely lacking in their biocompatibility and bioactivity, providing overall poor remodeling. Natural materials provide much better remodeling, both of vasculature and the surrounding tissue, but inferior

mechanical properties and difficulties reproducing proper geometries lead to difficulties in use. Despite this, scaffolds are highly promising and very important to the success of a vascular graft.

2.3.2: Cellular Vascular Engineering Strategies

Cellular vascular engineering typically involves a scaffold seeded with cells and growth factors among other signals to induce the growth of the desired vascular tissue. Multiple cell types must be used to create a graft sufficiently similar to vascular tissue to be clinically and theoretically relevant. These cells include endothelial cells, fibroblasts, and smooth muscle cells [5]. Besides the proper type, it is vital that these cells are also nonimmunogenic, highly proliferative, and most importantly that they are able to function normally [5]. Among these cell types, endothelial cells might be the most imperative. Endothelial cells line the inner layer of all vasculature and help to provide thromboresistance, preventing pseudo-intimal hyperplasia [7]. This subsection discusses a few broad techniques used for the development of engineered cellular vascular grafts, their benefits, and their limitations.

Prevascularization *in vitro* is the process by which a scaffold is seeded with appropriate cells in a lab environment and carefully cultured to obtain the desired cell functionality before implantation [1]. This technique has been shown to greatly reduce the time necessary for vasculature to grow *in vivo*, as it eliminates the need for host endothelial cells to grow to the center of the tissue, and it promotes rapid anastomosis [1, 23]. These *in vitro* prevascularized scaffolds are not, however, surgically attached to host vasculature. This severely limits the diffusion and perfusion rates of these scaffolds, as pre-built vasculature often does not develop a physiologically relevant vascular network able to diffuse up to 200µm [1]. This is opposed to the *in vivo* prevascularized scaffolds. The *in vivo* technique involves surgically inserting a scaffold into non-ischemic tissue within the host without cells and allowing it to vascularize *in vivo* [1]. The scaffold is then removed and reinserted into the damaged tissue. The

vasculature built this way has a wider spread and vascularizes the implant more completely. Unfortunately, this is a slower process and requires three surgeries to implant into ischemic tissue [1].

Another cell based vascular engineering strategy involves the induction of neoangeogenesis *in vitro*. The use of growth factors promotes vessel formation, cell assembly, and migration of endothelial cells [1]. These growth factors, including vascular endothelial growth factor (VEGF), basic fibroblast growth factor (bFGF), hepatocyte growth factor-regulated tyrosine kinase substrate (HGS), platelet derived growth factor (PDGF), transforming growth factor beta (TGFbeta), and angiopoietin, initiate this host derived vascularization and can be applied directly to the site that needs them most [1]. Unfortunately, these growth factors, once applied to the desired site, are both highly unstable and difficult to control [1]. Improvements in biomaterials, such as poly lactic-co-glycolic acid (PLGA) and polylysine (PLL), have improved the delivery of these growth factors, but it remains an imperfect system [1].

The use of cell sheets in vascular engineering has shown significant promise on several fronts. It involves the culture and then careful removal of monolayers of cells from temperature sensitive plates in a bioreactor. Thermoresponsive plates change hydrophobicity with external temperature, allowing cells to lift off the surface in sheets. The cell sheets can then be layered or shaped as desired [1, 5]. Structures made with these cell sheets have very good mechanical properties and show promise as a method of pursuing scaffold free vascular tissue engineering [5]. Unfortunately, this is limited as well. The cell sheets take a very long time to mature within their bioreactors and are difficult to remove without tearing [5]. Additionally, while cell sheets do show promise for scaffold free engineering. There is still no reliable method to make these custom shaped tissues with any degree of reproducibility, speed, or precision [19].

2.3.3: General Limitations of Vascular Engineering

In the previous subsection, the benefits and limitations of multiple vascular engineering strategies were discussed in depth. While understanding limitations of individual strategies is important, it is also vital to discuss what is limiting the field of vascular engineering and what has not yet been fully addressed. First and foremost among these is that there is no perfect material for vascular tissue engineering [7]. Whether it be due to a mismatch of mechanical properties, poor cell integration, immune reaction, or other factors, all polymers and natural materials have shortcomings [1, 7]. There are also additional factors that affect remodeling in ways that are not fully explored and understood, such as shear stress, stretch, immune response, and the specific properties of each matrix [7]. Cells are also a major limiting factor. The cells used in vascular engineering must be renewable and functional, as well as capable of rapid proliferation with minimized immune response [7], [5]. Additionally, it has been found that the endothelial cells seeded onto synthetic grafts are only 10% as functional as their native tissue counterparts, and tend to experience premature senescence [7]. Limitations with vascular engineering are varied, from material properties to reproducibility to cell functionality, but it is still a wide and important field of study for the treatment of a multitude of dangerous and debilitating conditions.

2.4: Microfluidics for Vascular Modeling

Besides the need for engineered vascular tissue, a considerable amount of work is being done to build a reliable vasculature model *in vitro*. These models became extremely popular with the introduction of polydimethylsiloxane (PDMS) [24]. PDMS is optically clear, relatively simple and inexpensive to work with, non-cytotoxic, and capable of precisely and accurately molding to patterns on a micron scale through soft lithography. It is the current state-of-the-art and most popular platform for microfluidics [24]. In the realm of vasculature, microfluidics primarily focus on reconstructing blood vessels *in vitro* to study vasculature in relation to disease modeling, drug screening, and small scale

versions of full vascular environments [2]. Microfluidic models of vascular networks can be created in several different ways to fulfil the requirements of each application.

2.4.1: Microfluidic Techniques for the Creation of Vascular Models

The most common techniques used for vascular modeling in microfluidics are cell patterning, patterned microchannels, sacrificial molds, and self-assembly. These techniques (pictured in Figure 3 below) each provide different benefits to the user and have seen considerable success in vascular engineering.

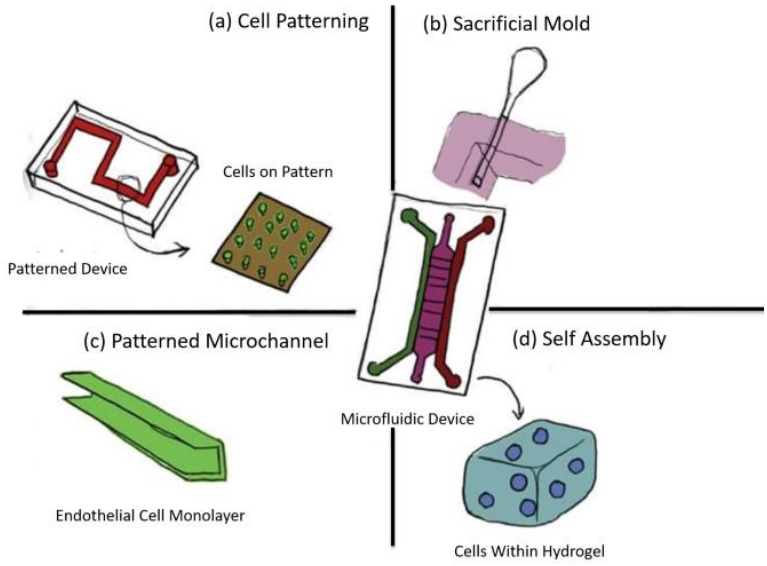

Figure 3:Schematic of vascular microfluidics fabrication methods. (a) Cell patterning within a PDMS device (b) sacrificial channels in hydrogel (c) patterned microchannels (d) self-assembled vasculature within a hydrogel matrix. Adapted from Kim et al. by Hugh Long

Cell patterning is among the simpler methods of vascular microfluidics and is most frequently used for studying shear forces on endothelial cells and diffusion through lined membranes [2]. A nano-scaled pattern is created using photolithography and imprinted into PDMS through soft lithography [2]. The PDMS can then be treated to be capable of cell culture, and cells can be grown directly onto the

patterns created through the soft lithography, and multilayered devices can be made to establish flow in cell seeded channels [2]. This method is also versatile enough that it is not limited to PDMS alone. Channels can be lined with a variety of patterned polymer membranes to achieve similar effects [2, 25]. The Stroock lab, for example, has patterned microchannels onto calcium alginate gel using PDMS, then combined two alginate layers by holding them together using an aluminum rig and injecting the material with primary chondrocytes. This system was then used to calculate diffusion through cell seeded bulk material [26]. Cell patterning is a simple technique to learn and utilize, and it is high throughput, making it ideal for a lot of researchers.

Patterned microchannels are made in a similar fashion as the cell patterned microfluidic devices but used for different applications. Patterned devices are made using PDMS soft lithography and layered together [2]. Channels are then typically filled with cell seeded hydrogels [2]. Cells can then be stimulated to grow in the desired alignment to the desired size within the hydrogel [2]. Stimuli within the channels are highly controllable, thus making this technique capable of reproduceable vasculature, and has made fully patent and confluent endothelialized channels within layers of PDMS[27]. This ease of use makes the method high throughput as well [2]. This method of microfluidic vascular engineering also shows considerable promise as it is capable of being translated to various hydrogels and biomaterials, such as collagen and polylactic glycolic acid (PLGA) [2, 28].

Another popular method of channel formation for vascular microfluidics involves the use of a sacrificial mold, or a sacrificial structure. Sacrificial structures are designed to create space within a hydrogel or other material and be removed immediately prior to cell seeding, leaving behind channels of predetermined dimensions [2]. It is common to secure those spaces with needles or rods within the hydrogel base. It is also common to use gelatin as a sacrificial structure. Gelatin has the added benefit of being able to be molded into a variety of shapes [2, 24, 29]. Sacrificial molds also promote the usage of materials besides PDMS for the bulk of the microfluidic device. The Chen lab uses sacrificial structures

made from micropatterned gelatin, which are placed against a treated glass slide and casts collagen gel over the surface within a larger PDMS mold in order to make complex channels against the surface of the glass [30]. A similar method has been used in the Tien lab where gelatin based meshes were fabricated as narrow as 6 µm in width [29]. In some cases, such as in work done by the Kaplin lab, complex multichannel networks can be made without the use of additional PDMS to encase the hydrogel fluidic device. In this instance, complex sacrificial structures were encased in multiple layers of silk hydrogel to obtain a self-contained network of channels [24].

Self-assembly of microfluidic vasculature is much different from the other methods discussed above. In self-assembly, vascular growth is not guided by structures [2]. Endothelial cells are simply seeded inside of a hydrogel matrix and allowed to grow themselves [2]. This is controlled only by growth factors and signals, and the vasculature grown using this method is the most physiologically similar to native tissue [2]. Coculturing different cell types can mimic several different physiological environments[2]. It is, however, very difficult to work with due to the necessity for extreme control of the experiment at all times. It has, however, been successful *in vitro*. The George lab at UC Irvine has proven the viability of this method by seeding human umbilical vein endothelial cells (HUVECs) onto microbeads and embedded them into a fibrin gel matrix. Assisted by signaling from media and a monolayer of dermal fibroblasts, the HUVECs sprouted capillary networks[11]. This experiment was done to facilitate the creation of a complex, prevascularized, anastomosing capillary network, as well as to observe the diffusion of oxygen through thick hydrogel layers [11].

Each of the methods discussed above provide different benefits and vascular environments for a wide range of research applications.

2.4.2: Applications of Vascular Microfluidics

Currently, there are only very limited *in vivo* applications of the vascular microfluidic techniques discussed above. The field is more focused on *in vitro* studies to increase understanding of various

diseases, both vascular based and cancer, how various drugs interact with vasculature, and the development of organ on a chip technology [2]. The advent of vascular microfluidics has made each of these areas of interest easier to study *in vitro* and allowed for greater understanding.

Engineered vascular networks are especially useful for the study of endothelial dysfunction, or malfunctions in the vascular wall [2]. It allows the observation of underlying principles of this endothelial dysfunction to gain a better understanding of its causes without the need to induce disease within an animal model. *In vitro* study of endothelial inflammation has given scientists and engineers a model for how vascular dysfunction impacts blood flow, and how that change in flow impacts the permeability and thrombotic factors of the endothelium [2]. Findings from the use of vascular microfluidics include the process by which atherosclerotic lesions and thrombus formation occur at points of endothelial inflammation [2]. By making a viable model for endothelial dysfunction *in vitro*, it has allowed for a deeper understanding of dangerous vascular diseases without the complications and ethical concerns involved in the use of *in vivo* animal models.

When a tumor forms, the blood vessels in the surrounding environment go through a series of changes, altering the surrounding microenvironments, and connecting to the tumor, simultaneously feeding it and promoting metastasis [2]. Before the advent of vascular microfluidic models, it was very difficult to study tumor angiogenesis *in vitro* [2]. Now, it is commonplace to observe and measure this process by coculturing tumor cells with endothelial cells within a microfluidic network. This is especially useful because it allows for the observations of how processes change in different microenvironments, in reaction to various signals in differing concentrations, and the process of proliferation [2]. Having vascular microfluidic devices has allowed for a much deeper understanding of cancer metastasis and allowed for all of this to happen in small scale environments, which again reduce the need for animal models.

As discussed, vascular microfluidic models provide a platform to study diseases. One of the greatest benefits of these models is that they can also be used as drug screening models. The vasculature contained within a microfluidic device can be exposed to a large number of drugs at a high throughput all within a small, contained environment, and the behavior of the cells can be observed in real time [2]. Because the vasculature in this environment is contained, and many can be manufactured at one time, it is possible to measure different doses and treatment times of a variety of drugs at once [2]. This is especially popular for anti-cancer compounds where dosage and exposure time needs to be precise to prevent unintended toxicity. Microfluidic drug screening also allows observation of the efficacy of different drug delivery methods [2]. The ability to simulate healthy and diseased vasculature *in vitro* with microfluidic networks has made drug screening, while still difficult, a much more streamlined process.

All of the above applications combine into one in the form of organs on a chip. The vascular microenvironments of different organs and tissues, including bone, kidneys, arterial tissue, lung tissue, skin, cardiac tissue, liver tissue, skin, the blood brain barrier, and the lymphatic system, can all be mimicked through very careful control of the microfluidic channels and the coculture of various cell types [2]. This is a very difficult and precise process, but it is possible to make systems biologically similar enough to all of these physiological environments to be able to study diseases, tumor metastasis, and test drugs within each of the specific environments to observe biological reactions within different microenvironments [2].

The multiple and varied applications of *in vitro* vascular modeling have been vital to establishing our understanding of vascular disease and how to treat it, and it has proven an accurate model for several organ systems. Unfortunately, however, despite all of its benefits, microfluidic vascular models have several limitations.

2.4.3: Limitations of Microfluidic Vascular Models

As previously mentioned, microfluidic vascular models are almost exclusively used *in vitro*. This is primarily because of the materials most commonly used to make the devices. PDMS is an extremely useful material due to its optical clarity, ease of use, and ability to pick up patterns on the nanometer scale using soft lithography, and, as previously mentioned, it is the gold standard for nearly all microfluidics research [2]. It is not, however, a particularly useful biological material. PDMS cures at high temperatures during manufacturing, which prevents the combination of PDMS with any biological factors [24]. It is also not particularly conducive to either cell infiltration or attachment, meaning that bioactivity of PDMS is very limited without surface treatment [24]. PDMS is also not degradable *in vivo*, meaning that it is not an ideal material for remodeling or for *in vivo* implants [24].

Some of the microfluidics methods mentioned in Section 2.4.1: Microfluidic Techniques for the Creation of Vascular Models above discuss the possibility of using non-PDMS materials, such as natural biomaterial hydrogels. Microfluidic devices with bases of gelatin, agarose, collagen, and other ECM proteins have all been developed and tested, and see much better biofunctionality than PDMS [24]. These hydrogels, however, tend to be much more difficult to work with. The lack of mechanical stiffness and strength means that only very simple vasculature can be developed within these matrices [24].

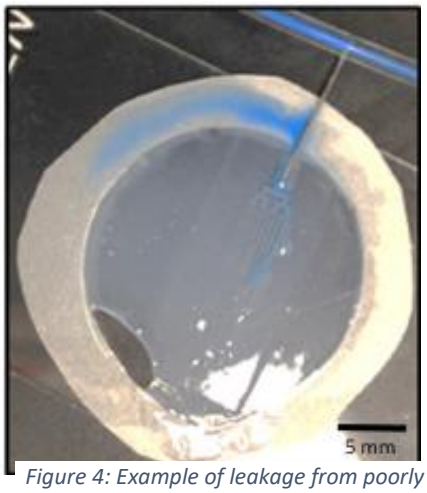

Figure 4: Example of leakage from poorly bonded hydrogel layers. Taken from Borenstein et al. [7]

Another limitation observed with the use of hydrogels as a microfluidic matrix is the prevalence of leakage between layers. Traditional plasma bonding is not possible with these materials, so methods such as enzymatic reactions, biomaterial based glues, chemical and UV crosslinking, and differential casting have been used to seal layers with varying levels of success [6, 24]. Poorly bonded layers in microfluidics, especially vascular microfluidics, compromise the integrity of the perfusion, and can cause device failure, such as in

Figure 4. Overall, the field of vascular microfluidics is rapidly developing, and has seen great success in many applications. While it is not capable of widespread *in vivo* implantations yet, it has proven an incredibly valuable tool for the study of physiologically similar vasculature *in vitro*.

2.5: Project Materials

This section includes a brief discussion of the two materials most prevalently used in this thesis: fibrin and gelatin.

2.5.1: Fibrin

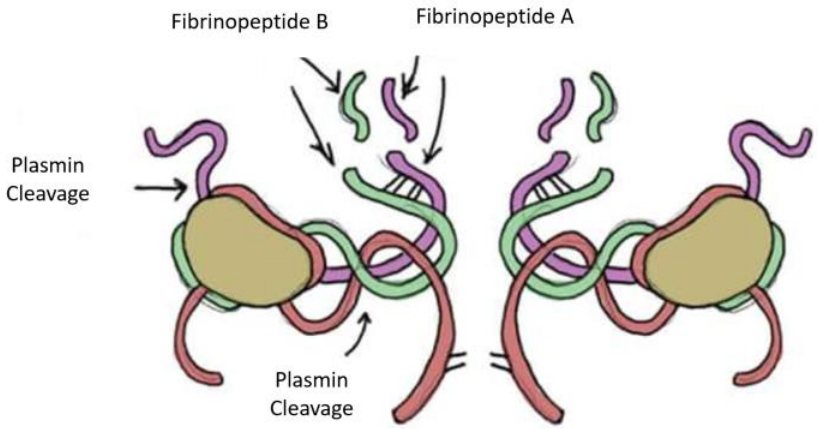

Figure 5: Structure of fibrin. Adapted from Sigma Aldrich by Hugh Long

Fibrin, the structure of which is shown in Figure 5 is a natural biopolymer created by thrombin cleaving fibrinopeptides A and B from fibrinogen, creating the matrix which makes up the bulk of blood clots [31]. Fibrin is a popular biomaterial in regenerative medicine. This is primarily because of fibrin's considerable remodeling potential and ability to improve the survival rate of implanted cells [32]. Fibrin implanted directly into wounds has shown significant promise for improved regeneration and healing. Grafts implanted into venous tissue have consistently showed considerable ingrowth of elastin and remained patent at 12 weeks, and fibrin injected into ischemic cardiac tissue has reduced the expansion

of infarcted tissue [5, 32]. Additionally, part of what makes fibrin especially attractive for vascular engineering is the fact that it induces neovascularization [32]. All of this has been successful despite fibrin's generally poor mechanical properties [5]. These mechanical properties, however, are highly tunable.

Besides its natural regenerative and cell adhesive properties, another attractive property of fibrin is that it is highly tunable, both in mechanical and degradation properties [32]. The mechanical properties of fibrin are primarily controlled by the concentration of fibrinogen and thrombin, and modulating these factors have shown significant impact on the mechanical properties of the fibrin microstructure [33]. While this change in stiffness can greatly improve the mechanical properties for specific applications, it has also been shown to have impacts on adherent cell morphology, protein expression, and migration [33]. Despite this, successful modulation of fibrin porosity, stiffness, viscosity, and tensile strength has allowed the development of several successful products, including tissue sealants, growth factor and drug delivery vehicles, and cell seeded implants [33].

While the concentration of fibrinogen and thrombin are used to alter the mechanical properties of fibrin, degradation properties are more commonly adjusted with the addition of aprotinin, a protease inhibitor which slows fibrinolysis [32]. The addition of aprotinin also increases the infiltration of capillaries and reduces the fibrous encapsulation of implanted fibrin [32]. While aprotinin is used to slow fibrin degradation, it isn't possible to stop this process entirely. The degradation products of fibrin are not only nontoxic, but also stimulate the migration of neutrophils and monocytes to the site of fibrin implantation, and signals for the neutrophils to commence phagocytosis at the wound site, thus further promoting healing [32], [34].

Overall, fibrin is an attractive material to be using for the purposes of regenerative tissue modeling due to its cell adhesive and regenerative properties, and viable for microfluidic experiments due to its highly tunable mechanical properties and architecture.

2.5.2: Gelatin

Gelatin was chosen for this project primarily because of its utility as a sacrificial material. A 10% weight volume solution of gelatin has multiple properties that make it highly desirable for this application [24]. Once a gelatin structure is made, it is highly resistant to deformation, and is able to preserve the patency of the formed channels, even if considerable pressure, up to 80 cm H_2O, is applied [29]. The material is strong enough to be made as narrow as 6µm without compromising shape or structure [29]. Gelatin also has a melting point below 35°C, which is well below the melting point of most materials used in hydrogel based microfluidics, allowing it to fully melt within the bulk gel [24, 29]. While these properties are all favorable for the use of gelatin, there are some drawbacks to consider. If gelatin is removed from a mold while not completely dry, or is rehydrated from a dried state, it tends to swell slightly, and not in an entirely uniform manner. This means that the channels created by gelatin sacrificial structures, while highly similar to each other, are unlikely to be identical [24, 29]. That being said, gelatin's positive characteristics still make it highly favorable for use in sacrificial structures.

2.6: Summary

To summarize this background, while a great deal has been done to combat the difficulties of vascularization in full thickness engineered tissue constructs, there has been no ideal method developed that combines the reliability of synthetic materials with the biofunctionality of natural hydrogels. While microfluidic models have shown great promise *in vitro*, current cell-, synthetic-, and natural-material-based vascular engineering have yet to produce a reliable and functional method of perfusion. Overall, there is a need for an engineered vascular device that will be capable of creating reliable channel geometries while maintaining a functional cell population without being rejected by the body..

To address this need, I propose a unique single layered fibrin vascular device which will be of a physiologically relevant arterial size, and capable of physiologically relevant flow and diffusion. This device will also have the capability to supply a cell population on the surface by diffusion from the

encapsulated channels. This will be done using a robust fibrin gel and a gelatin based sacrificial structure to create a seamless device to minimize the problem of leakage seen with other similar devices.

Chapter 3: Goal and Objectives

In order to ensure cell viability within large scale, tissue engineered constructs for long term applications, there is a need for a method of perfusing constructs with blood or media. Due to the developmental and technical nature of this project, this thesis was defined by a goal and a series of objectives rather than a hypothesis and aims. **The goal of this project was to develop a novel method for the fabrication of a single layered fibrin based vascular network that was able to reliably produce channels, had flow properties that were physiologically relevant, and had a diffusion rate that was capable of sustaining a viable cell population on the surface. If successful, this project would result in a unique platform technology for advancement in engineered scaffolds, *in vitro* fabricated tissues, and *in vitro* drug testing.**

The three objectives outlined in detail below were directed at the characterization of microfluidic channels within the fibrin device, establishing flow and diffusive properties of the channels and fibrin gel, as well as establishing the ability to maintain a cell population on the surface of the device.

Objective 1: Develop a novel technique for creating a consistently sized vascular network within a fibrin gel matrix.

The approach for this objective involved using a sacrificial structure encapsulated in fibrin gel in order to produce a branched microfluidic device without bursting or leakage. The first set of experiments to achieve this objective focused on developing physiologically relevant sacrificial structures to mimic small arteries. Small arteries were chosen because this thesis was framed as a proof of concept designed to address problems seen in previous iterations of this project such as leakage and continuous perfusion [6, 35]. We decided that the best way to tackle the problems seen in previous iterations was to start with an easier to manufacture large scale structure capable of being scaled down in the future.

The next step was to create a method to consistently generate fluid flow through a block of fibrin using the sacrificial structure method. Once this was determined, characterization of channels began. This was done through imaging and measurement of the sacrificial structures. Finally, in order to measure channel height, devices were sectioned, imaged and measured using histology techniques. Averages and standard deviations were measured for each experiment and compared between the sacrificial structures and the produced networks.

While a significant amount of discussion has touched on the need for microvasculature, the goal of this project was not to mimic those sizes exactly, but instead to work with channels the size of small arteries for this proof of concept developmental study. To mimic small arteries, the goal of this study is to achieve a channel diameter between 0.1.4 and 2.0 mm [8, 9]. Success in this objective was defined as the ability to reliably produce and perfuse channels of consistent size without experiencing device leakage.

Objective 2: Determine flow properties of liquids passing through the channels and the rate of diffusion through the gel

The purpose of this objective was to prove that the channels produced within the first objective were comparable to physiological structures. The approach for this two-part objective focused on perfusing channels of the fibrin vascular device with different fluids. The first set of experiments was used to measure the flow properties within the channels. A suspension of microbeads was perfused through the channels and individual particles were tracked in order to determine volumetric flow rate, Reynolds number, and wall shear force. Flow within native vasculature is laminar and applies enough wall shear force to allow endothelial cells to function normally. Proving physiological values lends credibility to fibrin vascular devices being used as vascular models. The second set of experiments targeted diffusion rates of molecules through the fibrin vascular device. One of the major functions of

vasculature is to diffuse oxygen and nutrients to the surrounding tissue. Determination of the diffusive properties was done to show that fibrin vascular devices were capable of diffusion from the channels into the surrounding gel. This was done by measuring the grey value of a line through the gel over the course of several minutes to observe changes in brightness. This was done with multiple sizes of fluorescent particles. Success of this objective was defined as collecting clear and accurate values for a variety of flow and diffusive properties and having said values fall within physiologically relevant ranges.

Objective 3: Determine zones of cell uptake on top of the device and observe how these zones change over time

The final objective was approached by measuring cellular uptake zones on the surface of the fibrin vascular device. This was performed in order to prove that the fibrin vascular devices were capable of diffusing particles through the bulk of the gel to the surface at sufficient rate and volume to observe intake into live cells. The experiment done to fulfill this objective involved culturing cells onto gelatin coated cover slips and placing these on the surface of the fibrin vascular device perfusing live staining dye for several hours. Images were taken at two time points to observe changing zones of cell uptake. Success of this objective was defined as the ability to see fluorescent cells on the surface of the fibrin vascular device, and to see the area of fluorescence growing over time.

Chapter 4: Methods

This section provides a thorough description of the procedures used to achieve each specific goal of this project. The topics discussed include the manufacture of sacrificial structures, the alteration of fibrin gels, the development of fluid flow within a fluidic device, the characterization of the fluidic channels, measurements of flow properties including flow rate, Reynolds number, and wall shear stress, diffusivity calculations, and viable zone identification.

4.1: Sacrificial Structures

This subsection is focused on the process of developing the gelatin sacrificial structures used in the fabrication of the fibrin vascular devices. This process included the development of the computer model, mold fabrication, gelatin pouring protocol, and identifying the most effective lamination protocol.

4.1.1: Computer Modeling

To design a mold for the production of sacrificial structures, SOLIDWORKS computer modeling software was used to create a basic two channel mold with evenly sized channels, inlets, and a divider at 2 mm wide. An isometric view can be seen in Figure 6 . A full drawing of the mold can be found in Appendix 1: SOLIDWORKS Drawing of Acrylic Mold. These dimensions were chosen in order to make a structure that would produce a size similar to small arteries.

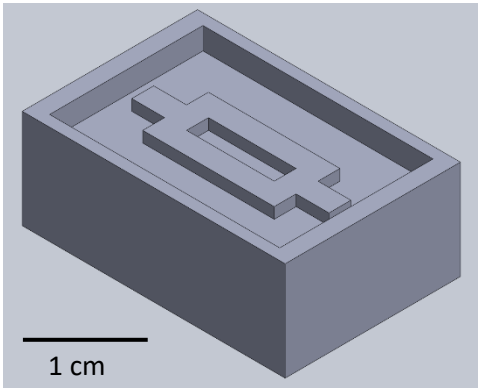

Figure 6: Isometric view of SOLIDWORKS model

4.1.2: Mold Fabrication

To convert the computer model to a usable mold, the SOLIDWORKS file was converted into an AutoCAD file. A Universal Laser Systems Versalaser VLS-4.60 laser cutter was used to cut several pieces

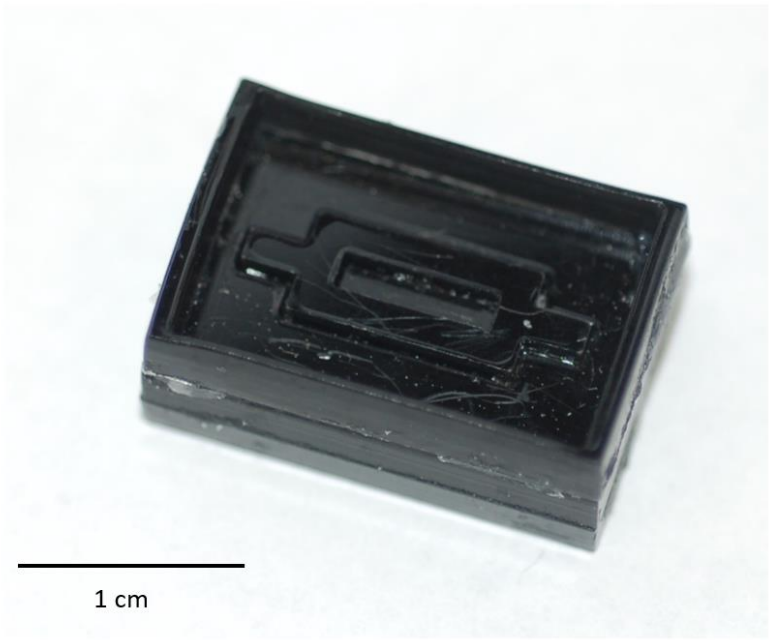

Figure 7: Laser cut acrylic mold

out of 3mm acrylic. These pieces included a flat rectangular base, a base with the channel shape cut out of it, the channel shape, and an 0.75mm thick wall. An additional channel shape was cut out of 1mm acrylic. These pieces were then layered together with acrylic glue to create a mold with a 1mm high raised channel shape (Figure 7).

The mold was treated with a coating of 1% pluronic F-127 for one hour, and then filled with a 10:1 elastomer to curing agent ratio of polydimethylsiloxane (PDMS) and allowed to cure overnight in a 37°C oven. The PDMS negative was then removed. These PDMS molds were rectangular with a precise imprint of the channel structure in the center. This process is known as soft lithography (Figure 8).

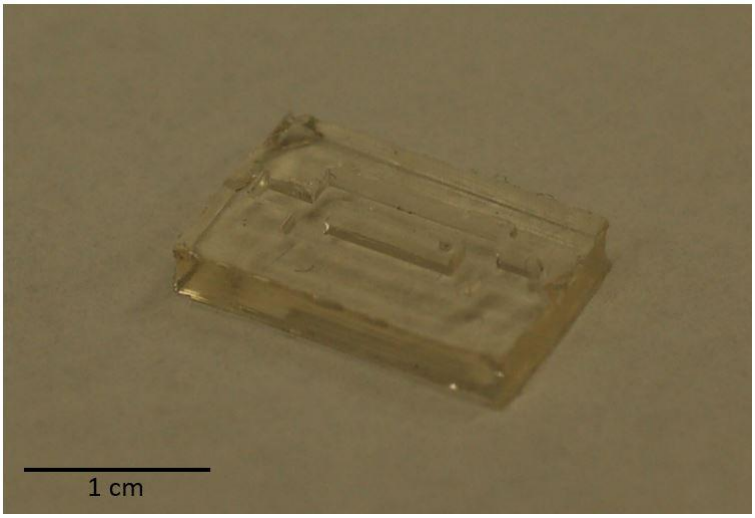

Figure 8: PDMS negative mold

4.1.3: Sacrificial Layer Creation

To make single layers of gelatin, the PDMS molds were coated with 1% pluronic F-127 (Sigma P2443) for one hour. Once removed, the channels were then filled with a solution of melted 10% gelatin (Sigma G2500) in 1X phosphate buffered saline (PBS). All 1X PBS was diluted from a 10X stock (OmniPur 6505) and brought to pH 7.4. Structures were allowed to dry overnight in the molds.

It was found that structures maintained their shape best when PDMS molds were coated once per 10 uses.

4.1.4: Lamination Techniques

In order to make a structure of physiologically relevant dimensions, two gelatin layers needed to be laminated together. A single dehydrated sacrificial layer was found to be too thin to structurally support itself and was not similar to physiologically relevant structures. Structure lamination was done to thicken the structure to make a shape more similar to *in vivo* vasculature. Four methods were attempted, as shown in Figure 9. A structure was considered hydrated if the gelatin had completely set, and still held most of its moisture but was set enough to remove from the PDMS mold to be stacked. Dehydrated layers were defined as layers that had been allowed to dry overnight. Partially rehydrated was defined as a dehydrated structure allowed to soak in 1X PBS until it was soft enough to be malleable, but not so soft that it lost its shape. This process was controlled by initially soaking structures for five seconds, removing from PBS to observe pliability, and continuing to soak in two second intervals until desired point was reached. The gelatin glue used was melted 10% gelatin that had not yet been allowed to set. Lamination strategy A was performed by removing two hydrated structures from their molds and laying one on top of the other with no additional adhesive. Strategy B was also fabricated from two hydrated structure, but 0.05 mL of gelatin glue was spread over the full surface of the bottom structure using a syringe and a 20-gauge needle before the other structure

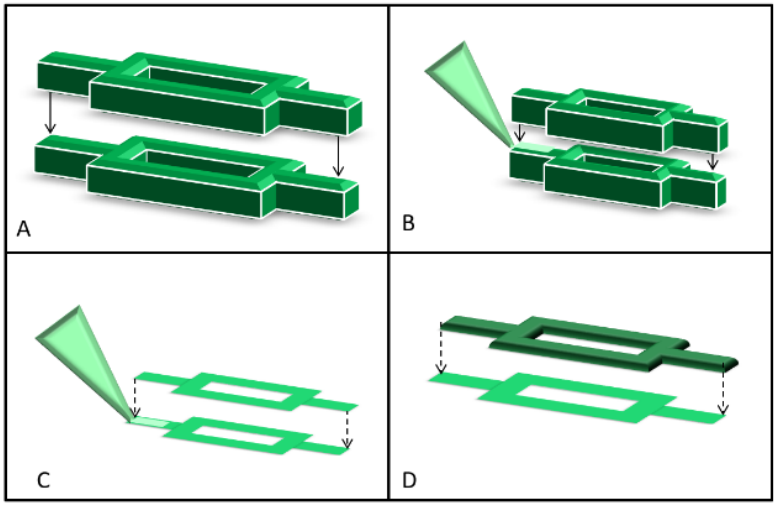

Figure 9: Lamination strategies. (A) Two stacked hydrated layers (B) Two hydrated layers with gelatin glue (c) Two dehydrated layers with gelatin glue (D) One dehydrated layer and one layer partially rehydrated in 1X PBS

was placed on top. Lamination strategy C was performed very similarly to strategy B, but structures were allowed to dehydrate overnight before lamination. Finally, lamination strategy D involved partially rehydrating one gelatin layer and placing it on top of a dehydrated gelatin layer and allowed to dry again.

4.1.5: Final Structure Fabrication

To make gelatin sacrificial structures, we developed the process shown below in Figure 10.The PDMS negative was filled with pluronic F-127 for one hour, which was then removed and replaced with 10% gelatin. The gelatin was allowed to dry overnight on the bench top and was then removed from the mold. Two structures were laminated together and dehydrated again on the benchtop. Any poorly

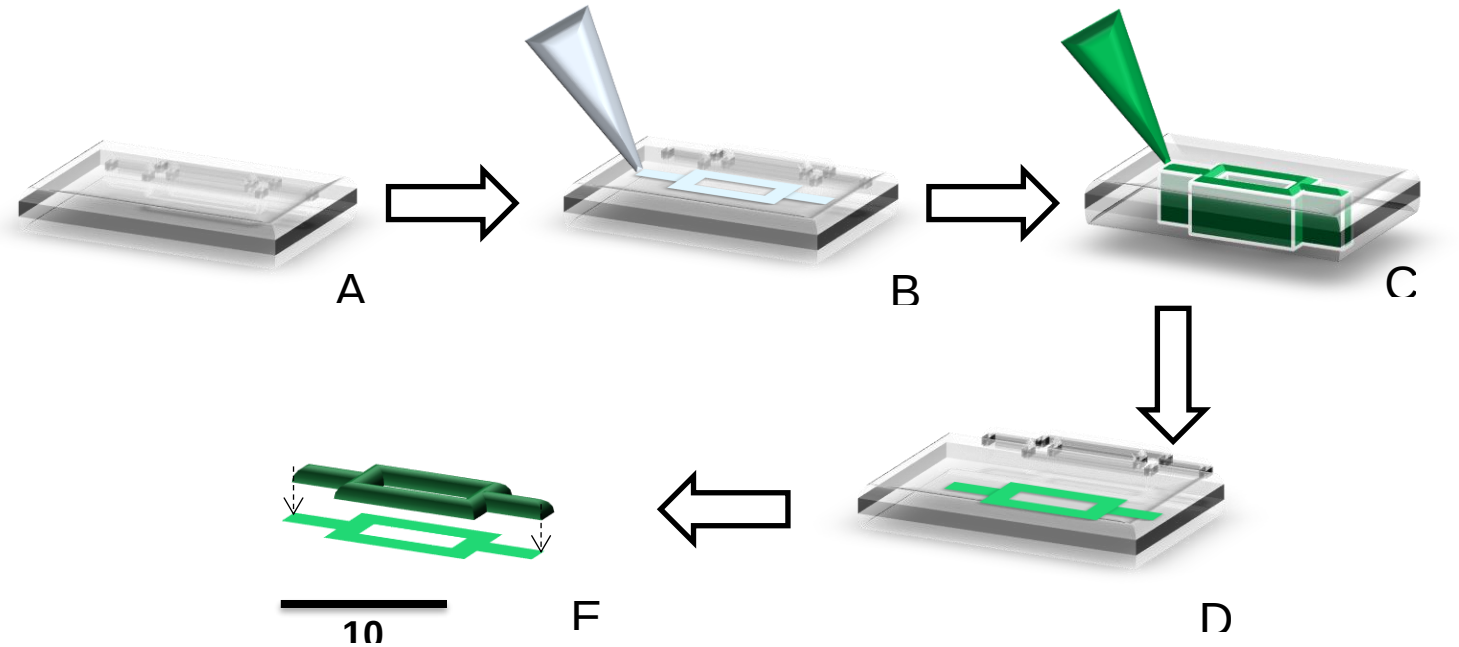

Figure 10: Fabrication of a sacrificial layer (A) PDMS mold (B) Pluronic F-127 coating (C) Filling with 10% gelatin (D) Dehydrating structure overnight (E) Laminating two layers together

shaped sacrificial structures were partially rehydrated and left to dehydrate again under a thin piece of PDMS. All dehydrated structures were stored at room temperature.

4.2: Fibrin Fluidic Devices

The first part of Objective 1 was to fabricate and perfuse a fibrin based vascular device. This section details how this was done. The three subsections discuss the formulation of a robust fibrin gel, the building of a vascular device, and finally how fluid flow was initiated.

4.2.1: Fibrin Gel

To ensure the structural integrity of the fibrin vascular channels, we altered the formulation of our fibrin gel to better maintain its shape. Increased fibrinogen and thrombin concentrations have independently been shown to increase gel stiffness [33]. Several gel formulations were tested, shown in Table 1: Fibrin Hydrogel Formulations below. Batches of each formulation were poured onto 1% pluronic F-127 treated PDMS and a vellum frame to see how well they maintained shape and structure once removed.

Table 1: Fibrin Hydrogel Formulations

Component	Formulation A	Formulation A2	Formulation B	Formulation C	Formulation D
Bovine Fibrinogen (MP 0882021/ Sigma F8630)	670 µL of 9.65 mg/mL solution in HBS	670 µL of 9.65 mg/mL solution in HBS	290 µL of 11 mg/mL solution in HBS	290 µL of 70 mg/mL stock	500µL of 70 mg/mL stock
Thrombin (Sigma Aldrich 9002-04-4)	100 µL of 2.35 units/mL solution in HBS	100 µL of 4.7 units/mL solution in HBS	40 µL of 40 units/mL stock	40 µL of 40 units/mL stock	150µL of 40 units/mL stock
$CaCl_2$ (EM Science CX0130-1)	80µL of 40 Mmolar stock	80µL of 40 Mmolar stock	N/A	N/A	60µL of 40 Mmolar stock
1x PBS	150µL	150µL	N/A	N/A	112µL
DMEM (Gibco 11960-044)	N/A	N/A	670µL	670µL	N/A

4.2.2: Fibrin Fluidic Devices

To provide a final platform for future experiments, we created fibrin vascular devices with the most favorable fibrin gel formulation. This multistep process began with the creation of a PDMS well. This well is a standard 10:1 PDMS elastomer to curing agent ratio poured into a 1% pluronic treated 3.5cm petri dish over a 2cm x 1.5cm x 0.3cm block of acrylic and allowed to cure at 37°C overnight. The next three steps, outlined in Figure 11 , involved piercing the edges of a sacrificial structure with two 27-gauge needles, encasing the structure in fibrin gel, and allowing it to polymerize on the bench top for 30 minutes.

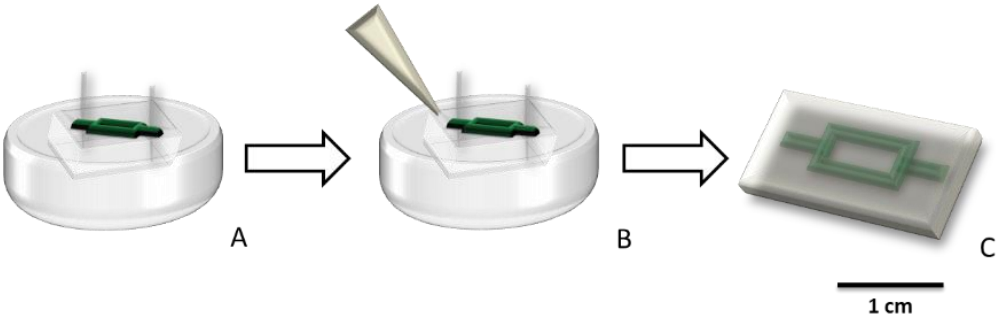

Figure 11: The fabrication of a fibrin vascular device. (A) The pierced sacrificial structure suspended in a PDMS well (B) 70 mg/mL fibrin was poured over the sacrificial structure. Any resulting bubbles were removed (C) Fibrin polymerizes around the structure

4.2.3: Fluid Flow Initiation and Continuous Perfusion

To create channels within the device, the sacrificial structure was melted and removed. After the fibrin gel polymerized around the gelatin sacrificial structure, the block was removed from the PDMS well and moved into a petri dish with 3 mL of 1X PBS. The petri dish was left in a 37°C incubator for at least 30 minutes. During this time, the gelatin structure hydrated and melted within the fibrin block. As shown in Figure 12, the melted gelatin could then be removed. The

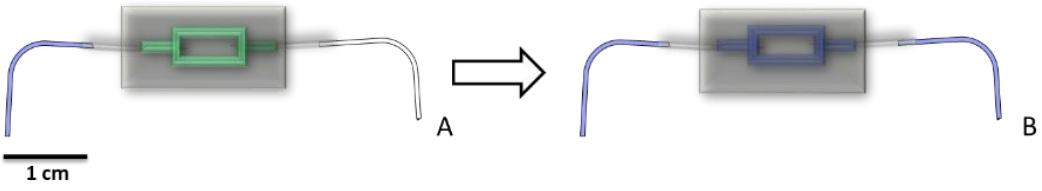

Figure 12: The removal of a gelatin sacrificial structure from within a block of fibrin gel. (a) Incubated vascular device with intact gelatin structure (b) Fluid pushed through fibrin vascular device, removing gelatin structure

sides of the device were pierced with a 20-gauge needle, and the gelatin was flushed out with 1mL of the warm PBS, in which the device had been incubated.

Once the gelatin had been removed, continuous perfusion was achieved with a syringe pump (Cole-Parmer 74902-00). A syringe filled with the desired liquid was tipped with custom microfluidic tubing. The polyethylene tubing was 16cm long with an inner diameter of 0.86mm (Intramedic 427421), with a flat-tipped 20g needle inserted 0.75cm into one end, and the removed tip of a second flat-tipped 20g needle cut to 1.25cm inserted into the other end. One of these pieces of tipped tubing was attached to the syringe in the syringe pump. A second piece of this custom tubing was attached to a syringe full of diH_2O. This was used to make drop-to-drop contact with the liquid within the channels of the fibrin vascular device in order to maintain a fluid gradient without bubbles. Once this was connected, the syringe pump was started and allowed to flow at 0.75 mL/ hour until a drop appears at the end of the tubing. This was then inserted into the other end of the fibrin device. The syringe not attached to the syringe pump was then removed and the tubing was allowed to flow into a waste container.

4.3: Channel Characterization

The second major part of Objective 1 was to verify the fidelity of the sacrificial structures, as well as to establish channel geometry. This subsection looks at how the structures were characterized morphologically along the x- and y-axes, as well as in the cross-sectional area. It also details the histology performed to measure the resultant channels. Finally, it covers what statistical analysis was performed to compare the structures and the channels.

4.3.1: Sacrificial Structure Characterization

To determine the average size of the gelatin sacrificial structures, photographs of 20 sacrificial structures were taken next to a ruler used as a scale bar. Structures were then measured using the imaging software ImageJ along several points, shown in Figure 13 to the right. Measurements were averaged across the samples with standard deviations.

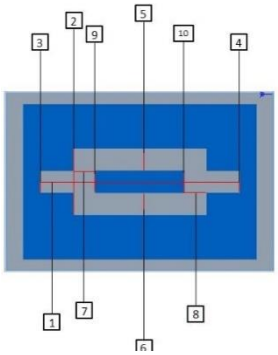

Figure 13: Measured points of a sacrificial structure. (1) end to end (2) width (3,4) inlet and outlet width (5,6) channel width (7,8) crossbar width (9,10) divider width

4.3.2: Sacrificial Structure Cross-Sections

To measure the sacrificial structure cross sections, a PDMS disc was made in a 3.5cm petri dish and cured overnight. The disc was removed and a shallow cut was made in the center of the disc. Sacrificial structures were snapped in half until there were seven intact samples. Samples were mounted within the PDMS disc, and the ends of each channel and inlet were photographed on a AmScope FMA050 stereoscope with a Basler acA1920-50gc camera (Figure 14). A calibrated scale bar image was taken at the same magnification. Images were scaled according to the calibrated scale bar, and the height, width, and area were each measured using ImageJ. Calculations were made to exclude outliers, and means and standard deviations were calculated for each measurement ($n = 21$).

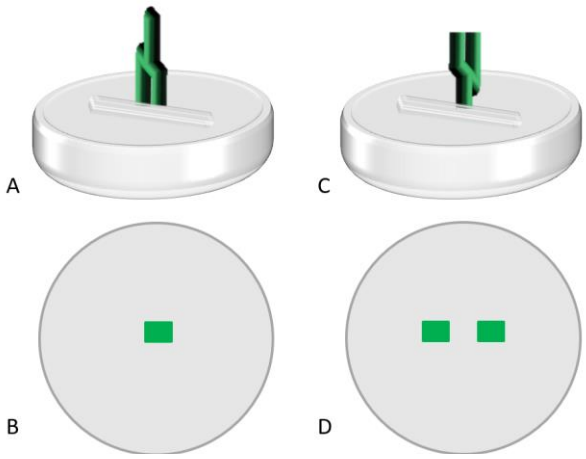

Figure 14: Cross sectional imaging of sacrificial structures. (A) Side view and (B) top view of structure inlet or outlet. (C) Side view and (D) top view of structure channels.

In ImageJ, measurements were taken from corner to corner on all four sides (Figure 15). The sacrificial structures were not necessarily even throughout each cross section. For this reason, both height measurements and both width measurements were taken and averaged for each observed structure to reach a measured value. Quartile calculations were performed to remove all outliers from height and width measurements. Due to the non-uniform rectangular shape, area measurements were calculated both by multiplying height and width, as well as by tracing the outer edge of the sacrificial channel

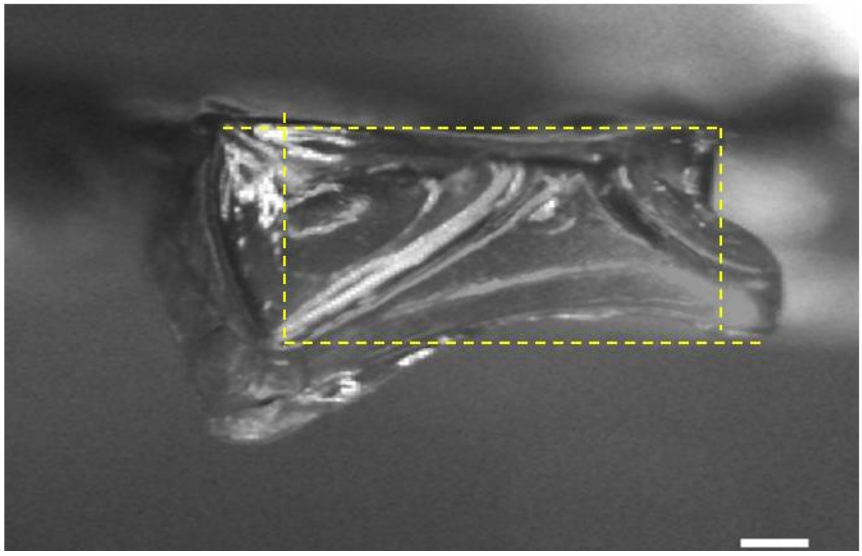

Figure 15: Representative image of sacrificial structure cross section with lines of measurement

4.3.3: Histology

This experiment was performed to measure the dimensions of the channels resulting from the removal of the gelatin sacrificial structures. Fibrin vascular devices were perfused to remove the sacrificial structures and were then fixed in 10% neutral buffered formalin (NBF) for one hour. The devices were then rinsed in PBS three times for five minutes each. All NBF and PBS used in the rinses were disposed of in a hazardous waste bottle. The samples were then cut into quarters along the long edge and each quarter was placed into a nylon tissue specimen bag (Thermo Scientific 6774012). The specimen bags were folded gently and placed into plastic tissue cassettes. The cassettes were loaded into a Tissue-Tek VIP® 6 AI tissue processing machine on a "Short No Fix" cycle, detailed in Table 2 below. Samples were removed the next morning and embedded on a Leica EQ 1160 embedding table.

Table 2: Short No Fix Cycle

Step	Bath	Time	Step	Bath	Time
1	70% Ethanol	30 minutes	7	100% Ethanol	20 minutes
2	80% Ethanol	30 minutes	8	Xylene	30 minutes
3	95% Ethanol	20 minutes	9	Xylene	20 minutes
4	95% Ethanol	20 minutes	10	Xylene	20 minutes
5	100% Ethanol	20 minutes	11	Paraffin	30 minutes
6	100% Ethanol	20 minutes	12	Paraffin	30 minutes

Table 3: Eosin Staining

Step	Bath	Time	Step	Bath	Time
1	Eosin	1 minute	5	100% Ethanol	1 minute
2	95% Ethanol	1 minute	6	Xylene	2 minutes
3	95% Ethanol	1 minute	7	Xylene	2 minutes
4	100% Ethanol	2 minutes	8	Xylene	2 minutes

Blocks were then sectioned on a Leica RM2235 microtome at 8µm. These sections were placed in a warm water bath and collected onto charged slides (VWR 48311-703). Slides were deparaffinated by constant movement in two five-minute xylene washes, followed by two three-minute 100% ethanol washes. The slides were dried thoroughly between each wash. The slides were then stained with alcoholic eosin with phloxine (Sigma HT110332) according to the bath and time information in Table 3 above. The sections were then covered with cover slips using Cytoseal 60 cover slipping medium (Thermo Scientific 8310-4). Ten slides were made of each well-formed channel.

Slides were observed and photographed at 5X-magnification on a Leica DMIL LED inverted microscope with an Image source DFK 41BU02 camera. A calibrated scale bar image was also taken at this time. Images were scaled according to this scale bar and analyzed using ImageJ. The length and

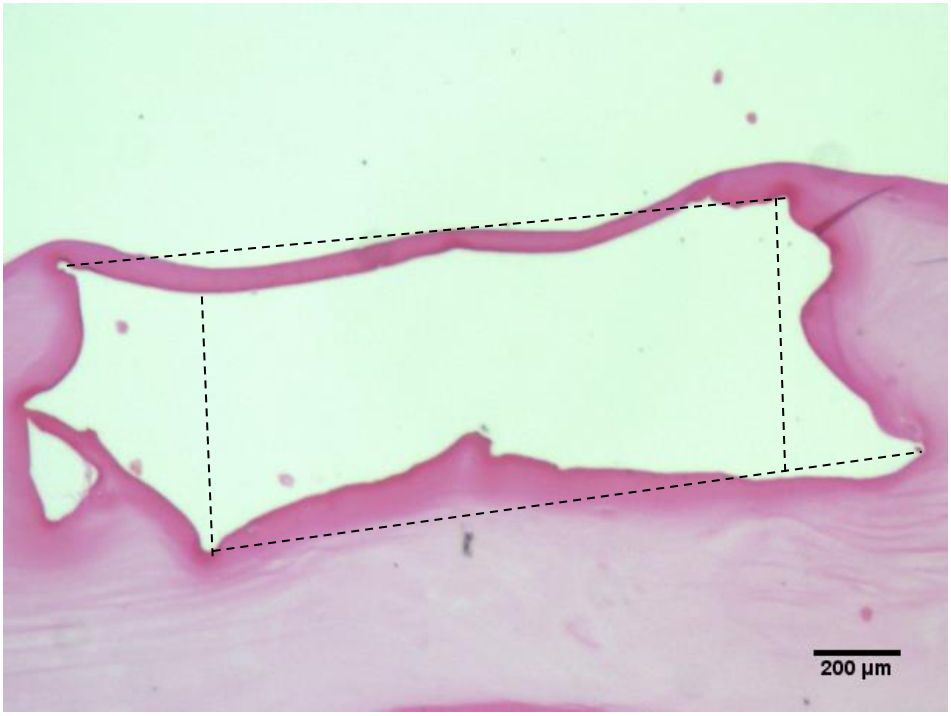

Figure 16: Histological section of fibrin vascular device with lines of measurement

width were measured according to the clearest visible corners (Figure 16), and the area was taken both by measuring around the outside of the channels, and by multiplying the measured length and width. The ten slides were averaged, and the standard deviation was found for the seven channel samples.

4.3.4: Statistical Analysis

To compare channel size to the size of the cross-section of the sacrificial structure, a student's t-test was run using the means and standard deviations of the lengths and widths of the samples. Statistical significance was defined as a P value of $P < 0.05$.

4.4: Flow and Diffusion Properties

This subsection focuses on the second objective. This involved calculating flow properties, including flow rate, Reynolds number, and wall shear force. Physiological blood flow in small arteries

have a mean flow rate of 3.5 mm^3/s, but can be as low as 0.04 mm^2 /s ,and exhibit laminar flow, so our system targets properties in this range [32]. This section also covers quantification of the diffusivity of macromolecules through the fibrin vascular device.

4.4.1: Microbead Flow Analysis

To determine flow properties within the fibrin channels, three fibrin vascular devices were perfused at 0.75 mL/hour by a Cole-Parmer single syringe infusion pump with 1X PBS and with a suspension of 6µm polystyrene beads (Polysciences Inc. 15714). The tubing connecting the 1 mL syringe to the fibrin vascular device was 16cm long with an inner diameter of 0.86mm (Intramedic 427421), with a flat-tipped 20g needle inserted 0.75cm into one end, and the removed tip of a second flat-tipped 20g needle cut to 1.25cm inserted into the other end. Waste tubing was identical and led from the outlet of the fibrin vascular device to a 100 mL beaker full of diH_20. The 6 µm bead size was chosen to mimic the size of neutrophils, which travel through vasculature. Six 15-second-long videos were recorded on a Nikon SMZu stereoscope at 20X with a Spot INSIGHT CMOS camera. Videos were taken as a series of time lapse images captured at an average of 6 frames per second. A calibrated scale bar image was taken at the same magnification, and all videos were scaled accordingly.

ImageJ was then used to track the distance traveled by ten particles in each video. These distances were recorded and averaged per video, as well as overall.

4.4.2: Determining Parabolic Flow

In this section, the parabolic nature of the flow within the fibrin vascular devices was measured to determine if the flow patterns within the fibrin vascular channels mirrored the parabolic properties of native tissue.

To calculate parabolic flow, the average width of each individual microfluidic channel was measured and split into six even regions (Figure 17). The measured particles were put into regions based on their distance from the top of the channel. The average velocity of particles in the top three regions was calculated over the 15 second video, and particles in each region were averaged.

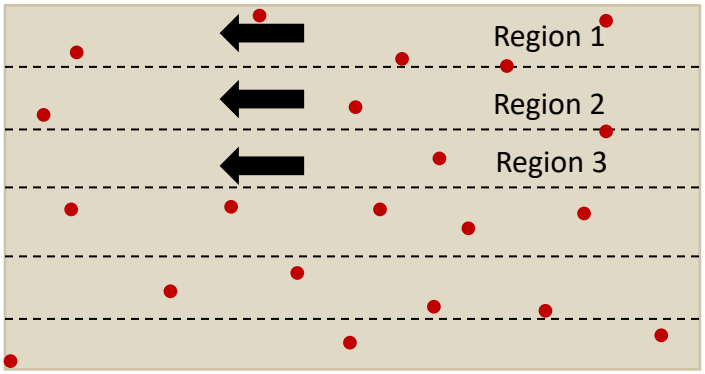

Figure 17: Regions of Analysis for Parabolic Flow

4.4.3: Flow Property Calculations

Three different calculations were performed to determine the flow properties within the fibrin vascular device. The first calculation run was to determine the volumetric flow rate, using Equation 1 below, where Q is volumetric flow rate, v is mean flow velocity, and A is channel area. For this equation, we assumed the area was the mean channel area determined in the first objective.

Equation 1: Volumetric Flow Rate

$$Q = v \cdot A \tag{1}$$

The next calculation done was a Reynolds Number calculation to determine the turbulence of the flow. The equation can be seen below in Equation 2 Equation 2, where ρ is density of the fluid, 1000 kg/m^2, v is the velocity of the fluid, L is the length of the channel, and μ is the viscosity of the fluid, 1.0 N.s/m. Any *Re* value under 2300 is considered laminar flow. For this equation, we need to assume that density and fluid viscosity are constant.

Equation 2: Reynolds Number

$$Re = \frac{\rho \cdot v \cdot L}{\mu} \tag{2}$$

The last calculation made was wall shear stress, shown in 3Equation 3. For this equation, we assume a no slip boundary condition, and that we have laminar flow.

Equation 3: Wall Shear Stress

$$\tau = \mu \frac{du}{dy} \tag{3}$$

Which can be derived to Equation 4 Equation 4, where τ is wall shear stress, μ is the viscosity of the fluid, *umax* is the maximum speed, *y* is the distance from the location at which the fluid moves at maximum speed and the wall, and *h* is the height of the channel.

Equation 4:Wall Shear Stress Derivation

$$\tau = \frac{-8 \cdot \mu \cdot umax \cdot y}{h^2} \tag{4}$$

The particle speed tracked in this experiment gives us an average value rather than an absolute maximum. In order to account for this, I used the average function value, Equation 5 , to solve for my velocity in the center of the channel, where, due to laminar parabolic flow, we assume flow was the fastest. In this equation, a is -h/2, b is h/2, where h is the channel width.

Equation 5: Average Function Value

$$f_{avg} = \frac{1}{b-a}\int_a^b f(x)dx \tag{5}$$

The equation in relation to particle speed is shown below in Equation 6where u is particle speed, h is channel width, and y is distance from the center of the channel.

Equation 6: Average Function Value in Reference to Particle Speed

$$u_{avg} = \frac{1}{\frac{h}{2} - \frac{-h}{2}}\int_{\frac{-h}{2}}^{\frac{h}{2}} u_{center}\left(1 - \frac{4y^2}{h^2}\right)dy \tag{6}$$

By solving this integration (the steps of which can be seen in Appendix 2: Maximum Particle Speed Formula Integration) we arrive at Equation 7 Equation 7 [36].

Equation 7: Particle Maximum Speed

$$u_{center} = \frac{3}{2} u_{avg} \quad (7)$$

4.4.4: FITC-Dextran Diffusion

Diffusivity of the fibrin vascular devices was measured by perfusing devices with different molecular weights of fluorescein isothiocyanate-dextran (FITC-dextran). Two molecular weights, 40 kDa (SigmaFD40S) and 250 kDa (Sigma FD250S), were used to see a difference in diffusion rates between macromolecules of different sizes. While a direct comparison cannot be made due to molecular shape, the 40 kDa dextran was meant to represent small proteins and molecules, such as albumin, and the 250 kDa dextran was meant to mimic larger molecules, like globulins. Perfusion was set up identically with a flow rate of 0.75 mL/hour by a Cole-Parmer single syringe infusion pump. The tubing connecting the 1 mL syringe to the fibrin vascular device was 16cm long with an inner diameter of 0.86mm (Intramedic 427421), with a flat-tipped 20g needle inserted 0.75cm into one end, and the removed tip of a second flat-tipped 20g needle cut to 1.25cm inserted into the other end. Waste tubing was identical and led from the outlet of the fibrin vascular device to a 100 mL beaker full of diH_20. Fluorescent time lapse videos were recorded for 18 minutes with a Spot INSIGHT CMOS camera on a Nikon Eclipse E600 upright microscope at 2X-magnification. Images were taken once every 30 seconds. Three fibrin vascular devices were perfused with each molecular weight. Videos were calibrated using the SPOT software (SPOT54B).

The videos were moved to ImageJ for analysis. They were calibrated within the SPOT software and appropriate scale bars were added. Images where the channel was changing position or perfusion was not yet complete were removed from the stacks. The videos were normalized by measuring the average brightness in two 50x50 pixel squares 500µm on either side of the channel edges at the center point of the video. The average of the two means was rounded to the nearest whole number and the minimum brightness of the videos was adjusted accordingly. To measure diffusion on each video, three

lines were drawn across the channels, covering the full width of the channel and 500µm on either side. The brightness profile was taken for each image in the stacks and recorded. These values were then graphed. If any section of the graph hit the saturation point, the dataset was excluded.

4.4.5: Intensity Curves and Diffusivity Calculations

Intensity curves were graphed to observe the changing fluorescent intensity at the channel edge, and at 0.01 cm increments away from the edge. The intensity ratio, calculated as the left-hand side of Equation 8 below, at each time was plotted in relation to these distances to observe how the passing time impacts the concentration at each point.

Diffusivity was calculated using Equation 8 below, derived from Fick's law of diffusion. Here, C_A is defined as the measured brightness at a certain point, C_{A0} is the brightness at time zero, C_{AS} is the mean brightness of the surface of the channel, *erf* is the error function, *x* is the distance from the channel surface, D_{AB} is the diffusivity, and *t* is time. Assumptions and boundary conditions for the use of this equation include that the channel intensity is consistent, we assume that the other boundary has a value of zero, flow is constant, and because we never reach out outer boundary, we can assume that it is an infinite system for the sake of these calculations.

Equation 8: Diffusivity Equation (8)

$$\frac{C_A - C_{A0}}{C_{AS} - C_{A0}} = \operatorname{erfc}\left(\frac{x}{\sqrt{4D_{AB}t}}\right)$$

This equation was solved for diffusivity at five different distances from the channel edge in 0.01cm increments.. The inverse error function was computed in Microsoft Excel as the square root of the inverse gamma function[37].

4.5: Cell Uptake

This final subsection details how cell viability was assessed on the surface of the fibrin vascular device according to the final objective. It covers how cell culture was performed as well as the experiment used to establish and measure viability.

4.5.1: Cell Culture

To measure cellular uptake over time, a culture of cells was needed for use in uptake experiments. C2C12 mouse myoblasts were continuously cultured in proliferation media of 43.8% DMEM (Gibco 11960-044), 43.8% Hamm's F12 Nutrient Broth (Gibco 11765-054), 10% Fetal Bovine Serum (INFO HERE), 1% Penicillin Streptomycin (Gibco 15140), 1% Amphotericin B (Sigma Aldrich A2942), and 0.4% Aprotinin (Sigma Aldrich A1153) all from stock. This media is designed to limit bacterial and fungal infections of cells while maintaining their ability to proliferate quickly. Cells were subcultured every two or three days depending on confluency.

C2C12 mouse myoblasts were chosen for this experiment for several reasons. First, we wanted a cell type that it was likely for vasculature to come in contact with. C2C12 cells being skeletal muscle cells made them a good candidate for this.

4.5.2: Gelatin Coated Cover Slip Preparation

To obtain a cell population for cellular uptake studies, coverslips needed to be coated for cell adhesion. Glass cover slips were cut down to 1cm by 1cm squares using a diamond tipped pen and a ruler. Cover slips were then wrapped in autoclave mats, sealed in a sterilization pouch, and autoclaved to sterilize. The day before an experiment was to be run, sterile glass cover slips were placed into a 5cm petri dish, and 10µL of sterile 1% gelatin in diH_20 was spread over the surface of the cover slip. The gelatin was then allowed to set for two hours at room temperature. At this point, 200,000 C2C12 mouse myoblasts and 5 mL of C2C12 proliferation media were placed into the petri dish with the gelatin coated

cover slips, and the plate was moved to the incubator overnight. From this process, we expect 10,000 cells per square centimeter. This process is illustrated in Figure 18 below.

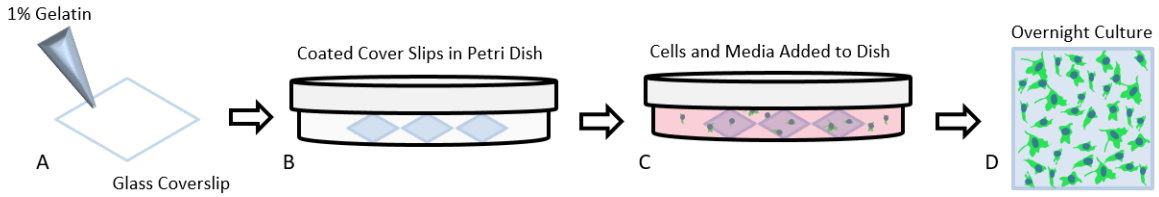

Figure 18: Myoblast seeded cover slips. (A) cover slips coated with gelatin (B) gelatin coated slips allowed to set for two hours (C) 200k C2C12 mouse myoblasts and C2C12 proliferation media added to plate (D) myoblast adhesion to gelatin coated cover slips

4.5.3: Calcein AM Perfusion

To observe cellular uptake of fluorescent dye, C2C12 cells were cultured on gelatin coated cover slips overnight, then washed with sterile 1X PBS twice for five minutes each. A fibrin vascular device was set up for perfusion as described in Figure 18 above. To make dye loaded media, 2 µL of calcein AM dye (Invitrogen L3224) was added to 4mL of serum free media, made with 44.2% DMEM, 44.2% Hamm's F12 Nutrient Broth, 10.1% HEPES buffer (Sigma H3375), 1% Penicillin Streptomycin, and 0.4% Aprotinin, and inverted to mix. The use of calcein AM dye required serum free media, as calcein AM, which is used as a live cell fluorescent dye due to it becoming cleaved upon passing through cell membranes, can also be cleaved when exposed to FBS. In order to ensure that cells would fluoresce, serum free media needed to be the perfused liquid for these experiments.

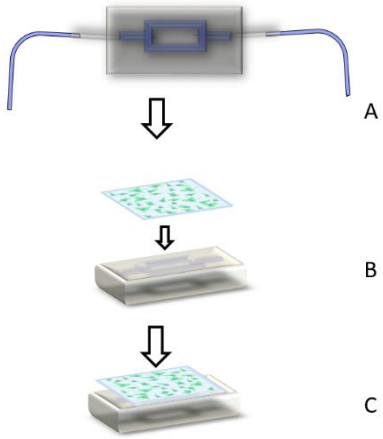

Figure 19: Experimental setup for calcein dye perfusion. (a) Fibrin vascular device being perfused with calcein loaded media (b) myoblast seeded cover slip placed on surface of fibrin vascular device (c) device perfused for four hours

The experiment was set up on the microscope stage. Fluid flow was initiated with the calcein AM loaded media, and a myoblast seeded cover slip was inverted onto the top surface of the vascular

device as in Figure 19Fluorescent and brightfield images were taken with a Spot INSIGHT CMOS camera on a Nikon Eclipse E600 upright microscope at 4X-magnification at t=one hour and t=4 hours. Images were properly scaled, and the size of fluorescing zones were measured using ImageJ. Positive controls for this experiment took the form of gelatin coated cover slips allowed to sit in calcein loaded media for four hours, with images taken at the same time points as for the perfusion study.

4.5.4: Image Processing and Calculations

Images were processed similarly to the fluorescent diffusion videos. Color channels were split, blue and red were discarded, and green was measured and normalized, as calcein AM is optimally excited at a wavelength 495nm. Images were normalized by drawing two 100x100 pixel boxes, one inside and one outside of the channel, being careful not to capture any cells within the boxes. The average brightness of those two boxes was taken and averaged together before that value was made the minimum brightness of the image.

For analysis, the channel edge was marked on each image, and the area of cell spread on the outside of the channel was measured, as in Figure 14. This area was divided by the length of the channel in the image to estimate the average diffusion plane of calcein AM dye. The difference between the average area change and the average limit of cell uptake were also calculated.

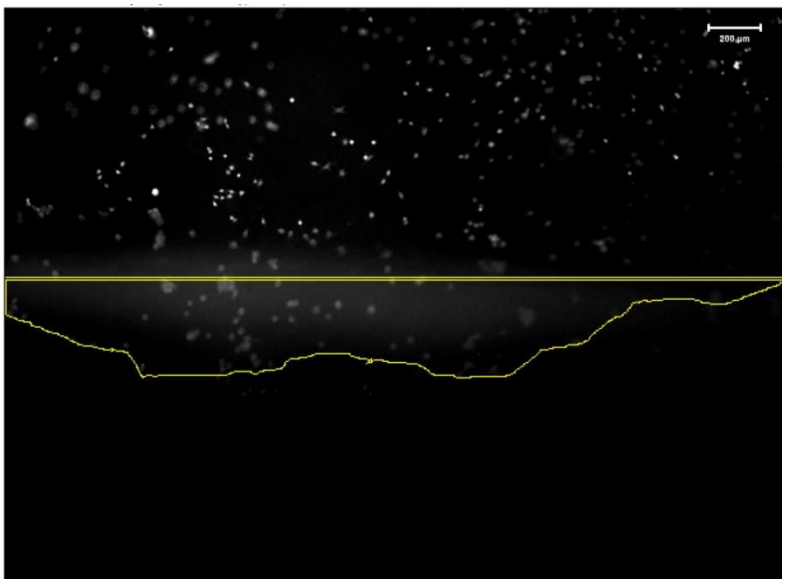

Figure 20: Example of traced calcein AM diffusion curve from channel edge at t=1 hour

Chapter 5: Results

5.1: Fluid Flow Initiation within Consistent Fibrin Vascular Devices

This section presents results acquired from experiments developed to achieve the first major objective of this project, which aimed to produce a fibrin-based device with channels capable of supporting continuous perfusion. The experiments in this section focused on the ability to manufacture and perfuse fibrin vascular devices, as well as assess the consistency of the channels within said devices. These experiments included: fibrin gel development, sacrificial structure fabrication and lamination, sacrificial structure morphometric analysis, and histological analysis of the resultant channels.

5.1.1: Fibrin Hydrogel Formulation

As outlined in the methods chapter, five different formulations of making a suitable fibrin gel were tested for the formulation of vascular devices. Results for this section were entirely qualitative. In order to maintain an encased channel, the matrix material had to be able to maintain its shape. The same volume of each formulation was poured onto vellum frames and allowed to polymerize. After each iteration, however, the only formulation that was able to consistently maintain its structure without tearing upon removal from the PDMS base was formulation D, which had a concentration of 4.26% fibrin. This formulation was also tested in a complexly shaped PDMS mold. The results are shown in Figure 21. This gel was able to maintain the shape of the mold from which it was removed, including ridges and holes. Since formulation D was the only one capable of being removed from a frame and manipulated, it was chosen as the formulation for further development of fibrin vascular devices.

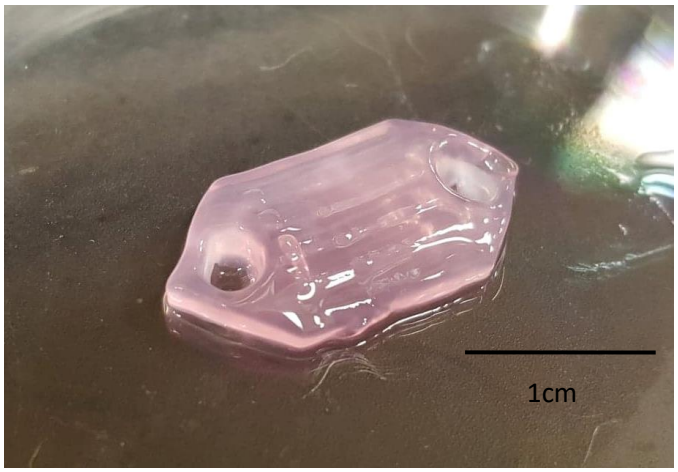

Figure 21: Fibrin Gel D removed from complex mold

5.1.2: Sacrificial Structure Fabrication

As discussed in the methods section, a mold was made for the fabrication of sacrificial structures from laser cut acrylic. The mold, pictured inFigure 7, was reusable, and through soft lithography, dozens of identical PDMS based negative molds were produced, one of which is pictured **Error! Reference source not found.**Figure 8. These negative molds were in turn treated with pluronic f127, which was then removed, and the molds filled with 10% gelatin, which was allowed to dehydrate before removal. One of these single layers of gelatin can be seen in Figure 22. The PDMS negative molds and the single layers of gelatin could be mass produced to ensure a consistent supply of sacrificial structures.

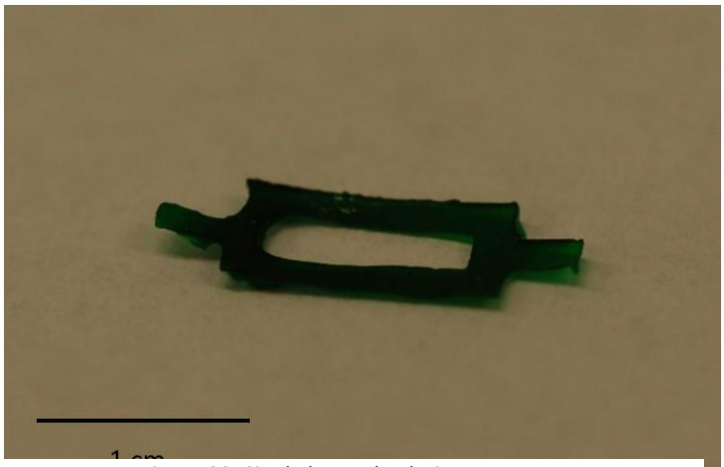

Figure 22: Single layered gelatin structure

5.1.3: Sacrificial Structure Lamination

Initial experiments with single layer sacrificial structures proved difficult, as the structure was buoyant and would float in the fibrin gel. If the structure was pierced and suspended with needles, it became extremely fragile and prone to breaking. Additionally, there is no vasculature within the body with similar geometries to the single layered sacrificial structures, which maintained their 1.5 mm width but were only approximately 0.04 mm in height. To address these issues, structures were laminated in four different ways to thicken the structures discussed in Section 4.1.4: Lamination Techniques. A representative image of the top and side of each of these lamination method follows. . The structure made using method A, Figure 23, did not retain its rectangular top geometry, nor did it have a flat, even, well bonded layers. shows the structure made using method B. This structure maintained its top

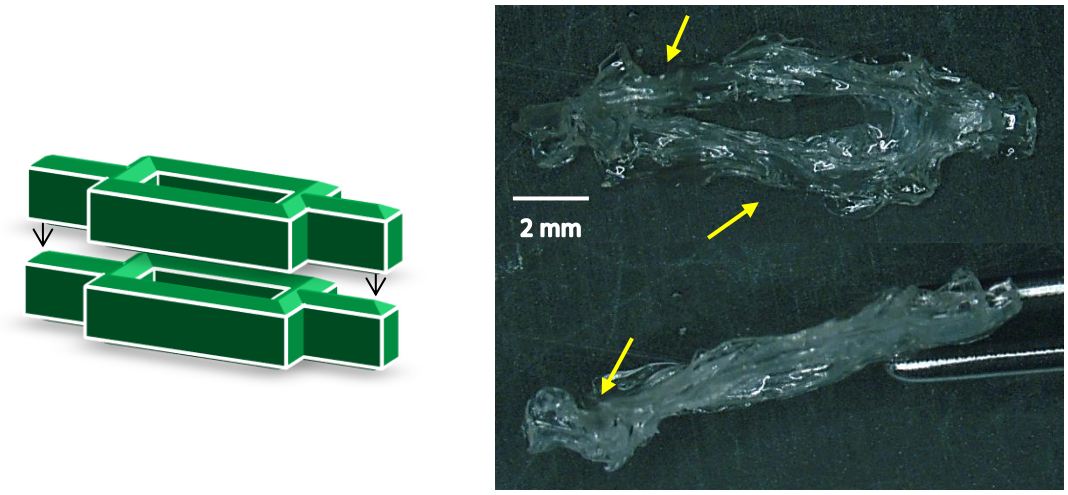

Figure 23: Schematic drawing, top and side view of a sacrificial structure using lamination method A, stacking two hydrated gelatin layers. Arrows point to deviations from rectangular channel shape and delamination between layers.

geometry with greater accuracy, but remained poorly bonded between layers, and showed some leakage of gelatin glue. Method C is pictured in **Error! Reference source not found.**Figure 25. This structure kept its

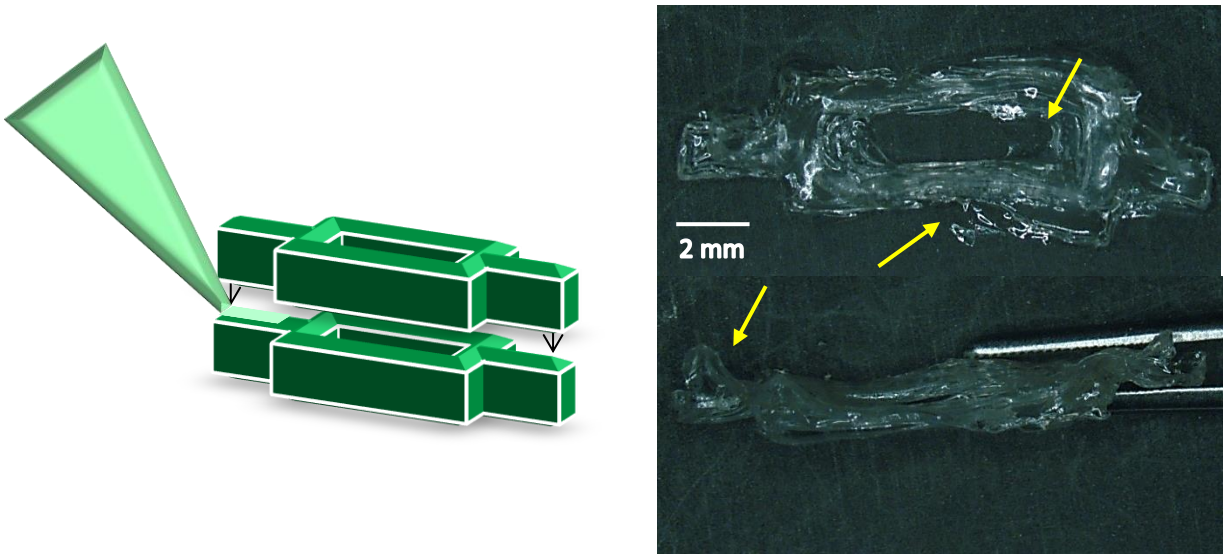

Figure 24: Schematic drawing, top and side view of a sacrificial structure laminated using method B, stacking two hydrated gelatin layers with a layer of fibrin glue between. Arrows point to leakage of gelatin glue and delamination between layers.

rectangular top geometry very well, maintaining clear straight lines. However, the layers were not evenly bonded, and were separating in the side view. . Finally, we attempted method D, illustrated in This lamination method provided not only unchanged top geometry, but also no visible separation between the layers. For this reason, method D was the lamination strategy of choice for future experimentation.

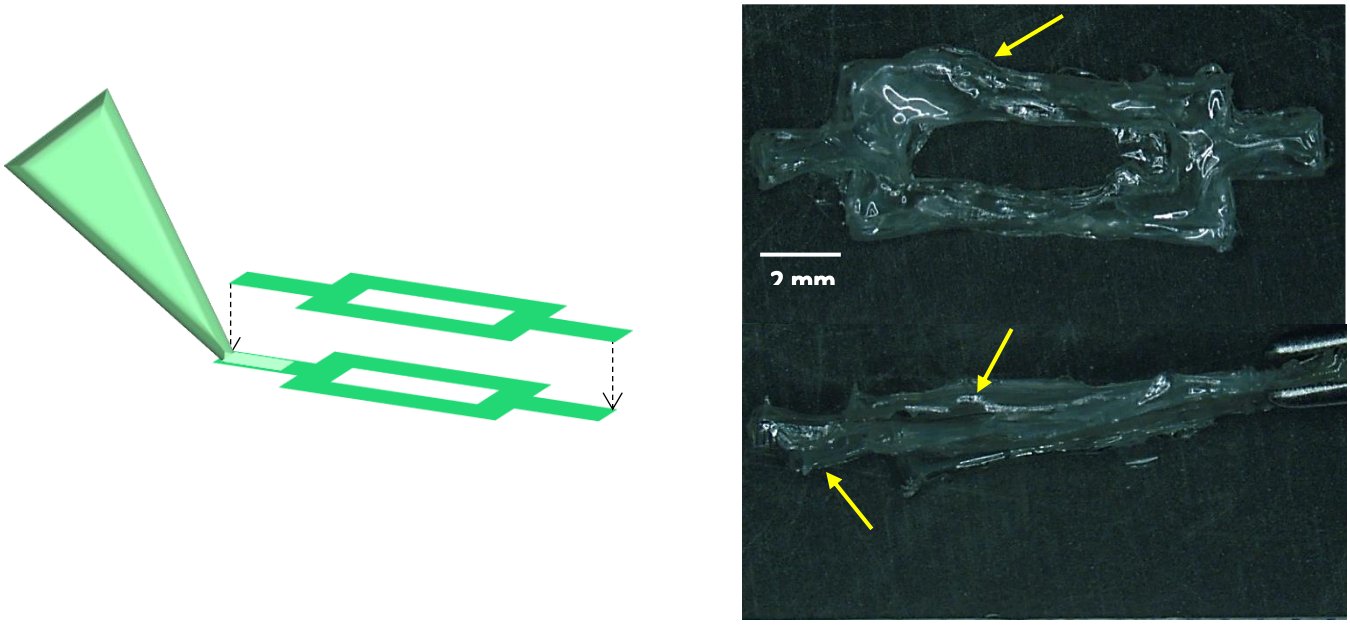

Figure 25:Schematic drawing, top and side views of a sacrificial structure laminated using method C, two dehydrated structures with a layer of gelatin glue. Arrows point to areas of delamination and leakage of gelatin glue.

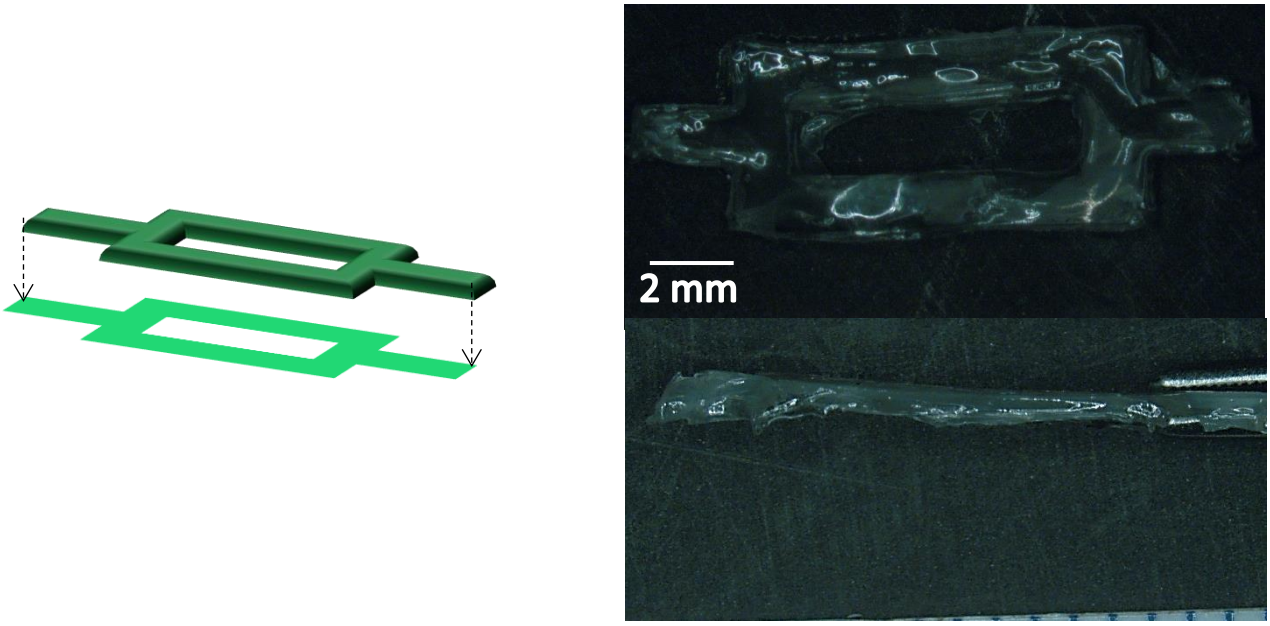

Figure 26: Schematic drawing, top and side view of a sacrificial structure made using lamination method D, one dry structure and one Partially rehydrated structure

5.1.4: Initiation of Fluid Flow

Once the gel formulation, sacrificial structure lamination technique, and the proper method of suspending a structure within a block of hydrogel were established, continuous perfusion was initiated by melting the gelatin structure, puncturing both ends of the fibrin vascular network, and initiating flow from a syringe pump. The QR code pictured in Figure 27: QR Code leading to video showing perfusion of fibrin vascular device leads to a video showing said flow.

Figure 27: QR Code leading to video showing perfusion of fibrin vascular device

5.1.5: Sacrificial Structure Morphometric Analysis

Two experiments were performed for the morphometric analysis of the gelatin sacrificial structures. First, structures were photographed dry next to a scale. These analyses were not capable of measuring cross-sectional area, so a second round of experiments was performed on the dry sacrificial structures. Structures were snapped in half, and the cross-section of each channel and inlet were photographed and measured.

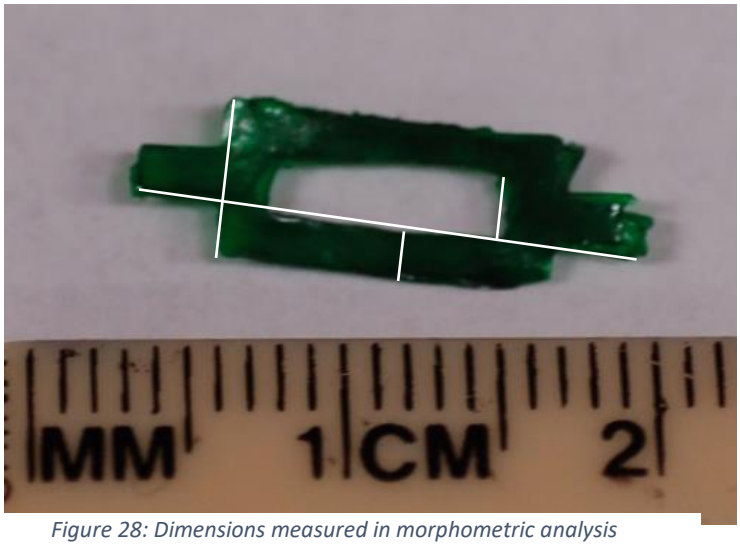

Figure 28: Dimensions measured in morphometric analysis

The measured dimensions for the first experiment are shown as overlays on Figure 28, as well as in Chapter 4: Methods. Measurements were performed using ImageJ to an n of 20. The mean values for each of these dimensions, as well as standard deviations, range and median, can be found in Table 4.

Table 4: Dry Sacrificial Structure Statistics

Dimension	Range (mm)	Median (mm)	Mean ± SD (mm)
Structure Length	13-19	15	15 ± 1.4
Structure Width	3.5-5.2	4.7	4.5 ± 0.52
Divider Width	0.73-2.4	1.7	1.6 ± 0.32
Channel Width	0.91-2.0	1.4	1.4 ± 0.30

The cross-sectional areas of the sacrificial structure channels were measured by standing them in a block of PDMS and imaging from the top. Figure 29 is an illustration of this process. A total of 21 channels (inlets or outlets) were photographed in this manner. A representative image of one of these points can be seen in Figure 30. The heights and widths were measured of each channel cross section.f. Average results and standard deviations from these measurements can be seen in Table 5. The median values and range were also recorded. Overall, while the top

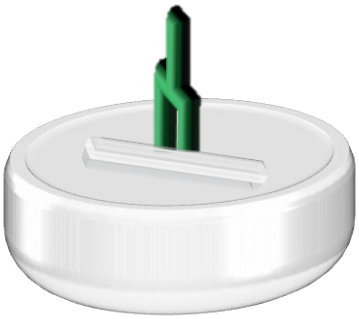

Figure 29: Illustration of how sacrificial structures were oriented for cross-sectional photography

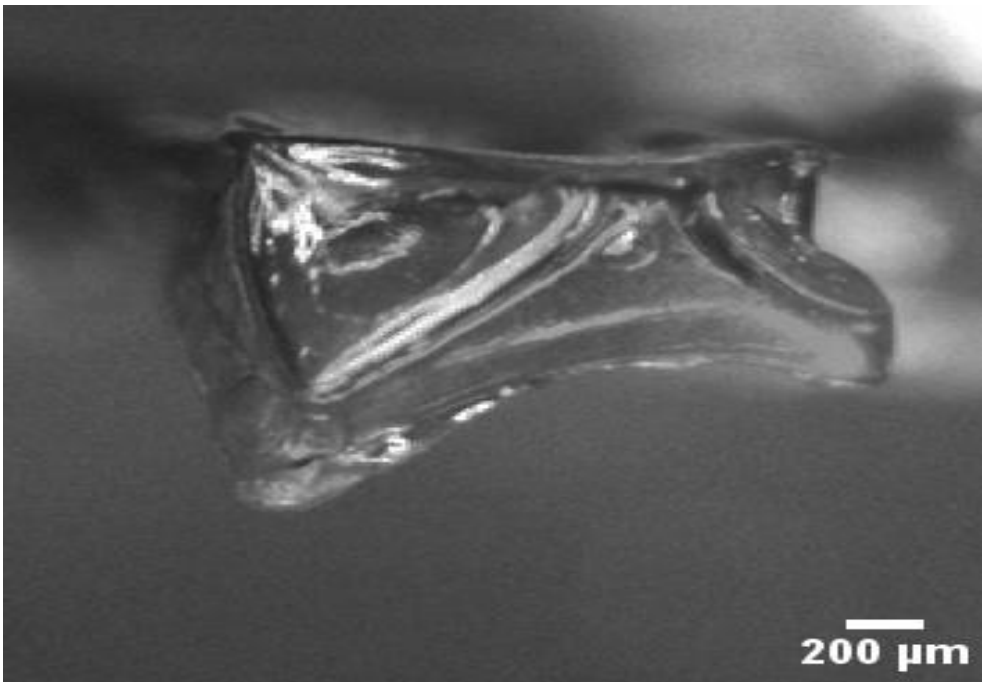

Figure 30: Representative image of a sacrificial structure inlet.

view of the sacrificial structures saw very limited deviation across samples, the cross-sectional area measurements saw significant irregularity. The calculated and measured areas were very similar, but standard deviations for both values were over 45% of the mean.

Table 5: Mean values and standard deviations of sacrificial structure cross-sections

Dimension	Range	Median	Mean ± SD
Height (mm)	0.37-1.07	0.74	0.73 ± 0.20
Width (mm)	1.19-1.57	1.75	1.33 ± 0.39
Calculated area (mm^2)	0.434-1.67	1.63	0.99± 0.45
Measured Area (mm^2)	0.41-1.36	1.1	0.96 ± 0.45

5.1.6: Histological Analysis of Vascular Channels

The final experiment for the first objective of this thesis was a histological analysis of the channels left behind after the sacrificial structure has been removed. Figure 31 is a representative image of one of these sections. Channels were then measured using ImageJ

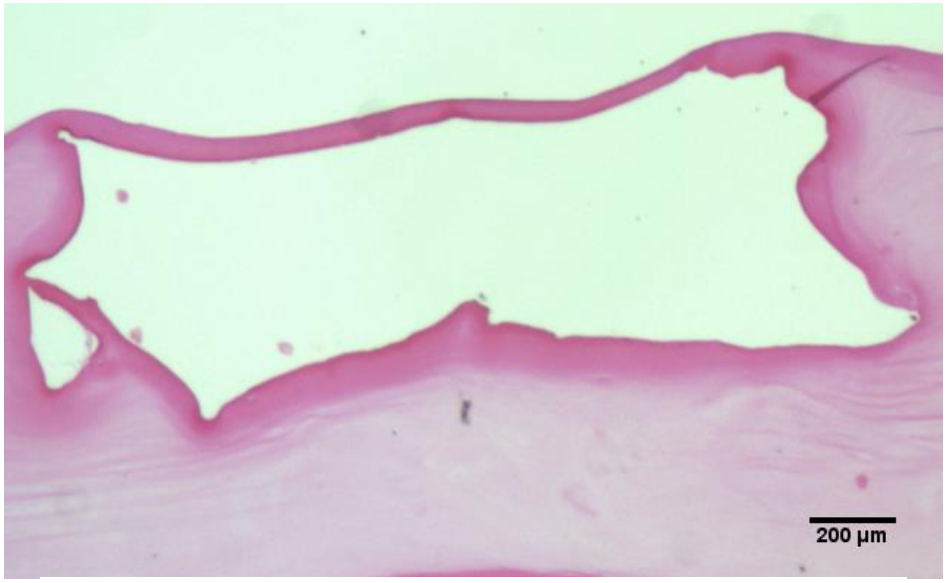

Figure 31: Histological section of fibrin vascular device.

Ten slides were taken from each sample ($n = 7$), and all sample averages were used to obtain the average value across all samples. Values for the average dimensions across all seven samples can be found in Table 6.

Table 6: Histological Analysis of Channel Dimensions

Dimensions	Sample 1 ± SD	Sample 2 ± SD	Sample 3 ± SD	Sample 4 ± SD	Sample 5 ± SD	Sample 6 ± SD	Sample 7 ± SD	Mean Value ± SD
Height (mm)	0.73±0.06	0.68±0.04	0.81±0.19	0.77±0.05	0.70±0.19	0.64±0.06	0.63±0.04	710.0±66.52
Width (mm)	1.51±0.07	1.64±0.05	1.36±0.10	1.56±0.11	1.04±0.25	1.57±0.05	1.81±0.06	1.50±0.24
Calculated Area (mm^2)	1.11 ±0.11	1.11±0.06	1.09 ±0.02	1.19 ±0.84	0.73 ±0.23	1.01 ±0.08	1.14±0.07	1.06 ±0.15
Measured Area (mm^2)	0.98 ±0.19	1.07±0.16	1.22 ±0.03	1.31 ±0.11	0.75±0.22	1.06±0.10	1.30 ±0.14	1.10 ±0.20

This table shows that while there may be some major differences between channels, the standard deviations within a single sample tend to be rather low, with the largest being 31%, for the calculated area of sample 5.

5.1.7: Comparison Between Sacrificial Structures and Channels

A student's t-test was performed using the average heights and widths of the channels and the sacrificial structure cross-sections to find if the channels made by the sacrificial structures were statistically different from the structures themselves. The results shown in Figure 32, both with P>0.05, show that there is no statistically significant difference between the size of the structure and the size of the produced channels. The T value of the height comparison was 0.04, and the t value for the width comparison was 1.32. The channels were measured at an n of 7, while the structures were measured at an n of 21.

It was found that there was a height scaling factor of 0.36 between the measured height of the channels and structures when compared to 2 PDMS molds, and a width scaling factor of 0.71, meaning

that we can predict the shrinkage of a gelatin based sacrificial structure made using this method, and the size of the resulting channels.

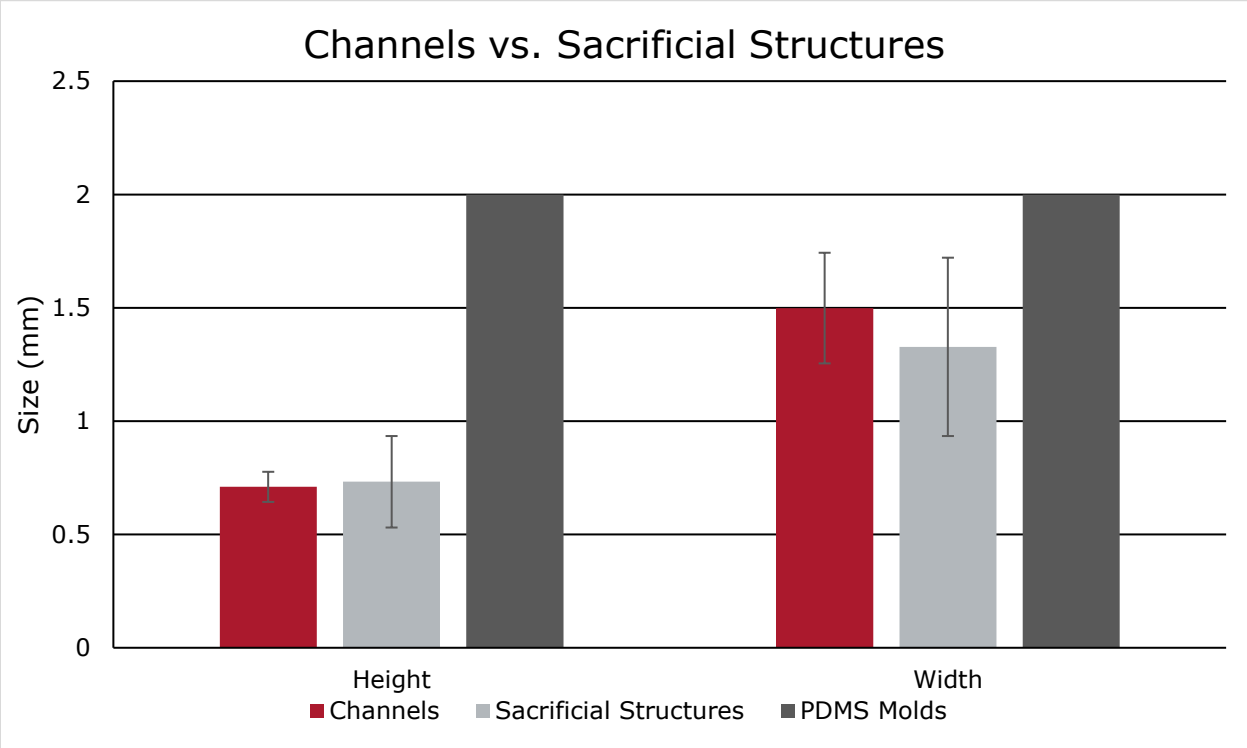

Figure 32: Student's t-test between sacrificial structure and channel height and width compared to PDMS molds. In both cases, P>0.05 means that there is no statistically significant difference between the structures and the channels that they create.

5.2: Diffusive and Fluid Flow Properties of Fibrin Vascular Devices

This section presents the results obtained from experiments focusing on the flow and diffusive properties of the robust fibrin gel devices, encompassed by the second objective. Two experiments were run to fulfill this goal. The first was designed to observe properties of flow to compare to physiological values. The second was to measure the diffusion of differently sized particles through the bulk of the fibrin hydrogel.

5.2.1: Fluid Flow Properties:

The experiment used to establish flow properties involved the perfusion of a fibrin vascular device with a suspension of polystyrene microbeads in PBS. A total of 15 videos were recorded for 15 seconds each. Ten particles from each video were identified and the distance between their starting and ending position measured. The starting position of each particle tracked was recorded, as in Figure 33. The averages of each group of ten particles was calculated. The distance traveled by all particles can be found in Appendix 3: Particle Tracking Measurements. The final average particle speed was found to be 0.096 ± 0.038 mm/s. The standard deviation of this value is so large because in the videos, flow could be seen moving faster towards the center of the channels than the edges, meaning that the fibrin vascular channels displayed parabolic flow. From the average particle speed and other known values, several flow properties were calculated, including volumetric flow rate, the Reynolds number, and wall shear stress.

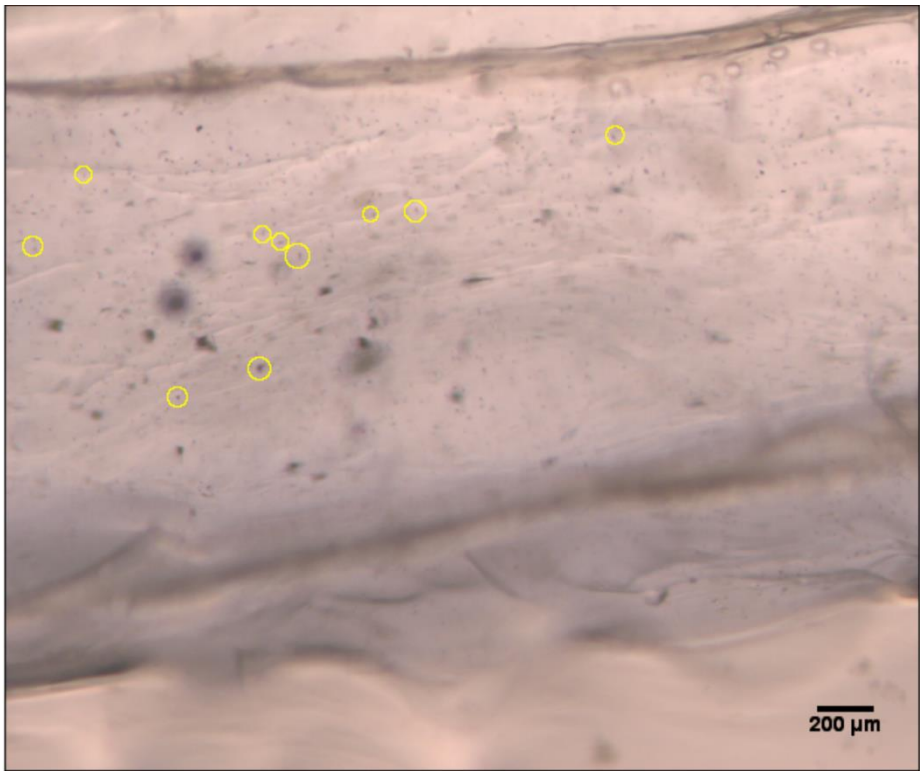

Figure 33: Representative image of the starting positions of microbeads within a fibrin vascular channel. The chosen particles were scattered throughout the full width of the channel, and large enough to easily visualize.

5.2.1.A: Volumetric Flow Rate

The volumetric flow rate was calculated using Equation 1 Equation 1, found in Section 4.1.4: Lamination Techniques. Both the expected volumetric flow rate, based on the output of the syringe pump, and the measured flow rate, based on average particle velocity, were calculated. The average particle velocity was based on measurements as discussed in Section 4.2.1. The results are below.

$Q_{expected}$ was calculated based on the flow rate of the syringe pump.

$$Q_{expected} = \frac{7.5 * 10^{-7} m^3}{hour} * \frac{1\ hour}{3600\ seconds} = 2.08 * 10^{-10} \frac{m^3}{second} = 0.208 \frac{mm^3}{second}$$

$$Q_{actual} = \frac{9.62 * 10^{-5} m}{second} * 2.12 * 10^{-6} m^2 = 2.04 \times 10^{-10} \frac{m^3}{second} = 0.204 \frac{mm^3}{second}$$

The actual volumetric flow rate was calculated to be nearly identical to the predicted value once both fluidic channels within the fibrin vascular device were considered. Slight differences can be attributed to relying on average channel geometries to calculate the flow rate, rather than the actual channel geometries for each video recorded.

5.2.1.B: Parabolic Flow and Reynolds Number

Reynolds number determines if flow is considered laminar, transitional, or turbulent. Equation 2 (Section 4.4.1: Microbead Flow Analysis), requires values for the density of the liquid (in this case PBS), the velocity of the fluid flow, the length of the channel, and the viscosity of the liquid. The density of PBS is 1000 kg/m3 and the viscosity is 1 N*s/m2. One Newton is equal to one kg*m/s2. Substituting this value allows for all units to cancel out, as Reynolds number is a dimensionless value.

The Reynolds number calculation is below.

$$Re = \frac{1000\,{}^{kg}/_{m^2} * 9.62 \times 10^{-5}\frac{m}{s} * 0.012m}{1.0\frac{Ns}{m^2}} = 1.15 \times 10^{-3}$$

$$Re = \frac{1000\,{}^{kg}/_{m^2} * 9.62 \times 10^{-5}\frac{m}{s} * 0.012m}{1.0\frac{kg * m * s}{m^2 * s^2}} = 1.15 \times 10^{-3}$$

This Reynolds number value is well under 2300, meaning the flow created within the fibrin vascular device is laminar.

Flow within a laminar system is also parabolic in nature, meaning that flow towards the center of the channel is faster than towards the edges. We confirmed that our flow matched this profile by measuring the velocity of particles within regions of the fibrin vascular devices. Figure 34and Table 7 show the mean and standard deviation of particle velocity passing through the channels. The standard deviations of these values are quite high due to differences between channels. Figure 34shows that there is a parabolic fit between channels.

Table 7: Average Flow Velocities across Channel Regions

	Average Flow Velocity (mm/s)
Region 1	0.08±0.01
Region 2	0.09±0.03
Region 3	0.10±0.04

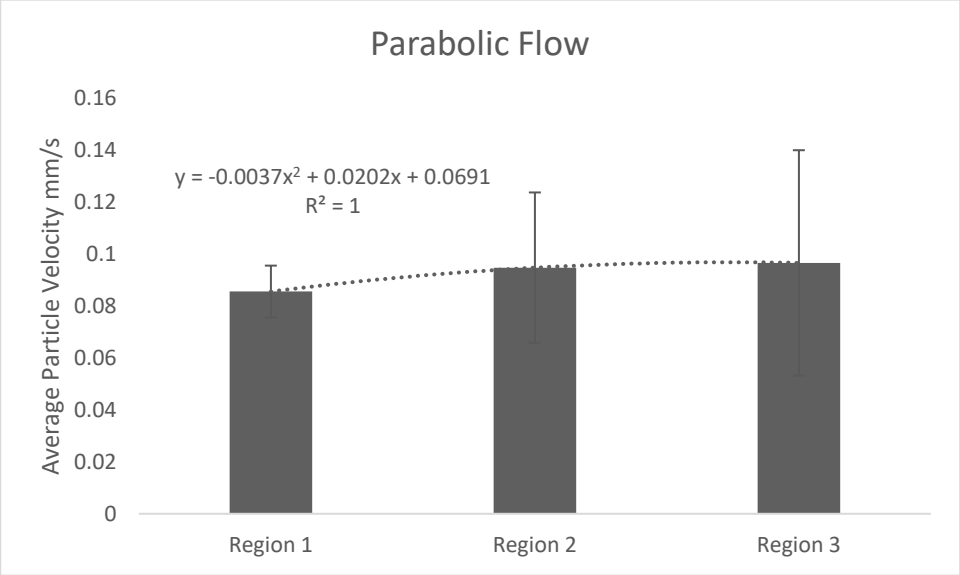

Figure 34: Parabolic Flow within Fibrin Vascular Devices

5.2.1.C: Wall Shear Stress

To calculate wall shear stress, an additional calculation had to be run. The shear force equation requires maximum speed, and what was calculated from the particle flow study was the average speed. Due to the nature of flow within channels, the maximum particle speed will come at the center of the channel. This is calculated from Equation 7 Equation 7 (Section 4.4.1: Microbead Flow Analysis). This value is below.

$$u_{center} = \frac{3}{2}(9.62 * 10^{-5})\frac{m}{second} = 1.44 \times 10^{-4}\frac{m}{second}$$

With this maximum speed value and Equation 4 Equation 4, the wall shear stress was calculated where τ represents wall shear stress:

$$\tau = \frac{-8\left[1 * (1.44 \times 10^{-4}\frac{m}{second}) * (7.49 \times 10^{-4}m)\right]}{(1.50 \times 10^{-3}m)^2} = -0.385\frac{N}{m^2}$$

5.2.1.D: Non-Uniform branching of fluid flow While all values calculated above are based on average values obtained over the analysis of 150 individual particles from 15 videos. These videos were taken from a total of five different channels within three different devices. The consistency of fluid flow between channels is an important consideration for this work. If channels are perfectly bifurcated and channels are identical, fluid velocity and volumetric flow rate should be identical across all channels. Unfortunately, as outlined in Table 8, this does not appear to be the case. While this discrepancy exists, it is most likely the result of regional Non-uniformities in the channels, and slight differences in channel size.

Table 8: Individual Channel Velocities and Volumetric Flow Rates

Channel	Average Velocity (mm/s)	Channel Area (mm^2)	Volumetric Flow Rate ($\frac{mm^3}{s}$)
Experiment 1 Channel 1	0.08±0.02	0.88	0.09
Experiment 2 Channel 1	0.05±0.01	1.20	0.07
Experiment 2 Channel 2	0.12±0.05	1.46	0.17
Experiment 3 Channel 1	0.10±0.01	1.28	0.12

Experiment 3 Channel 2	0.13±0.02	1.81	0.24

5.2.2: Diffusive Properties of Fibrin Vascular Devices

An experiment was run to measure the diffusive properties of fibrin vascular devices. In this experiment, FITC-dextran was perfused through the channels. Two different sizes of dextran were used for this experiment to observe how differently sized particles diffuse through the fibrin gel. The molecular weights used were 40 kDa and 250 kDa.

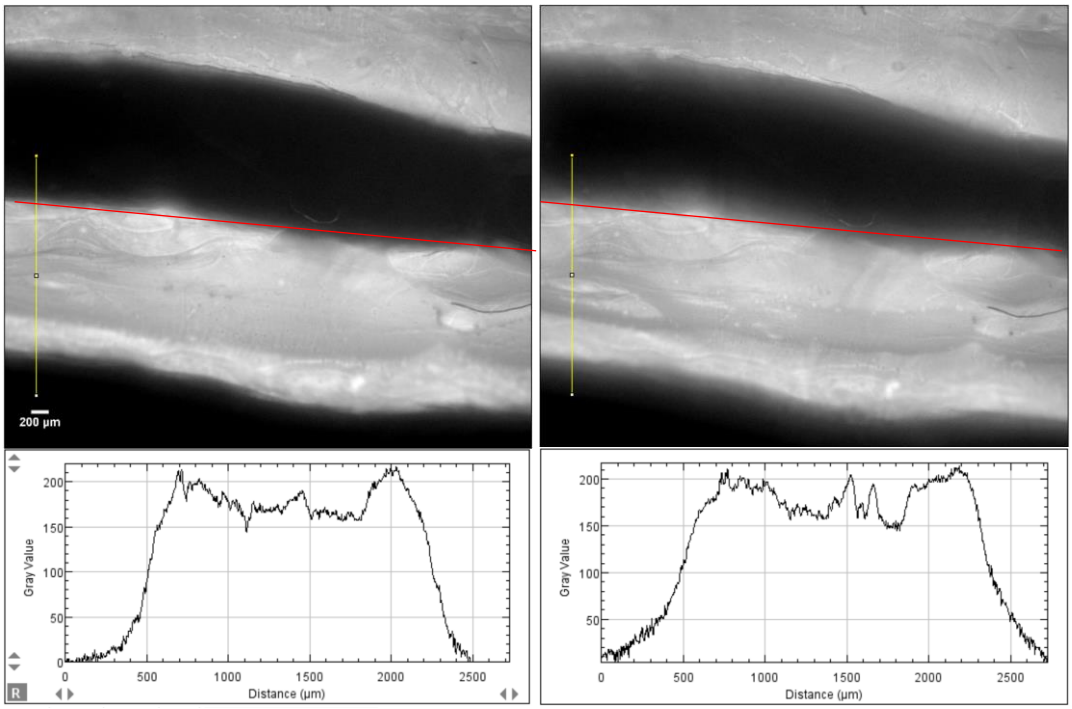

Figure 35: Intensity profiles of a microfluidic channel in the first (left) and last (right) frames of a 15 minute long time lapse video diffusing 40 kDa FITC Dextran. Red lines represent channel edges. Channels are fluorescing white as dextran diffuses into the black area of the fibrin device. The graphs show diffusion spreading and increasing in intensity.

Time lapse videos were recorded, and three lines that stretched through the channel and 0.5 mm on either side were selected along the length of the channel for analysis d. The intensity profile was taken along the lines for each frame of the video. Figure 35 shows the change in intensity profile from

the first to the last frame of an 18-minute-long time lapse video. The specific pixel values were taken from the List function at the bottom of the intensity plots and put into a Microsoft Excel sheet. These values were then plotted per time point. If a plateau occurred at any point on a graph, this meant that the video had become saturated, and data from that region of interest would not be usable, as the maximum recorded intensity may not be representative of the actual level of diffusion. Figure 36 below shows one of these graphs with a visible plateau, circled, unlike Figure 37. On Figure 37, each consecutive timepoint is plotted in a lighter shade of green. As more time elapsed in this diffusion, the intensity increased both in maximum value, but in spread as well.

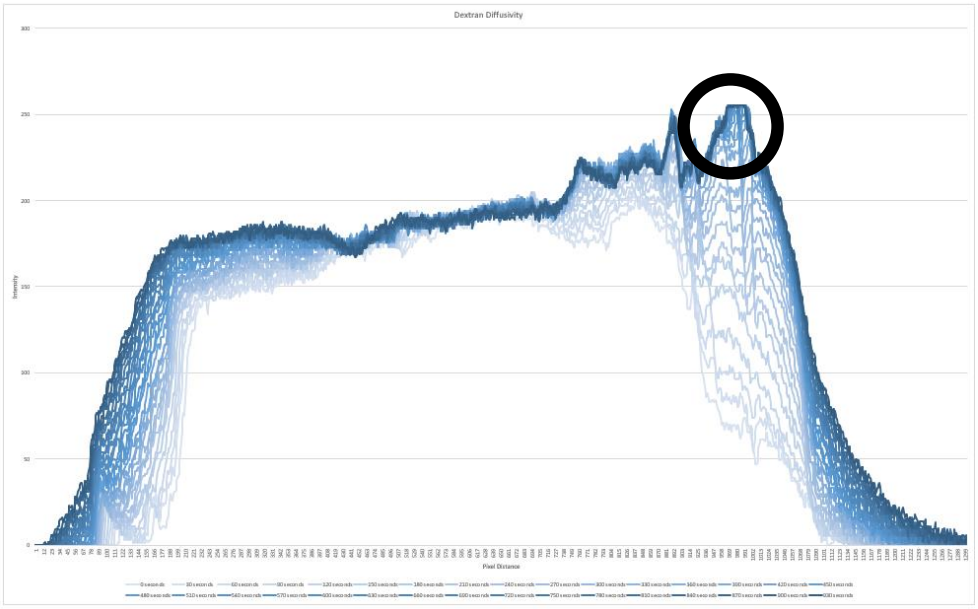

Figure 36: Graph of a diffusion video with an area of saturation (circled)

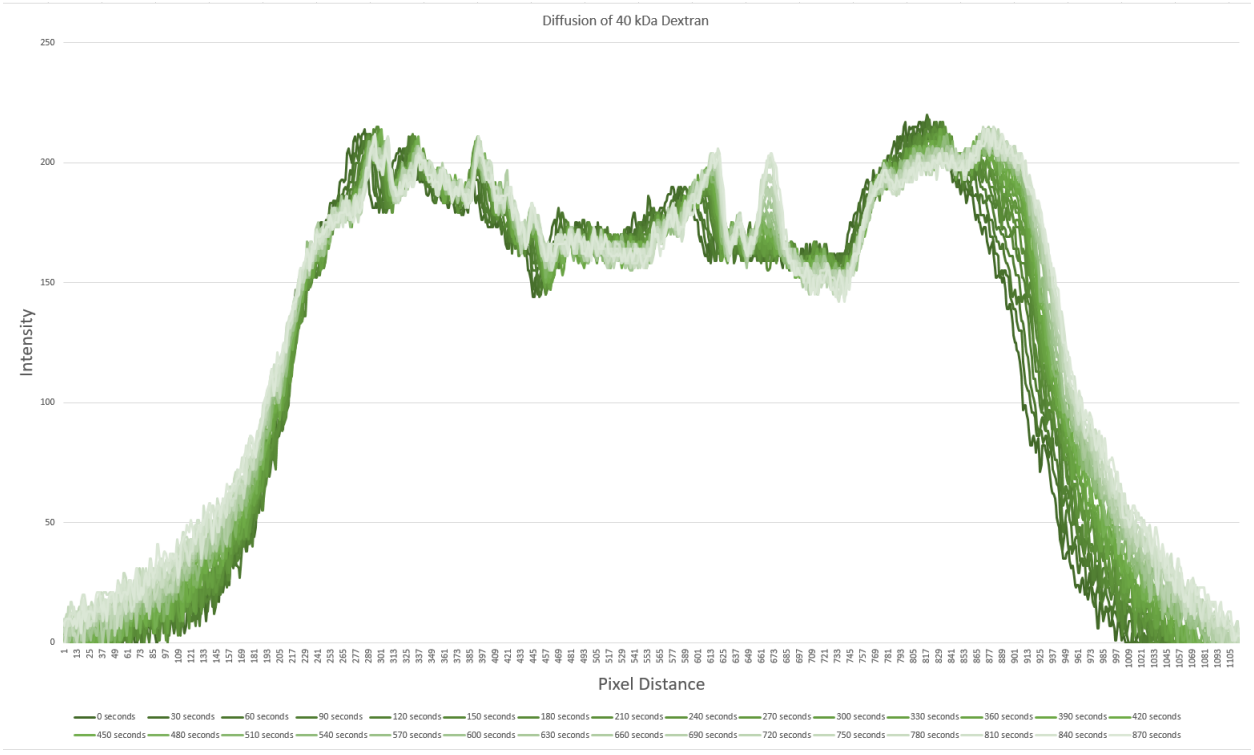

Figure 37: Graph of a region of interest from the same diffusion video as the previous figure. There are no visible plateaus in this image.

From the recorded fluorescent intensities, we graphed intensity ratios against the channel average at each time point at several distances from the channel edge. As time passed, represented by

the darkening line, the fluorescent intensity at each point increased, while remaining highest at the

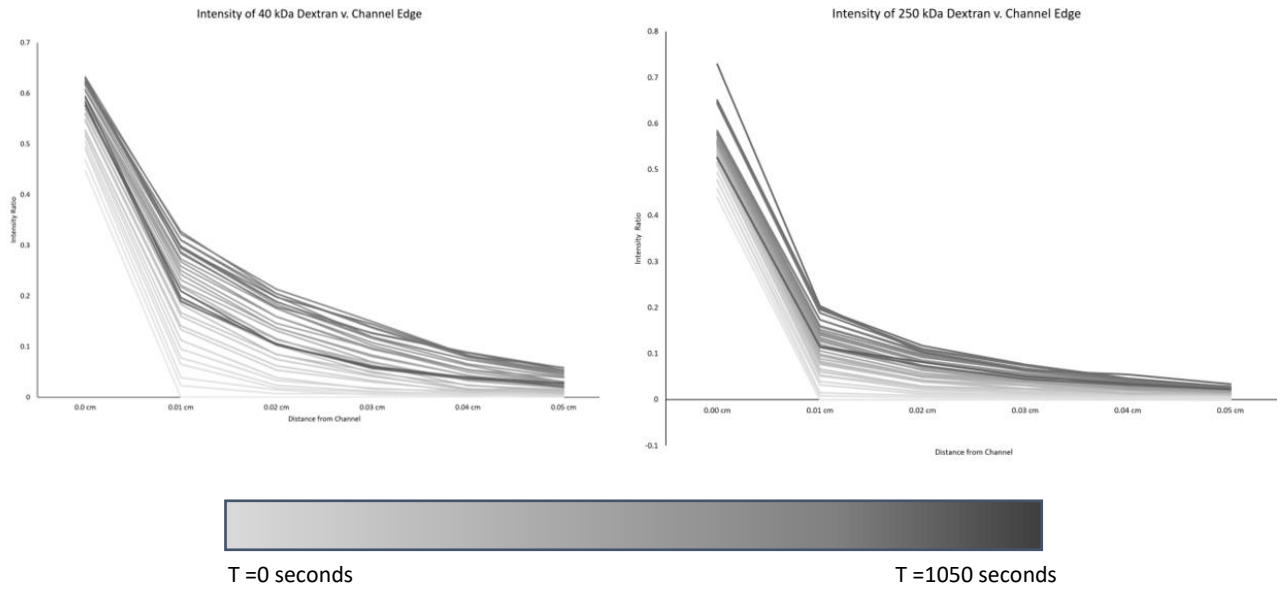

Figure 38: Intensity curves for 40 kDa and 250 kDa dextran at various distances from channel edge

channel edge (Figure 38).

The diffusivity of that region was calculated using Equation 8. The mean and standard deviation for these values for each size of FITC-dextran can be found in Table 9.

Table 9: Diffusivity of 40 kDa FITC Dextran and 250 kDa FITC Dextran

Diffusivity Mean ± SD (mm^2/s)		
Distance from Channel Edge (mm)	40 kDa FITC Dextran	250 kDa FITC Dextran
0.1	$1.00 \pm 0.67 \times 10^{-5}$	$5.72 \pm 5.17 \times 10^{-6}$
0.2	$2.47 \pm 2.30 \times 10^{-5}$	$1.71 \pm 1.98 \times 10^{-5}$
0.3	$4.31 \pm 4.67 \times 10^{-5}$	$3.55 \pm 4.88 \times 10^{-5}$

0.4	$6.34 \pm 7.99 \times 10^{-5}$	$5.64 \pm 8.07 \times 10^{-5}$
0.5	$9.31 \pm 12.72 \times 10^{-5}$	$8.36 \pm 11.74 \times 10^{-5}$
Mean	$4.69 \pm 3.27 \times 10^{-5}$	$3.96 \pm 4.56 \times 10^{-5}$

Values in this table show some standard deviations that are larger than their means. While not ideal, this is because the means are recorded across all 35 time points (every 30 seconds for 18 minutes). A full table of average diffusivities can be found in Appendix 4: Mean Diffusivity Measurements. There is also a trend of higher diffusivity at the points further away from the channel edge.

5.3: Cellular Uptake of Fibrin Vascular Devices

This section presents the results acquired from the experiment designed to fulfil the third objective of this project: determining zones of cellular uptake. As mentioned in Chapter 4, this was done by perfusing a fibrin vascular device with calcein AM dye loaded, serum-free media for a total of four hours with images taken at one and four hours. The images were then normalized and the area in which calcein AM was taken up by cells was outlined and measured to determine the cellular uptake area of

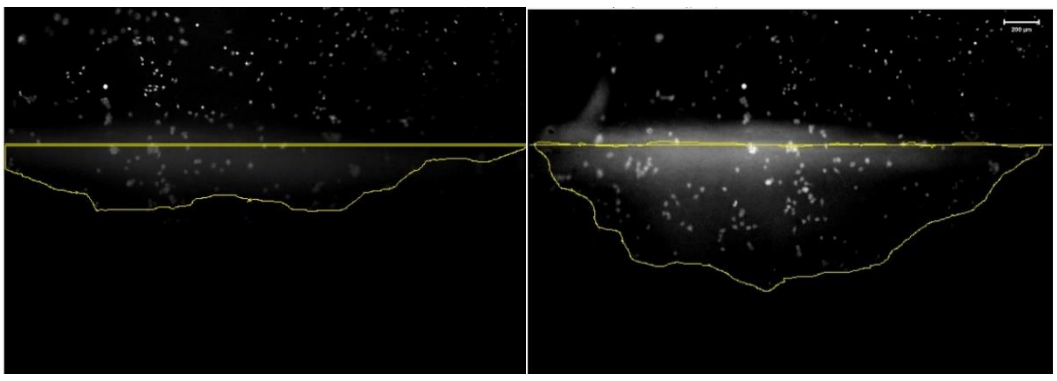

Figure 39: Calcein AM uptake study at t=1h (left) and t=4h (right). Yellow lines show the outline of dye uptake region.

the calcein AM dye. Visualization of these regions can be seen in Figure 39. The measurements taken from these studies can be seen in Table 10 below. In both the change in area and the average uptake distance from the channel edge, the values approximately doubled between the 1 hour and 4 hour time points. Calcein AM was chosen for this set of experiments because it only becomes fluorescent when cleaved by intracellular esterases, meaning it must pass through a live cell membrane to fluoresce. Thus, all of the visible cells in Figure 39 are still alive after the elapsed time.

Table 10: Average uptake area and diffusion plane of calcein AM dye ($n = 3$)

Time (hours)	Average Uptake Area (mm^2)	Average Change in Area (mm^2)	Average Distance of Cellular Uptake (mm)	Average Change in Cellular Uptake Distance(mm)
1	0.79 ± 0.27	0.72±0.11	0.26 ± 0.09	0.24 ± 0.04
4	1.51 ± 0.35		0.50 ± 0.12	

Chapter 6: Discussion

The long-term goal of this project was to develop a monolayered fibrin based vascular network for use in *in vivo* vascular repair, vascularization of full thickness tissue engineered constructs, as well as a possible *in vitro* platform for drug testing and vascular modeling. Currently, when vasculature is damaged or diseased *in vivo*, there are limited options for treatment. Depending on the disease or damage type, it is sometimes possible to treat macrovasculature such as veins and arteries with stents or vascular autografts from a patient's own saphenous vein [5]. In the case of microvasculature, the most common treatment is pedicle flaps [16], [17], [18]. While these methods have seen some considerable success, they both see problems with morbidity, both at donor site and implant site, shifting and degradation over time, and limited availability of donor material [5], [16], [17]. Tissue engineered constructs are currently limited to skin and cartilage, as these are some of the only tissues capable of surviving more than 200µm away from vasculature [1]. These limits persist because, while considerable work has been done towards this goal, there has yet to be a suitable substitute for vasculature which can provide a platform for full thickness tissue engineering [19, 20]. Current *in vitro* vascular models have been extremely successful in creating various organ environments, but the gold standard, PDMS, has proven a poor matrix for cell attachment and signal incorporation, and often saw leakage from within fluidic channels [2], [6, 24]. Towards this goal of creating a versatile platform with the capability to be developed to address any and all of these limitations of vascular engineering, a monolayered fibrin based vascular device was developed, characterized for its channel reliability, its flow and diffusive properties, and its ability to maintain a cell population on the surface.

In this study, a seamless fibrin vascular network was created using gelatin as a sacrificial layer to eliminate the need for layering hydrogels, which is a common cause for the leakage seen in hydrogel derived fluidic systems. The system was designed in two major parts: a fibrin gel capable of maintaining a stable network of channels and sacrificial structures capable of reliably exhibiting physiologically

relevant dimensions and producing channels of predictable size. Photographs were taken of sacrificial structures to measure both the 2D and cross-sectional dimensions of the produced sacrificial structures and compared to measurements taken from histological sections of a perfused fibrin device.

6.1: Development of a Reliable Fibrin Based Vascular Network

6.1.1: Manufacture of fibrin vascular devices

This section consisted of a series of trials for choosing the proper materials and proper fabrication methodology for making a fibrin based vascular device. For the first several experiments, namely the testing of various formulations of fibrin gel and the fabrication and lamination of sacrificial structures, the results were nearly entirely qualitative. Fibrin gels were assessed based on their ability to be lifted from a surface and manipulated. This is because in the use of these fluidic devices, they are at least briefly handled in order to access the edges for piercing and perfusion and need to maintain an enclosed channel without collapse. Forming channels within lower concentration fibrin gels had been problematic in previous iterations of this work, with channels frequently leaking or collapsing within the gel [35]. When the first attempts at fibrin gel, formulation A, failed to maintain their integrity when simply lifted from a cured PDMS surface before a sacrificial structure was involved, it confirmed that this gel would not function satisfactorily, and the other gel formulations were attempted. Knowing that increases in concentrations and volumes of both fibrinogen and thrombin could be used to change the mechanical properties of fibrin gels gave a direction for future attempts [33]. In the end, only formulation D could be consistently lifted from the surface of treated PDMS without tearing and remained intact when handled. This made it the best choice for use in the fibrin vascular devices. The material and channel were more structurally sound, and throughout the course of this project, there was no case of channel collapse. It was still possible for leaks to form when gelatin structures rose to the surface of the device during polymerization, another problem detailed in previous iterations, but during the completion of this thesis, these were fairly rare [35]. This increased structural integrity was due to

the higher concentrations of both fibrinogen and thrombin increasing the fiber length within the gel[33]. The fact that we were able to develop a fibrin gel that was capable of maintaining structural integrity as well as being capable of movement and manipulation will allow for more complex scaffold builds and experiments in the future.

The lamination of sacrificial layers was also a qualitative set of experiments directed towards finding the best possible method for structure production. In order to produce channels which are completely open without risk of fibrin infiltration which could disrupt flow, it is necessary to have well bonded layers without gaps or bubbles. For the structure to be considered reliable and reproduceable, it is also essential for it to maintain the intended shape and dimensions as designed for with the SOLIDWORKS model and PDMS negatives. Of the methods attempted, it was found that structures that had been allowed to completely dehydrate within the PDMS mold were the best at keeping their shape. The two methods involving dry structures also bonded the best, but gelatin glue tended to not always make full contact across the entire monolayers during bonding, which caused some separation between layers, leaving the partially rehydrated as the best option, both in full bonding and in the retention of shape. It was the method used going forward from this point.

6.1.2: Morphometric Analysis of Sacrificial Structures and Histological Analysis of Fibrin Fluidic Channels

One of the most important goals of this project was to have the channels within the fibrin devices mimic physiological values for vasculature. Past iterations of this project had seen considerable difficulty in producing microscale vascular channels, so for the sake of this thesis, the intention was to scale the channels up to a larger, but still physiologically relevant channel size [6]. The range of physiologically relevant values was taken from textbooks by Berger and Frietas, and can be found in Table 11[8, 9].

Table 11: Physiological Values for Vascular Size and Flow Rate

Vasculature	Diameter (mm)	Mean Flow Rates (mm^3/s)
Large Arteries	2.0-6.0	1600-5700
Small Arteries	0.3	3.5
Arterioles	0.01-0.14	0.025

The morphometric analysis was performed both by photographing the 2D top surface of the sacrificial structures and by photographing the cross-sections using a stereoscope and measuring all dimensions in ImageJ. These were then compared to channels made within a fibrin vascular device. Results from this set of experiments showed that we were successful in creating channels and sacrificial structures that mimicked the size of small arteries. While this cannot be considered microvasculature, the experiments succeeded in creating a bifurcated perfusable network of physiological relevance within a block of fibrin hydrogel.

Another important finding from this set of experiments was that there is no statistical difference between gelatin sacrificial structures and the fluidic channels they create within a block of fibrin gel. We were also able to calculate a scaling factor for this particular method of channel fabrication based on the differences between expected and experimental geometries. This means that, despite the fact that these channels are not currently considered microvascular, the same method used in this thesis could apply to later iterations of this project directed towards scaling down channel size and increasing complexity. Because we also know by what percentage structures shrink while being developed, we have a better understanding of how molds should be fabricated in order to achieve desired dimensions. This greater understanding will be vital for when this method is further developed towards microvasculature rather than the meso-vasculature modeled in this thesis.

Gelatin has been used as a sacrificial structure multiple times in the creation of hydrogel based fluidic devices, so while it was expected, the fact that it has been experimentally shown that this method

works in a robust fibrin gel fluidic network means that a gelatin based sacrificial structure method is reliable and a viable option for future development [24, 29, 30].

6.2: Assessing Flow and Diffusive Properties of Fibrin Vascular Devices

6.2.1: Flow Properties of Fibrin Vascular Devices

The flow properties of the fibrin vascular channels were calculated based on a series of perfusion experiments using 6µm polystyrene beads. These beads were chosen to mimic the size of neutrophils in the vascular system and were recorded in time lapse videos at 6 frames per second. Particles were tracked over the course of these 15-second-long videos to find an average speed, which was then used to calculate volumetric flow rate, Reynolds number, and wall shear stress.

While volumetric flow rate is an important property of fluid flow, it is determined primarily by the syringe pump's settings. The point of these calculations was not to test the viability of the syringe pump. The pump was set to perfuse at a rate of 0.21 mm^3/s, which is a physiologically relevant rate for small arteries(Table 11). Instead, this experiment was intended to prove that flow through the channels could match expected flow properties based on conservation of flow from the tubing into the channels themselves. The measured value is nearly identical to the calculated expected value, with a margin of approximately 0.004 mm^3/s. There are a few possible reasons for this very slight difference. First, the expected value based on conservation of flow calculations relies on an average channel size in calculations. Additionally, because particles to track were chosen for their size and visibility, it is possible that the average particle speed is slightly skewed. Overall, however, the results showed values similar to what was expected of the system, meaning that it abided by conservation of flow. Reynolds number was calculated to observe the turbulence of flow. In the body, flow is almost exclusively laminar, meaning that it has a Reynolds number below 2300. Because this project is intended to develop a vascular model, it is ideal to mimic the linear flow of blood vessels. The calculated Reynolds number for this experiment was 1.15×10^{-3}, which is a strongly laminar value. Turbulent flow within blood vessels

is seen only at branching points in large arteries, the ascending aorta, diseased vasculature, and in aneurisms [38]. The fact that we were able to achieve such a low Reynolds number indicates that our flow is similar to that within small and healthy vasculature. This is important because this vascular model should be as similar to native tissue as possible. If this model showed turbulent flow, rather than laminar, it would not be ideal for use in full thickness tissue engineered models, or in *in vitro* vascular modeling. Any results seen from diffusion or flow property experiments would be skewed by the unsteady flow.

All flow that is laminar is also parabolic. We were able to model this flow within our system, which contributes to the viability of this system. We did see, however, very large standard deviations within these values. These large standard deviations are most likely due to the overall difference in particle velocity seen due to uneven channel sizes throughout the study. These high standard deviations are not ideal, and do further emphasize that the non-uniform branching is a limitation to this system.

Finally, wall shear stress was calculated from this experiment. Wall shear stress is important because it plays a role in the structure and function of endothelial cells within vasculature [10]. Among these functions impacted by shear stress are the binding of transcription factors by shear stress responsive promoter elements [10]. While the physiological average shear stress within vasculature ranges between 1 and 4 N/m^2 in most arteries, areas of bifurcation often see stress dropping to as low as 0, or even negative values at branching points in blood vessels [10]. Thus, not only was the measured experimental value of 0.385 N/m^2 physiologically relevant, it was both well below the maximum value, and above the minimum value. This makes a promising argument that future experiments aimed at endothelializing the fibrin channels will see fully functioning endothelial cells. The wall shear stress value we calculated was below the average in vasculature, but it was also taken within a few millimeters of a branching point, where wall shear stress is expected to be lower. This means that our model system shows even further similarity to values within native vasculature.

One limitation of these fibrin vascular structures does, however, have to do with flow and flow rates. We found that between channels, even channels within the same device, the average speed of flow and thus the volumetric flow rate was not identical. This is likely due to the fact that the channel width of each channel changed slightly between each devices and structures (Table 8). As expected based on Equation 1, there was a greater flow rate within channels of larger areas. Despite the differences between structures, we remained successful in maintaining flow rates consistent with small arteries.

Further work will need to be done in order to improve bifurcation in order to make flow rate constant across the entire system.

Overall, the calculated flow properties of the fibrin vascular network have proven that flow is conserved and reliable within channels, flow is laminar, like in blood vessels, and the shear stress applied to the walls of the channel by fluid flow is within physiological norms. While we do see a limitation in non-uniform bifurcation, the overall flow within the fibrin vascular device meets the goal of being physiologically relevant.

6.2.2: Intensity Curves and Diffusivity of Fibrin Vascular Devices

The intensity curves seen in Figure 38 are a clear visualization of the diffusion of the FITC dextran. As expected, the fluorescence intensity is highest at the channel edge and dissipates quickly upon its diffusion into the fibrin hydrogel matrix. As time passes, and more dextran becomes diffused, the intensity curves increase, while maintaining the exact same shape. This means that our diffusivity is, while not consistent, predictable.

As mentioned in the results section and shown in Table 9, we see very high standard deviations within our system. This is because diffusivity is not consistent over time and distance. The averages seen in the table below are the averages not only over an 18 minute period, but also at five different points away from the channel edge. This led to a system average over a wide range of

conditions. The diffusivity tends to increase the further the measurement was taken from the channel edge. This is not necessarily an unexpected result. In Figure 38, the intensity ratio is lower, and Equation 8 shows that the diffusivity values and concentration ratios are inversely proportional. At lower concentrations of dextran, the chains entangle with each other less, allowing faster and easier diffusion down the gradient [39].

Diffusive properties are impacted by a variety of factors, including the size and shape of the molecule being diffused, and the concentration of the diffusive matrix. Fibrin changes properties such as stiffness, viscosity, and porosity with the concentration of fibrinogen and thrombin within the gel [33]. This means that, because a robust fibrin gel with a high concentration of fibrinogen and thrombin was used in this experiment, diffusivity values were observed to be very different from most published literature, which tends to focus on low concentration gels. Table 12 shows a comparison of our experimental values with literature values.

Table 12: Experimental values compared to literature value for diffusivity within fibrin gel. Experimental values highlighted in grey.

Dextran/molecule and size	Fibrin Gel	Diffusivity (mm^2/s)
3 kDa	~3.5% fibrin gel	$2.60 \pm 0.86 \times 10^{-4}$ [20]
10 kDa	~3.5% fibrin gel	$1.15 \pm 0.15 \times 10^{-4}$ [20]
40 kDa	0.40% fibrin gel	$\sim 4.00 \times 10^{-4}$ [18]
40 kDa Dextran	4.26% fibrin gel (42.6 mg/mL fibrinogen)	$4.69 \pm 3.27 \times 10^{-5}$
70 kDa	~3.5% fibrin gel	$0.99 \pm 0.19 \times 10^{-4}$ [20]

250 kDa Dextran	4.26% fibrin gel (42.6 mg/mL fibrinogen)	$3.96 \pm 4.56 \times 10^{-5}$
500 kDa	~3.5% fibrin gel	$0.34 \pm 0.07 \times 10^{-4}$ [20]

Diffusion within a physiological system is important because it is the method by which nutrients reach cells. The goal of this experiment was to establish the rate by which that happens within our system, and to compare the diffusion of differently sized macromolecules. As expected, our experimental values for 40 kDa dextran, highlighted in grey in **Error! Reference source not found.**Table 12, are higher than our experimental values for 250 kDa. This is a trend that can be seen throughout the table, specifically from Catalano et al., . which observed diffusion of four sizes of fluorescent dextran through a fibrin based wound sealant. Each successively larger molecular weight of dextran showed a lower rate of diffusivity. [20]

The lower diffusion rate of our experimental values may be contributed to the higher concentration of fibrin gel used. However, not only were diffusivity values within an order of magnitude of other published data for dextran in fibrin gel, but our diffusivity also falls within an order of magnitude of diffusivity into native tissue. Reissis et al. diffused 40 kDa dextran into articular cartilage, and found a diffusivity of $5.8 \pm 1.0 \times 10^{-5}$ mm^2/s [18]. While $5.8 \pm 1.0 \times 10^{-5}$ mm^2/s and $4.69 \pm 3.27 \times 10^{-5}$ mm^2/s are different from each other, we managed to create a vessel with diffusivity within the same order of magnitude as into native tissue.

Our diffusivity values also remained within reasonable range for particles diffusing out of native vasculature. Table 13 details the diffusion of small particles out of vasculature. We do, again, see differences on the scale of an order of magnitude, but the particles being diffused out of vascular tissue are much smaller than those being diffused out of the fibrin vascular devices. In the grand scheme,

further testing should be done, but we were able to acquire vascular diffusion rates similar to what was seen out of native tissue.

Table 13: Fibrin vascular device diffusivity compared to native vascular tissue. Experimental values highlighted in grey.

Particle	Molecular Weight (kDa)	Matrix	Diffusivity (mm^2/s)
H_2O	0.02	Arterial Wall	$0.79\pm0.04\times10^{-3}$ [40]
Glucose	0.18	Aorta	$1.43\pm0.24\times10^{-4}$ [41]
FITC Dextran	40	Fibrin Vascular Device	$4.69 \pm 3.27 \times10^{-5}$
FITC Dextran	250	Fibrin Vascular Device	$3.96 \pm 4.56 \times10^{-5}$

It is clear that the diffusive properties seen from our experiments did not exactly match those of published literature or native tissue. While our values remained within the range of an order of magnitude, a large difference in diffusivity is not ideal for a vascular model. As discussed above, the porosity of fibrin gel can be adjusted by changing concentrations of fibrinogen and thrombin, which would change the overall diffusivity [33]. Further testing of fibrin gel formulations may produce a gel with diffusive properties more similar to those of native tissue.

6.3: Cellular Uptake on Surface of Fibrin Vascular Devices

In order to achieve the long-term goal of the fibrin vascular devices being utilized in the vascularization of full thickness tissue engineered constructs or in tissue repair, it is imperative that the

robust fibrin gel is capable of providing nutrients and oxygen to cells found on the surface of the network. The experiments run to establish cellular uptake showed that not only were cells capable of taking up nutrients, in this case media loaded with dye, but the uptake zone increased over time. The visualization of live cells on the surface of these fibrin vascular constructs is promising for future development of these structures.

After the one-hour point however, the uptake by cells seemed to have slowed This is because the diffusion of the calcein AM would not have scaled linearly over time [42]. Visible uptake area could also have been effected if the cells that took up the dye were either dim or not in focus, and thus washed out by the normalization. The normalization itself may have cause further irregularities within the data obtained from these experiments. In the representative image, the area of cellular uptake appears to be rounded in nature. Given that the calcein loaded media was being flowed through the channels constantly at an even rate, the diffusion distance should have appeared linear. In Figure 39, one will notice that fluorescence is brightest along the channel edge, and there was a particularly bright area directly behind the furthest reach of the uptake area. It is possible that during normalization of these images that the brightness along the channel edges caused other cells that had taken up the calcein dye to be removed by the normalization.

Chapter 7: Future Work and Recommendations

This thesis focused on the fabrication of a monolayered fibrin vascular device that would be able to mimic physiological properties of flow and diffusion for the purpose of sustaining a cell population. The developed devices have been shown to be capable of reliable perfusion as well as being able to supply cells on the surface with media. These are promising results which lend themselves to further development in the future, for possible use in vascularizing full thickness cardiac patches and an *in vitro* vascular model for drug screening. For either of these to occur, further testing is needed to gain a better

understanding of this system, and to increase the physiological relevance of the encased vascular network.

7.1: Short Term Recommendations

There are several short-term recommendations which specifically target the fabrication of more complex networks, as well as the endothelialization of the inner channels. These short-term recommendations focus on making a more accurate model of a vascular network within a block of fibrin gel using our established methodology.

7.1.1: Increasing Network Complexity

While the two-channel network that has been established has shown good results, it was established in its current form for proof of concept studies. In order to make a true vascular network, it is necessary to build a larger, high complexity network of channels. This brings with it its own array of complications, such as pressure within channels, mold fabrication, and channel size.

As shown by COMSOL modeling by Borenstein et al., the best way to manage pressure drop across channels of decreasing size is to follow the principals of Murray's Law [6]. Murray's law, shown in Equation 9, states that the cubed width of the parent channel should equal the sum of all daughter channels cubed. Due to the maintenance of pressure across branched channels, future iterations of this project with more complex networks should be modeled according to this principal.

Equation 9: Generalized Murray's Law

$$W_{Parent}^3 = \sum W_{Daughters}^3 \tag{9}$$

The mold used in this thesis for the fabrication of sacrificial structures was laser cut from acrylic and was assembled out of multiple pieces. While this worked for this application, it did have some problems: slight damage, leakage, unknown additional height added due to the presence of adhesive layers, and difficulty to reproduce and replace. To address these concerns, I experimented with the use of thermoplastic shrinking polystyrene sheets, or "Shrinky-Dinks". These thermoplastic shrinking polystyrene sheets have been experimented with in several microfluidic applications, including 3D-chips, fluid flow containing Chinese Hamster Ovary cells, a simple immunoassay, and the fabrication of master molds for soft lithography [43-46]. Etching onto Shrinky-Dinks with a craft cutter obtained channels as small as 65µm in width [44]. These sheets however, often exhibit varying shrinkage tolerances from sheet to sheet [43]. In our own testing, done by cutting 20x20mm squares with 10x10mm windows with a Silhouette Cameo craft cutter, the average shrinkage between trials was found to be within an average of a 2% tolerance of each other. This data can be found in Appendix 5: Shrinky-Dink Analysis.

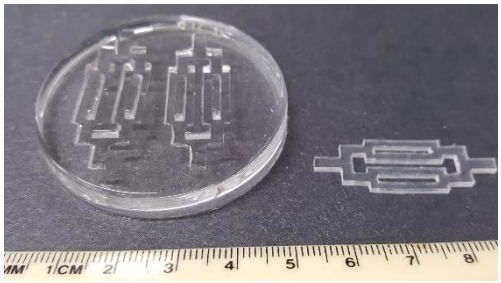

Figure 40: A Shrinky-Dink master mold (right) and PDMS negative (left)

Preliminary sacrificial structure manufacturing was performed with the use of Shrinky Dink based master molds. Shrinky Dinks were cut using the Silhouette Cameo printer, soaked in pluronic f127, then covered in PDMS shown in Figure 40 to the left. The PDMS was then also treated with pluronic f127, and filled with 10% gelatin, shown in Figure 41 to the right. While the molding of the gelatin was successful, it was found that these gelatin layers were very difficult to work with and were not able to be laminated the same way as the sacrificial structures used in experiments. The additional channels tended to stick together and become entangled when rehydrated, and became difficult to untangle without damaging

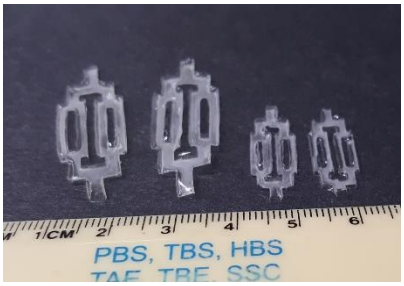

Figure 41: Gelatin structures made with Shrinky-Dink derived mold

the structure. That being said, the use of thermoplastic polystyrene sheets has proven promising for the future development of molds for sacrificial structures.

Finally, in these proof of concept studies, the gelatin structures made were large, and required a large volume of fibrin gel to encapsulate them. This is both wasteful, and not physiologically relevant. In order to create more complex networks, I suggest reducing channel size considerably to mimic smaller physiological structures.

7.1.2: Reducing Channel Size

In order to more closely mimic physiological vascular tissue, I suggest choosing a method to reduce the channel size. The current channel area of the fibrin vascular devices places them physiologically most similar to small arteries [8, 9]. To obtain a perfusion area more relevant to the fabrication of full thickness tissue engineered scaffolds, it is ideal to have a larger network of smaller channels. The target area should be a maximum of $0.015mm^2$ to match the area of arterioles [8, 9]. If the silhouette cameo printer is not capable of cutting Shrinky-Dinks of the appropriate size to make PDMS negatives, I propose cutting channels directly into Shrinky-Dinks, treating the surface with pluronic f127, and pouring gelatin directly into the channels on the polystyrene sheets.

7.1.3: Endothelialization of Channels

The results show that the fibrin vascular device is a viable model for vasculature, and is capable of maintaining a surface population of cells. In order to make a more accurate model for vasculature, however, it is essential to endothelialize the inner channels. Endothelial cells have been grown on fibrin before, as well as within PDMS microfluidic channels, so I propose combining some of these methods to hopefully obtain a confluent layer of endothelial cells. Researchers at the University of Zurich increased endothelial cell growth on fibrin gel by altering VEGF to be capable of binding to fibrin gel, and incorporating it into fibrin gel in varying concentrations [47]. In order to culture endothelial cells within the channels, I suggest following the method developed at Emory School of Medicine by the Lam

group[48]. PDMS channels were endothelialized by perfusing a 1 million cell/mL suspension of HUVECS in an endothelial growth media containing added dextran through microchannels for two hours at a low flow rate within an incubator environment (37°C and 5% CO_2). At this point, the cell suspension flow was stopped and replaced with a perfusion of the same growth media for between two and eight days to achieve a monolayer of endothelial cells [48]. I believe that a combination of these two methods will allow for complete endothelialization of the microfluidic channels.

Histological analysis should be performed to ensure complete confluence of endothelial cells within the microfluidic channels. Having fully endothelialized channels will make the fibrin vascular devices better endothelial models. However, it will also change the diffusive properties, possibly by as much as an order of magnitude [49]. This means that once a method has been fully established for creating the endothelial layer, diffusion and cellular uptake experiments should be repeated.

7.2: Long Term Recommendations

Once the work to develop a more complexly branched and endothelialized fibrin microvascular device is done, characterization should be run to assess how useful these devices will be *in vivo* and in *in vitro* drug testing analysis. For this, we should characterize *in vitro* degradation, *in vivo* degradation and biocompatibility, and finally attempt use of the fibrin microvascular device as a platform for drug testing.

7.2.1: Quantify Degradation *In Vitro*

Early stent studies showed that the average time required to fully endothelialize an implant *in vivo* is 28 days [50]. While this was measured on an untreated stent, and the endothelialization time of fibrin is much shorter, with Wong et al. running experiments on fibrin constructs after only nine days [51]. With that said, fibrin based implants *in vivo* have been found to be completely degraded by 21 days [52]. It is important to determine the speed of degradation of the fibrin microvascular devices to determine if they would be capable of survival until endothelialization is complete. The addition of

aprotinin in different concentrations can adjust the degradation rate of the fibrin microvascular devices to ensure device survival [32]. With this in mind, future researchers should quantify the degradation of the fibrin microvascular devices to ensure success. I suggest this be done through the use of an ELISA targeting fibrin degradation products, as was used in studies by Coffin and Gaudette [53].

7.2.2: *In Vivo* Biocompatibility and Degradation

As mentioned above, Kidd et al. have found that a fibrin based implant had fully degraded by 21 days [52]. The fibrin vascular devices from this thesis are made of a more robust fibrin gel than the implants used in that study, so experiments measuring the degradation rate of it *in vivo,* as well as the biocompatibility *in vivo,* should be run to establish a baseline. I suggest the use of a mouse model, as used by Page et al. in their fibrin microthread *in vivo* skeletal muscle regeneration study [54]. In order to line up with relevant endothelialization time and degradation estimates, I suggest time points of 8 days, 12 days, 16 days, 20 days, and 24 days. Samples should be histologically analyzed for endothelization, fibrous encapsulation, and scaffold degradation.

7.2.3: *In Vitro* Drug Testing Assay

Common uses of vascular microfluidics, as discussed in Chapter 2: Background, are the modeling vascular disease and the testing of pharmaceuticals *in vitro*, before moving to an *in vivo* model. I suggest a set of future experiments where the effects of a drug can be tested on cells on the surface of the fibrin vascular device. An ideal system to test would be intravenously delivered chemotherapy drugs, such as Doxorubicin, to a culture of tumor cells on the surface of the device, such as MOLT-4 leukemia cells, MCF7 breast cancer cells, or NCI-H522 small cell lung cancer cells, all of which are cancer types that Doxorubicin is used to treat. The fibrin vascular device can be recorded, and the cellular reaction can be measured in real time. If results of this experiment line up with expected cell behavior, then the fibrin vascular device can be established as a drug testing platform for the development of new intravenously delivered drugs.

7.3: Fabrication of a Fibrin Based Modulated Cardiac Patch

The thesis work of Megan Chrobak focused on the development of a modulated fibrin composite patch for cardiac regeneration [55]. This body of work was successful in developing a biomimetic cardiac patch capable of aligned contraction and shows promise as a functional ventricular wall replacement. Like most tissue engineered constructs, however, it is limited by thickness and the diffusion limit of oxygen [55]. In order to function as a full thickness tissue engineered construct, a vascular network needs to be put in place. The fibrin vascular devices may be a good solution to this problem.

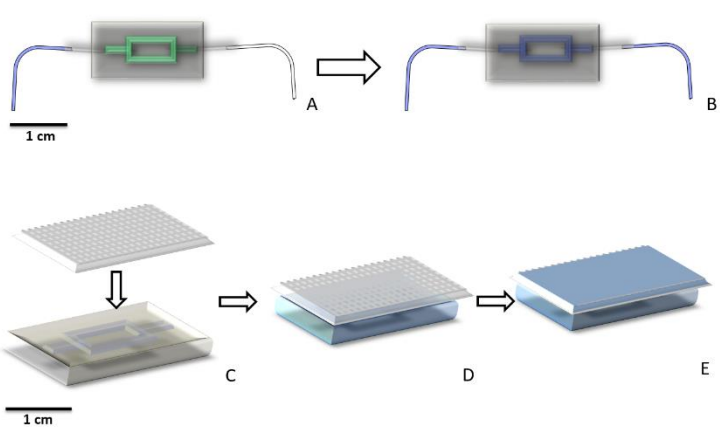

Figure 42: Cardiac patch and fibrin vascular device setup. (a, b) fibrin vascular device made and perfused to remove gelatin (c) cardiac patch laid on top (d, e) diffusion from microfluidic channels to cardiac patch

Preliminary testing was performed with layering one of these cardiac patches seeded with rat neonatal ventricular monocytes on the surface of a fibrin vascular device (Figure 42). The fibrin vascular device was perfused with a 2µL calcein AM loaded dPBS solution for 75 minutes to observe diffusion of dye to the surface. As previously mentioned, calcein AM becomes fluorescent only once hydrolyzed by intracellular esterases [55]. After this perfusion, images were taken at 40X on an upright fluorescent microscope. From these images, shown in Figure 43 below, it was clear to see that the calcein reached the cells within the cardiac patch, and the fibrin microthreads within the composite batch were clearly identifiable. While much work remains to be done to perfect the integration of cardiac composite patches with fibrin vascular devices, initial results show promise for the development of a full thickness, perfused fibrin cardiac patch.

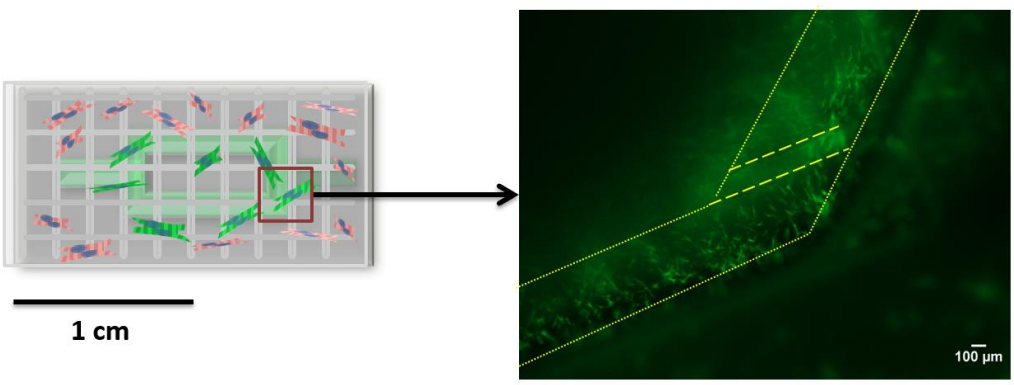

Figure 43: Diffusion of calcein AM dye to rat neonatal ventricular monocytes within a fibrin composite patch. Yellow lines indicate channel boundaries and microthread outline after 75 minutes of perfusion. Image credit Megan Chrobak.

Chapter 8: Conclusions

The goal of this project was to develop a novel method for the fabrication of a single layered, fibrin-based vascular network that was able to reliably produce channels, had flow properties within physiological relevance, and had a diffusion rate that was capable of sustaining a live cell population on the surface. A detailed protocol was developed for the fabrication of fibrin vascular devices involving the development of sacrificial structures and a robust fibrin gel capable of maintaining channels. This goal had three main objectives.

The first objective was the development of a novel technique for creating a consistently sized vascular network within a fibrin gel matrix. Success in this objective was defined as the ability to reliably produce and perfuse channels of consistent size without experiencing leakage. In this aim, these experiments were successful in creating sacrificial structures and fluidic channels that were not significantly different from each other, and reliably producing flow.

The second objective of this project was determining the flow properties of liquids passing through the channels and the rate of diffusion through the gel, with success defined as collecting clear and accurate values for a variety of flow and diffusive properties and having said values fall within physiologically relevant ranges. In this objective, these experiments were very successful in obtaining favorable flow properties, but the diffusive properties did not match published literature, though likely due to the use of a robust fibrin gel.

The final objective towards accomplishing the goal of this thesis was determining zones of cellular uptake on top of the device and observing differences in uptake zones between one and four hours of perfusion. Success was considered to be seeing and quantifying any change in uptake zones. In this objective, these experiments were also successful.

Overall, the morphological, diffusive, and flow properties of a monolayered fibrin vascular device showed strong correlation to physiological values, and several problems common with hydrogel

based fluidic systems were successfully addressed. These promising results, as well as preliminary future work studies directed at increasing complexity and decreasing the size of the vascular network, provide a strong argument for the continuation of development of this system, with the end goal of creating a functional microvascular network for an array of uses, including *in vivo* vascular repair, vascularization of full thickness tissue engineered constructs, and as an *in vitro* vascular model for drug testing.

Sources

[1] E. C. Novosel, C. Kleinhans, and P. J. Kluger, "Vascularization is the key challenge in tissue engineering," *Adv Drug Deliv Rev,* vol. 63, no. 4-5, pp. 300-11, Apr 30 2011.

[2] S. Kim, W. Kim, S. Lim, and J. S. Jeon, "Vasculature-On-A-Chip for In Vitro Disease Models," *Bioengineering (Basel),* vol. 4, no. 1, Jan 24 2017.

[3] N. G. Frangogiannis, "Pathophysiology of Myocardial Infarction," *Compr Physiol,* vol. 5, no. 4, pp. 1841-75, Sep 20 2015.

[4] J. M. Gonzalez-Rosa, V. Martin, M. Peralta, M. Torres, and N. Mercader, "Extensive scar formation and regression during heart regeneration after cryoinjury in zebrafish," (in English), *Development,* vol. 138, no. 9, pp. 1663-1674, May 1 2011.

[5] D. G. Seifu, A. Purnama, K. Mequanint, and D. Mantovani, "Small-diameter vascular tissue engineering," *Nat Rev Cardiol,* vol. 10, no. 7, pp. 410-21, Jul 2013.

[6] A. Borenstein, Gagnon, Keith, Moutinho, Thomas, and Ryer, Kevin, "Fibrin-Based Microvascular Network for the Modular Design of a Cardiac Patch," W. P. Institute, Ed., ed, 2015.

[7] Y. Naito *et al.*, "Vascular tissue engineering: towards the next generation vascular grafts," *Adv Drug Deliv Rev,* vol. 63, no. 4-5, pp. 312-23, Apr 30 2011.

[8] S. A. Berger, Goldsmith, W. and Lewis, E.R, *Introduction to Bioengineering*. Oxford University Press, 2004.

[9] R. Frietas, *Nanomedicine*. Austin, TX: Landes Bioscience, 1999.

[10] N. Resnick *et al.*, "Fluid shear stress and the vascular endothelium: for better and for worse," *Progress in Biophysics and Molecular Biology,* vol. 81, no. 3, pp. 177-199, 2003.

[11] C. K. Griffith *et al.*, "Diffusion limits of an in vitro thick prevascularized tissue," *Tissue Eng,* vol. 11, no. 1-2, pp. 257-66, Jan-Feb 2005.

[12] E. J. Benjamin *et al.*, "Heart Disease and Stroke Statistics-2017 Update: A Report From the American Heart Association," *Circulation,* vol. 135, no. 10, pp. e146-e603, Mar 07 2017.

[13] A. Skyschally, R. Schulz, and G. Heusch, "Pathophysiology of myocardial infarction: protection by ischemic pre- and postconditioning," *Herz,* vol. 33, no. 2, pp. 88-100, Mar 2008.

[14] M. B. Furtado, H. T. Nim, S. E. Boyd, and N. A. Rosenthal, "View from the heart: cardiac fibroblasts in development, scarring and regeneration," *Development,* vol. 143, no. 3, pp. 387-97, Feb 01 2016.

[15] J. M. Grasman, M. J. Zayas, R. L. Page, and G. D. Pins, "Biomimetic scaffolds for regeneration of volumetric muscle loss in skeletal muscle injuries," *Acta Biomater,* vol. 25, pp. 2-15, Oct 2015.

[16] B. J. Jank *et al.*, "Creation of a Bioengineered Skin Flap Scaffold with a Perfusable Vascular Pedicle," *Tissue Eng Part A,* vol. 23, no. 13-14, pp. 696-707, Jul 2017.

[17] E. D. Bar-Meir, J. H. Yueh, A. M. Tobias, and B. T. Lee, "Autologous fat grafting: a technique for stabilization of the microvascular pedicle in DIEP flap reconstruction," *Microsurgery,* vol. 28, no. 7, pp. 495-8, 2008.

[18] M. Reissis, D. Reissis, G. B. Bottini, A. Messiha, and D. C. Davies, "A morphometric analysis of the suitability of the transverse cervical artery as a recipient artery in head and neck free flap microvascular reconstruction," *Surg Radiol Anat,* Apr 9 2018.

[19] C. Norotte, F. S. Marga, L. E. Niklason, and G. Forgacs, "Scaffold-free vascular tissue engineering using bioprinting," *Biomaterials,* vol. 30, no. 30, pp. 5910-7, Oct 2009.

[20] E. Catalano, A. Cochis, E. Varoni, L. Rimondini, and B. Azzimonti, "Tissue-engineered skin substitutes: an overview," *J Artif Organs,* vol. 16, no. 4, pp. 397-403, Dec 2013.

[21] J. R. Gershlak *et al.*, "Crossing kingdoms: Using decellularized plants as perfusable tissue engineering scaffolds," *Biomaterials,* vol. 125, pp. 13-22, May 2017.

[22] H. C. Ott *et al.*, "Perfusion-decellularized matrix: using nature's platform to engineer a bioartificial heart," *Nat Med,* vol. 14, no. 2, pp. 213-21, Feb 2008.
[23] P. L. Tremblay, V. Hudon, F. Berthod, L. Germain, and F. A. Auger, "Inosculation of tissue-engineered capillaries with the host's vasculature in a reconstructed skin transplanted on mice," *Am J Transplant,* vol. 5, no. 5, pp. 1002-10, May 2005.
[24] S. Zhao *et al.*, "Bio-functionalized silk hydrogel microfluidic systems," *Biomaterials,* vol. 93, pp. 60-70, Jul 2016.
[25] E. W. Young, M. W. Watson, S. Srigunapalan, A. R. Wheeler, and C. A. Simmons, "Technique for real-time measurements of endothelial permeability in a microfluidic membrane chip using laser-induced fluorescence detection," *Anal Chem,* vol. 82, no. 3, pp. 808-16, Feb 1 2010.
[26] N. W. Choi, M. Cabodi, B. Held, J. P. Gleghorn, L. J. Bonassar, and A. D. Stroock, "Microfluidic scaffolds for tissue engineering," *Nat Mater,* vol. 6, no. 11, pp. 908-15, Nov 2007.
[27] M. Shin *et al.*, "Endothelialized networks with a vascular geometry in microfabricated poly(dimethyl siloxane)," *Biomed Microdevices,* vol. 6, no. 4, pp. 269-78, Dec 2004.
[28] Z. Z. Wang *et al.*, "Endothelial cells derived from human embryonic stem cells form durable blood vessels in vivo," *Nat Biotechnol,* vol. 25, no. 3, pp. 317-8, Mar 2007.
[29] A. P. Golden and J. Tien, "Fabrication of microfluidic hydrogels using molded gelatin as a sacrificial element," *Lab Chip,* vol. 7, no. 6, pp. 720-5, Jun 2007.
[30] B. M. Baker, B. Trappmann, S. C. Stapleton, E. Toro, and C. S. Chen, "Microfluidics embedded within extracellular matrix to define vascular architectures and pattern diffusive gradients," *Lab Chip,* vol. 13, no. 16, pp. 3246-52, Aug 21 2013.
[31] S. Aldrich, "Fibrin," ed: Sigma Aldrich.
[32] K. S. Thomson, S. K. Dupras, C. E. Murry, M. Scatena, and M. Regnier, "Proangiogenic microtemplated fibrin scaffolds containing aprotinin promote improved wound healing responses," *Angiogenesis,* vol. 17, no. 1, pp. 195-205, Jan 2014.
[33] H. Duong, B. Wu, and B. Tawil, "Modulation of 3D fibrin matrix stiffness by intrinsic fibrinogen-thrombin compositions and by extrinsic cellular activity," *Tissue Eng Part A,* vol. 15, no. 7, pp. 1865-76, Jul 2009.
[34] R. A. Clark, "Fibrin and wound healing," *Ann N Y Acad Sci,* vol. 936, pp. 355-67, 2001.
[35] K. Ackerman, J. Akid, A. Baltazar, D. Duo, and S. Fariello, "Bioreactor and a Novel Microengineered Vascular Network," Bachelor of Science, Biomedical Engineering, Worcester Polytechnic Institute, 2016.
[36] G. A. Truskey, F. Yuan, and D. F. Katz, *Transport Phenomena in Biological Systems*. Upper Saddle River, NJ: Pearson Patience Hill, 2004.
[37] J. Lewis. (2004). *Re. include inverse error function (erfinv and erfcinv) in Excel*.
[38] R. E. Klabunde. (2018). *Turbulent Flow*. Available: https://www.cvphysiology.com/Hemodynamics/H007
[39] U. Zettl *et al.*, "Self-Diffusion and Cooperative Diffusion in Semidilute Polymer Solutions As Measured by Fluorescence Correlation Spectroscopy," *Macromolecules,* vol. 42, no. 24, pp. 9537-9547, 2009.
[40] J.-F. H. Geschwind *et al.*, "Chemoembolization of Liver Tumor in a Rabbit Model: Assessment of Tumor Cell Death with Diffusion-Weighted MR Imaging and Histologic Analysis," *Journal of Vascular and Interventional Radiology,* vol. 11, no. 10, pp. 1245-1255, 2000.
[41] K. V. Larin, M. G. Ghosn, S. N. Ivers, A. Tellez, and J. F. Granada, "Quantification of glucose diffusion in arterial tissues by using optical coherence tomography," *Laser Physics Letters,* vol. 4, no. 4, pp. 312-317, 2007.
[42] O. G. Bakunin, *Turbulence and Diffusion: Scaling Versus Equations*. Springer, 2008.

[43] C. S. Chen *et al.*, "Shrinky-Dink microfluidics: 3D polystyrene chips," *Lab Chip,* vol. 8, no. 4, pp. 622-4, Apr 2008.
[44] A. Grimes, D. N. Breslauer, M. Long, J. Pegan, L. P. Lee, and M. Khine, "Shrinky-Dink microfluidics: rapid generation of deep and rounded patterns," *Lab Chip,* vol. 8, no. 1, pp. 170-2, Jan 2008.
[45] D. Taylor, D. Dyer, V. Lew, and M. Khine, "Shrink film patterning by craft cutter: complete plastic chips with high resolution/high-aspect ratio channel," *Lab Chip,* vol. 10, no. 18, pp. 2472-5, Sep 21 2010.
[46] M. H. Lee, M. D. Huntington, W. Zhou, J. C. Yang, and T. W. Odom, "Programmable soft lithography: solvent-assisted nanoscale embossing," *Nano Lett,* vol. 11, no. 2, pp. 311-5, Feb 9 2011.
[47] A. H. Zisch, U. Schenk, J. C. Schense, S. E. Sakiyama-Elbert, and J. A. Hubbell, "Covalently conjugated VEGF–fibrin matrices for endothelialization," *Journal of Controlled Release,* vol. 72, no. 1-3, pp. 101-113, 2001.
[48] D. R. Myers *et al.*, "Endothelialized microfluidics for studying microvascular interactions in hematologic diseases," *J Vis Exp,* no. 64, Jun 22 2012.
[49] L. Yang, S. V. Shridhar, M. Gerwitz, and P. Soman, "An in vitro vascular chip using 3D printing-enabled hydrogel casting," *Biofabrication,* vol. 8, no. 3, p. 035015, Aug 26 2016.
[50] E. Van Belle, F. O. Tio, T. Couffinhal, L. Maillard, J. Passeri, and J. M. Isner, "Stent Endothelialization: Time Course, Impact of Local Catheter Delivery, Feasibility of Recombinant Protein Administration, and Response to Cytokine Expedition," *Circulation,* vol. 95, no. 2, pp. 438-448, 1997.
[51] K. H. Wong, J. G. Truslow, A. H. Khankhel, K. L. Chan, and J. Tien, "Artificial lymphatic drainage systems for vascularized microfluidic scaffolds," *J Biomed Mater Res A,* vol. 101, no. 8, pp. 2181-90, Aug 2013.
[52] M. E. Kidd, S. Shin, and L. D. Shea, "Fibrin hydrogels for lentiviral gene delivery in vitro and in vivo," *J Control Release,* vol. 157, no. 1, pp. 80-5, Jan 10 2012.
[53] S. T. Coffin and G. R. Gaudette, "Aprotinin extends mechanical integrity time of cell-seeded fibrin sutures," *J Biomed Mater Res A,* vol. 104, no. 9, pp. 2271-9, Sep 2016.
[54] R. L. Page *et al.*, "Restoration of Skeletal Muscle Defects with Adult Human Cells Delivered on Fibrin Microthreads," *Tissue Engineering Part A,* vol. 17, no. 21-22, pp. 2629-2640, 2011.
[55] M. O. B. Chrobak, "Designing Modular Fibrin Composite Scaffolds for Enhanced Ventricular Myocardium Regeneration," PhD, Biomedical Engineering, Worcester Polytechnic Institute, 2017.

Appendices:

Appendix 1: SOLIDWORKS Drawing of Acrylic Mold

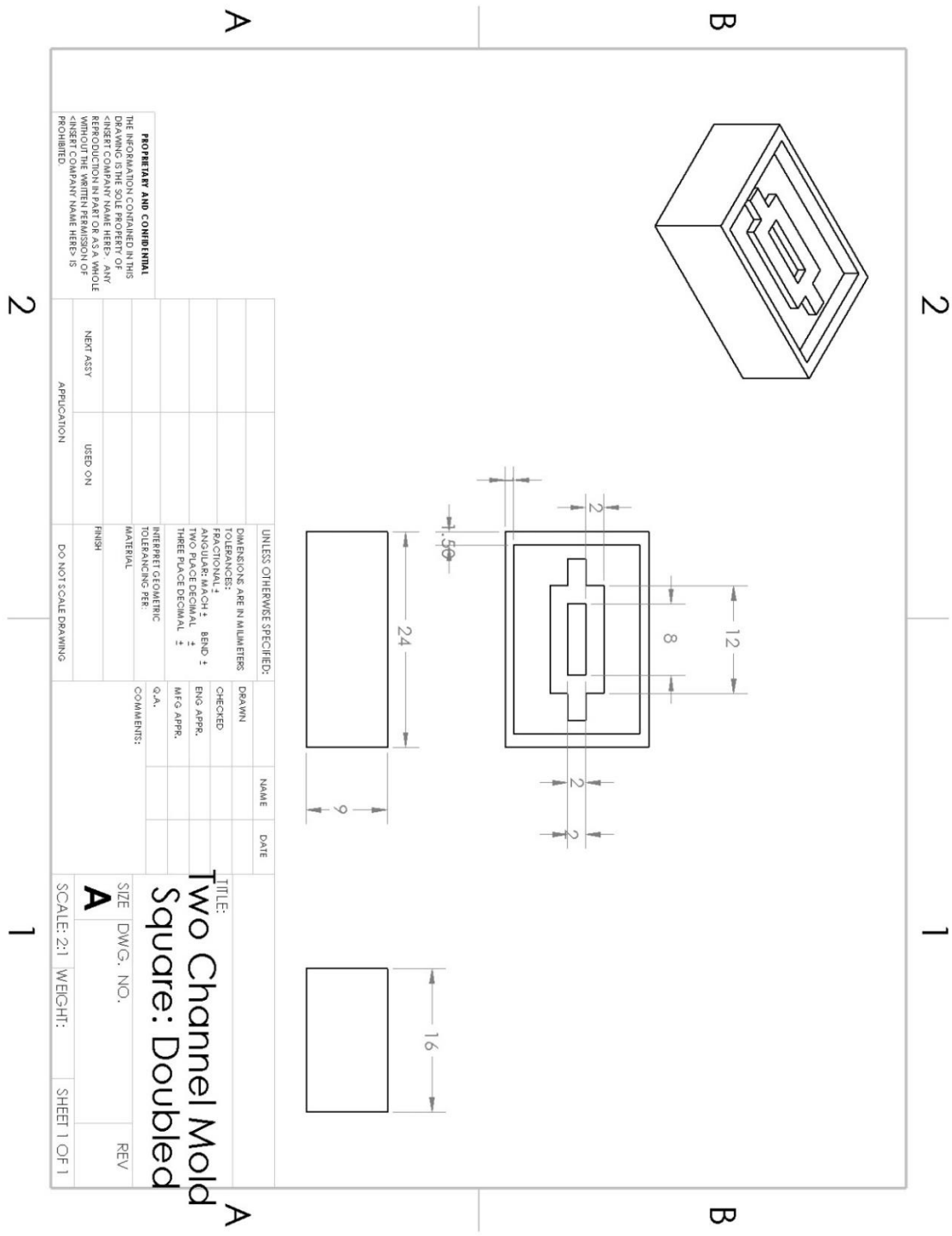

Appendix 2: Maximum Particle Speed Formula Integration

Below is the integration of the average function value equation. The bonds were chosen in order to calculate the speed of the particles at the center of the channel based on knowing the average speed of particles tracked. Here, “a” is -h/2, “b” is h/2, “u” is speed, “h” is the width of the channel, and “y” is the distance from the center point.

$$f_{avg} = \frac{1}{b-a}\int_a^b f(x)dx$$

$$f(x) = u(y) = u_{center}\left(1 - \left(\frac{2y}{h}\right)^2\right) = u_{center}\left(1 - \frac{4y^2}{h^2}\right)$$

$$u_{avg} = \frac{1}{\frac{h}{2} - \frac{-h}{2}}\int_{\frac{-h}{2}}^{\frac{h}{2}} u_{center}\left(1 - \frac{4y^2}{h^2}\right) dy$$

$$u_{avg} = \frac{1}{h} * u_{center}\int_{\frac{-h}{2}}^{\frac{h}{2}}\left(1 - \frac{4}{h^2}y^2\right)dy$$

$$u_{avg} = \frac{u_{center}}{h}\left(y - \frac{4}{h^2}\frac{y^3}{3}\right)\Big|_{\frac{-h}{2}}^{\frac{h}{2}}$$

$$u_{avg} = \frac{u_{center}}{h}\left[\left(\frac{h}{2} - \frac{4}{h^2} * \frac{1}{3} * \frac{h^3}{8}\right) - \left(\frac{-h}{2} - \frac{4}{h^2} * \frac{1}{3} * \frac{-h^3}{8}\right)\right]$$

$$u_{avg} = \frac{u_{center}}{h}\left[\left(\frac{h}{2} - \frac{1}{1} * \frac{1}{3} * \frac{h}{2}\right) - \left(\frac{-h}{2} - \frac{1}{1} * \frac{1}{3} * \frac{-h}{2}\right)\right]$$

$$u_{avg} = \frac{u_{center}}{h}\left[\left(\frac{h}{2} - \frac{h}{6}\right) - \left(\frac{-h}{2} + \frac{h}{6}\right)\right]$$

$$u_{avg} = \frac{u_{center}}{h}\left(\frac{h}{2} - \frac{h}{6} + \frac{h}{2} - \frac{h}{6}\right)$$

$$u_{avg} = \frac{u_{center}}{h}\left(h - \frac{h}{3}\right)$$

$$u_{avg} = \frac{u_{center}}{h}\left(\frac{2h}{3}\right)$$

$$u_{avg} = \frac{2u_{center}}{3}$$

$$u_{center} = \frac{3u_{avg}}{2}$$

Appendix 3: Particle Tracking Measurements

Trial one:

Sample Number 1		Sample Number 2		Sample Number 3	
Particle Number	Distance Traveled (um)	Particle Number	Distance Traveled (um)	Particle Number	Distance Traveled (um)
1	1442.08	1	1108.44	1	1736.59
2	1368.31	2	977.32	2	931.64
3	1452.73	3	863.18	3	996.23
4	1060.11	4	874.09	4	1196.89
5	1240.47	5	1043.67	5	1618.26
6	1318.21	6	1222.34	6	1668.16
7	1450.17	7	1346.82	7	1546.63
8	966.19	8	1089.94	8	926.32
9	986.97	9	1441.62	9	1163.27
10	1311.88	10	1414.86	10	1364.88
Mean	1259.712	Mean	1138.228	Mean	1314.887
Standard Deviation	190.1694868	Standard Deviation	211.5102732	Standard Deviation	313.9692828
Per Second	83.9808		75.88186667		87.65913333
	12.67796579		14.10068488		20.93128552

Trial 2:

Sample 1 (T1)		Sample 2 (B2)		Sample 3 (B3)	
Particle Number	Distance traveled (um)	Particle Number	Distance traveled (um)	Particle Number	Distance traveled (um)
1	493.029	1	3353.49	1	1361.85
2	876.368	2	1388.39	2	2246.05
3	546.817	3	1047.91	3	2552.42
4	929.901	4	1086.84	4	1221.33
5	831.999	5	1479.88	5	1350.58
6	696.711	6	1304.13	6	1348.61
7	885.604	7	2544.33	7	1552.86
8	733.605	8	1582.48	8	1149.23
9	776.985	9	1929.71	9	1323.597
10	730.908	10	1450.97	10	3729.01
Mean	750.1927	Mean	1716.813	Mean	1783.5537
Standard Deviation	143.3580542	Standard Deviation	720.8129941	Standard Deviation	825.1314025

Sample 4 (B1)	
Particle Number	Distance traveled (um)
1	3232.96
2	1368.64
3	2989.43
4	1247.51
5	1495.13
6	1477.15
7	1415.78
8	2498.57
9	957.464
10	1465.86
Mean	1814.8494
Standard Deviation	789.6236117

Sample 5 (t2)	
Particle Number	Distance traveled (um)
1	781.269
2	919.651
3	912.363
4	875.242
5	795.697
6	931.896
7	659.519
8	786.836
9	671.773
10	1026.663
Mean	836.0909
Standard Deviation	117.8841408

Sample 6	
Particle Number	Distance traveled (um)
1	943.251
2	995.984
3	890.675
4	912.363
5	972.527
6	848.291
7	628.388
8	711.188
9	869.264
10	534.803
Mean	830.6734
Standard Deviation	154.5359321

Trial 3:

Sample 1 (T1)	
Particle Number	Distance traveled (um)
1	1269.09
2	1284.99
3	1187.36
4	1429.93
5	1512.76
6	1204.62
7	1604.58
8	1217.59
9	1561.18
10	1732.33
Mean	1400.443
Standard Deviation	194.0535745

Sample 2 (T2)	
Particle Number	Distance traveled (um)
1	1521.53
2	1612.46
3	1383.47
4	1536.37
5	1324.59
6	1561.29
7	1640.13
8	1224.19
9	1588.09
10	1645.18
Mean	1503.73
Standard Deviation	144.1231985

Sample 3 (T3)	
Particle Number	Distance traveled (um)
1	1272.45
2	1395.78
3	1505.42
4	1495.99
5	1334.29
6	1417.19
7	1778.11
8	1197.53
9	1446.53
10	1569.77
Mean	1441.306
Standard Deviation	162.9975726

Sample 4 (b1)	
Particle Number	Distance traveled (um)
1	2184.49
2	1585.89
3	1773.49
4	2385.54
5	2179.24
6	2056.12
7	2274.49
8	2163.29
9	2179.94
10	1708.98
Mean	2049.147
Standard Deviation	265.7637021

Sample 5	
Particle Number	Distance traveled (um)
1	1257.33
2	2244.12
3	1282.04
4	1703.31
5	2307.85
6	2216.35
7	1281.01
8	1375.47
9	2233.43
10	2184.67
Mean	1808.558
Standard Deviation	469.6689481

Sample 6	
Particle Number	Distance traveled (um)
1	1403.77
2	2039.83
3	1757.72
4	2105.71
5	2326.01
6	2260.88
7	2163.02
8	1965.18
9	2350.54
10	1546.28
Mean	1991.894
Standard Deviation	326.1156491

Appendix 4: Mean Diffusivity Measurements

Appendix 4.1 40 kDa Dextran Diffusivity

Diffusivity of 40 kDa Dextran (mm^2/s)					
Distance from Channel Edge	0.1 mm	0.2 mm	0.3 mm	0.4 mm	0.5 mm
0 Seconds	0.000E+00	0.000E+00	0.000E+00	0.000E+00	0.000E+00
30 Seconds	4.107E-05	1.376E-04	2.655E-04	4.644E-04	7.201E-04
60 Seconds	2.261E-05	7.170E-05	1.524E-04	2.027E-04	3.426E-04
90 Seconds	1.832E-05	4.734E-05	9.321E-05	1.592E-04	2.400E-04
120 Seconds	1.642E-05	3.787E-05	7.433E-05	1.118E-04	1.597E-04
150 Seconds	1.446E-05	3.177E-05	6.297E-05	1.013E-04	1.558E-04
180 Seconds	1.278E-05	3.179E-05	5.199E-05	8.666E-05	1.311E-04
210 Seconds	1.196E-05	2.817E-05	4.831E-05	7.345E-05	1.200E-04
240 Seconds	1.154E-05	2.701E-05	4.384E-05	5.902E-05	1.020E-04
270 Seconds	1.087E-05	2.485E-05	4.315E-05	5.696E-05	8.745E-05
300 Seconds	9.560E-06	2.332E-05	3.576E-05	4.841E-05	7.771E-05
330 Seconds	9.648E-06	2.241E-05	3.617E-05	4.730E-05	7.512E-05
360 Seconds	9.149E-06	2.106E-05	3.391E-05	5.020E-05	6.985E-05
390 Seconds	9.190E-06	2.088E-05	3.306E-05	4.515E-05	6.209E-05
420 Seconds	8.601E-06	1.983E-05	3.035E-05	4.367E-05	5.548E-05
450 Seconds	8.557E-06	1.812E-05	2.954E-05	4.266E-05	5.984E-05
480 Seconds	7.927E-06	1.881E-05	2.928E-05	4.033E-05	5.563E-05
510 Seconds	8.039E-06	1.849E-05	2.862E-05	3.893E-05	4.654E-05
540 Seconds	8.028E-06	1.742E-05	2.768E-05	3.779E-05	4.847E-05

570 Seconds	7.738E-06	1.728E-05	2.882E-05	3.678E-05	4.612E-05
600 Seconds	7.867E-06	1.753E-05	2.753E-05	3.665E-05	4.494E-05
630 Seconds	7.757E-06	1.682E-05	2.562E-05	3.507E-05	4.812E-05
660 Seconds	7.665E-06	1.731E-05	2.592E-05	3.417E-05	4.302E-05
690 Seconds	7.939E-06	1.674E-05	2.559E-05	3.296E-05	4.171E-05
720 Seconds	7.738E-06	1.666E-05	2.573E-05	3.237E-05	4.136E-05
750 Seconds	7.825E-06	1.643E-05	2.492E-05	3.327E-05	4.093E-05
780 Seconds	7.859E-06	1.645E-05	2.426E-05	3.192E-05	3.949E-05
810 Seconds	7.695E-06	1.643E-05	2.578E-05	3.161E-05	3.981E-05
840 Seconds	8.114E-06	1.608E-05	2.509E-05	3.229E-05	4.135E-05
870 Seconds	7.494E-06	1.604E-05	2.569E-05	3.046E-05	3.892E-05
900 Seconds	5.618E-06	1.290E-05	2.202E-05	3.071E-05	3.794E-05
930 Seconds	5.789E-06	1.304E-05	2.122E-05	2.937E-05	3.537E-05
960 Seconds	5.657E-06	1.335E-05	2.278E-05	2.745E-05	3.576E-05
990 Seconds	3.000E-06	7.762E-06	1.252E-05	1.799E-05	2.492E-05
1020 Seconds	3.019E-06	7.421E-06	1.230E-05	1.830E-05	2.549E-05
1050 Seconds	3.172E-06	7.226E-06	1.223E-05	1.786E-05	2.204E-05
Mean	1.002E-05	2.468E-05	4.309E-05	6.340E-05	9.305E-05
SD	6.733E-06	2.300E-05	4.669E-05	7.990E-05	1.272E-04
System Mean	4.685E-05				
System SD	3.267E-05				

Appendix 4.2: 250 kDa Dextran Diffusivity

Diffusivity of 250 kDa Dextran (mm^2/s)					
Distance from Channel Edge	0.1 mm	0.2 mm	0.3 mm	0.4 mm	0.5 mm
0 Seconds	0.000E+00	0.000E+00	0.000E+00	0.000E+00	0.000E+00
30 Seconds	3.021E-05	1.118E-04	2.853E-04	4.647E-04	6.760E-04
60 Seconds	1.732E-05	6.051E-05	1.274E-04	2.162E-04	2.935E-04
90 Seconds	1.198E-05	4.737E-05	8.221E-05	1.379E-04	2.040E-04
120 Seconds	1.025E-05	2.994E-05	6.371E-05	1.074E-04	1.839E-04
150 Seconds	8.655E-06	2.556E-05	5.653E-05	9.503E-05	1.405E-04
180 Seconds	7.278E-06	2.218E-05	4.540E-05	7.195E-05	1.289E-04
210 Seconds	6.372E-06	2.061E-05	4.207E-05	6.735E-05	1.082E-04
240 Seconds	5.884E-06	1.698E-05	3.843E-05	6.041E-05	1.006E-04
270 Seconds	5.479E-06	1.502E-05	3.437E-05	5.210E-05	7.855E-05
300 Seconds	5.386E-06	1.523E-05	3.172E-05	4.796E-05	7.122E-05
330 Seconds	4.968E-06	1.414E-05	2.841E-05	4.861E-05	6.396E-05
360 Seconds	4.659E-06	1.313E-05	2.851E-05	3.758E-05	6.974E-05
390 Seconds	4.467E-06	1.312E-05	2.595E-05	4.091E-05	6.377E-05
420 Seconds	4.399E-06	1.209E-05	2.481E-05	3.835E-05	5.467E-05
450 Seconds	4.166E-06	1.163E-05	2.466E-05	3.647E-05	5.012E-05
480 Seconds	4.097E-06	1.143E-05	2.275E-05	3.366E-05	4.832E-05
510 Seconds	4.049E-06	1.139E-05	2.119E-05	3.286E-05	4.810E-05
540 Seconds	4.034E-06	1.065E-05	2.089E-05	3.178E-05	4.737E-05
570 Seconds	4.045E-06	1.059E-05	2.157E-05	2.945E-05	4.361E-05

600 Seconds	3.884E-06	1.004E-05	1.836E-05	2.926E-05	4.195E-05
630 Seconds	3.748E-06	9.913E-06	1.814E-05	2.875E-05	3.994E-05
660 Seconds	3.708E-06	1.006E-05	1.811E-05	2.814E-05	4.094E-05
690 Seconds	3.667E-06	9.632E-06	1.731E-05	2.634E-05	3.609E-05
720 Seconds	3.545E-06	9.480E-06	1.695E-05	2.680E-05	3.486E-05
750 Seconds	3.591E-06	9.497E-06	1.727E-05	2.669E-05	3.593E-05
780 Seconds	3.611E-06	9.457E-06	1.646E-05	2.436E-05	3.454E-05
810 Seconds	3.530E-06	9.011E-06	1.683E-05	2.374E-05	3.258E-05
840 Seconds	3.718E-06	9.050E-06	1.579E-05	2.265E-05	3.234E-05
870 Seconds	3.610E-06	8.865E-06	1.543E-05	2.418E-05	3.146E-05
900 Seconds	4.399E-06	8.866E-06	1.562E-05	2.082E-05	3.127E-05
930 Seconds	4.361E-06	8.816E-06	1.546E-05	2.133E-05	3.072E-05
960 Seconds	4.186E-06	8.835E-06	1.515E-05	2.057E-05	2.930E-05
990 Seconds	4.675E-06	7.695E-06	1.317E-05	2.126E-05	3.033E-05
1020 Seconds	1.989E-06	6.104E-06	1.083E-05	1.677E-05	2.558E-05
1050 Seconds	1.938E-06	6.268E-06	1.117E-05	1.692E-05	2.495E-05
Mean	5.718E-06	1.708E-05	3.550E-05	5.637E-05	8.355E-05
SD	5.168E-06	1.979E-05	4.876E-05	8.067E-05	1.174E-04
System Mean	3.964E-05				
System SD	4.558E-05				

Appendix 5: Shrinky-Dink Analysis

Shapes tested for these experiments were concentric squares, with the “big” dimension referring to the outer shape, and the “small” dimension referring to the cut-out window.

Normal Shrinky-Dinks

TRIAL 1			
Height big (mm)	Width big (mm)	Height small (mm)	Width small (mm)
8.36	8.32	4.18	4.21
8.25	8.29	4.13	4.1
8.28	8.36	4.18	4.25
8.24	8.31	4.25	4.22
8.18	8.23	4.15	4.15
8.28	8.13	4.18	4.07
8.25	8.13	4.1	4.14
8.24	8.3	4.12	4.3
8.26	8.24	4.25	4.11
8.19	8.27	4.08	4.27
8.3	8.09	4.1	4.11
8.31	8.12	4.15	4.17
8.08	8.22	4.08	4.15
8.1	8.46	4.12	4.1
8.28	8.11	4.05	4.17
8.23	8.3	4.18	4.22
8.34	8.13	4.18	4.23
8.33	8.12	4.03	4.21
8.07	8.42	4.02	4.1
8.05	8.21	4.04	4.06
avg height	avg width	avg sm height	avg sm width
8.231	8.238	4.1285	4.167
avg square dimensions		avg small square dimensions	
8.2345mm^2		4.14775mm^2	
original dimensions 20x20mm big 10x10mm small			

TRIAL 2			
Height big (mm)	Width big (mm)	Height small (mm)	Width small (mm)
8.3	8.34	4.08	4.08
8.28	8.11	4.09	4.01
8.27	8.36	4.1	4.12
8.09	8.48	4.02	3.89
8.21	8.47	4.06	4.3
8.3	8.04	4.1	4.03
8.27	8.42	4.14	4.24
8.11	8.36	4.03	4.09
8.23	8.35	4.07	4.17
8.18	8.32	4.07	4.2
8.33	8.19	4.08	4.23
8.44	8.25	4.12	4.12
8.28	8.07	4.05	4.01
8.27	8.17	4.08	4.06
8.03	8.34	4.17	3.99
8.19	8.37	4.11	4.22
8.35	8.24	4.12	4.09
8.3	8.07	4.2	4.07
8.39	8.39	4.18	4.14
8.18	8.31	4.01	4.19
avg height	avg width	avg sm height	avg sm width
8.25	8.2825	4.094	4.1125
avg square dimensions		avg small square dimensions	
8.26625mm^2		4.10325mm^2	
final avg square dimensions		final avg sm square dimensions	
8.205mm^2		4.106mm^2	
about .41025x original		about .41025x original	

TRIAL 3			
Height big (mm)	Width big (mm)	Height small (mm)	Width small (mm)
8.04	8.2	3.93	4.13
7.96	8.08	3.94	3.99
8.09	8.23	4.09	4.04
7.95	8.11	4.1	4.14
8.01	8.13	4.2	4.02
8.05	8.05	4.04	4.02
8.29	8.14	4.12	4.15
8.01	8.24	4.03	3.99
8.17	8.17	4.03	4.23
8.18	8.13	4.03	4.3
8.28	8.11	3.99	4.19
8.08	8.08	4.09	4.05
8.2	8.24	4.01	3.98
8.14	8.21	4.04	4.12
8.14	8.03	4.01	4.11
8.08	8.16	4.02	4.07
8.21	7.96	3.98	4.2
8.15	8.03	3.96	4.07
8.3	8.01	3.99	4.2
8.18	8.06	4.01	4.03
avg height	avg width	avg sm height	avg sm width
8.1125	8.1185	4.0305	4.1015
avg square dimensions		avg small square dimensions	
8.1155mm^2		4.066mm^2	

Ultra-Thick Shrinky-Dinks

TRIAL 1				TRIAL 2				TRIAL 3			
Height(mm)	Width(mm)	Small Height(mm	Small Width(mm)	Height(mm)	Width(mm)	Small Height(mm	Small Width(mm)	Height(mm)	Width(mm)	Small Height(mm	Small Width(mm)
7.41	8.29	3.69	4.14	7.45	8.25	3.5	4.18	7.11	7.88	3.32	3.85
7.3	8.5	3.65	4.2	7.19	7.93	3.58	3.99	7.12	7.69	3.51	3.78
7.34	8.34	3.69	4.1	7.23	7.91	3.69	3.97	7.23	7.92	3.59	3.85
7.36	8.32	3.7	4.11	7.3	7.92	3.64	3.84	7.22	7.85	3.6	3.81
7.3	8.5	3.73	3.94	7.24	8.07	3.62	3.94	7.36	7.75	3.63	3.83
7.29	8.32	3.66	4.18	7.18	7.97	3.57	3.91	7.25	8.05	3.63	3.89
7.41	8.6	3.68	4.27	7.12	8.06	3.5	3.99	7.22	8.03	3.55	4.04
7.23	8.38	3.65	4.32	7.22	8.08	3.55	4.04	7.33	8.08	3.55	4.13
7.29	8.51	3.71	4.21	7.17	8.02	3.55	3.85	7.31	8.02	3.58	4.05
7.3	8.43	3.69	4.11	7.24	8.11	3.52	4.12	7.19	7.92	3.48	3.9
7.25	8.33	3.68	4.12	7.24	8.01	3.64	3.78	7.38	7.87	3.62	3.92
7.29	8.27	3.67	4.09	7.22	7.76	3.67	3.68	7.14	7.86	3.56	3.82
7.63	8.44	3.67	4.01	7.14	7.94	3.5	4	7.2	7.93	3.62	3.94
7.32	8.32	3.65	4.07	7.33	8.12	3.51	4.06	7.26	7.74	3.61	3.75
7.27	8.5	3.7	4.22	7.29	8.19	3.28	4.17	7.21	7.83	3.58	3.81
7.31	8.56	3.7	4.28	7.21	7.91	3.59	3.85	7.18	7.94	3.6	3.82
7.29	8.37	3.7	4.1	7.31	7.96	3.67	3.97	7.17	7.76	3.56	3.86
7.32	8.54	3.68	4.2	7.28	7.91	3.64	3.83	7.25	7.82	3.61	3.81
7.22	8.48	3.69	4.16	7.16	7.93	3.57	3.91	7.34	7.83	3.61	3.99
7.34	8.39	3.65	4.14	7.36	8	3.65	3.92	7.19	7.93	3.59	3.67
Avg Height	Avg Width	Avg Sm Height	Avg Sm Width	Avg Height	Avg Width	Avg Sm Height	Avg Sm Width	Avg Height	Avg Width	Avg Sm Height	Avg Sm Width
7.3235	8.4195	3.682	4.1485	7.244	8.0025	3.572	3.95	7.233	7.885	3.57	3.876
avg square dimensions		avg small square dimensions		avg square dimensions		avg small square dimensions		avg square dimensions		avg small square dimensions	
7.8715mm^2		3.91525mm^2		7.62325mm^2		3.761mm^2		7.559mm^2		3.723mm^2	
original dimensions 20x20mm big 10x10mm small											
				final avg square dimensions		final avg sm square dimensions					
	7.3235	8.4195		7.6846mm^2		3.7798mm^2					
	7.244	8.0025		0.3842xoriginal		0.3779xoriginal					
	7.233	7.885									
	7.267	8.102									
	1.38	1.23									